METALLO-PORPHYRIN CONTAINING ZIRCONIUM PHOSPHONATE THIN FILMS: STRUCTURE AND CATALYSIS

By

CHRISTINE MARIE NIXON LEE

A DISSERTATION PRESENTED TO THE GRADUATE SCHOOL
OF THE UNIVERSITY OF FLORIDA IN PARTIAL FULFILLMENT
OF THE REQUIREMENTS FOR THE DEGREE OF
DOCTOR OF PHILOSOPHY

UNIVERSITY OF FLORIDA

2000

ACKNOWLEDGMENTS

First, I would like to thank some of the teachers who have pointed me toward chemistry and supported me in this long educational adventure. I thank Mr. Roger Craig from Lexington High School, for being so excited about chemistry, and Dr. Jim McCargar, for being a tireless ambassador of general and physical chemistry, and for encouraging (pushing?) me to pursue research opportunities outside of Baldwin-Wallace College. I would also like to thank Dr. Gary Kosloski, who cared about my music even after I defected to the other half of the liberal arts and sciences. And to Dr. John West and Dr. William Samuels, I extend many thanks for accepting me into their research programs and giving me two unique and valuable perspectives on research outside of the academic environment.

I must thank Dr. Dan Talham for his patience, the limits of which, I have surely tested. I would also like to thank him for accepting a physical polymer chemistry convert and for teaching me to appreciate materials and surface chemistry. I would also like to thank him for his time and effort in encouraging all of us to be organized and effective speakers and writers. For that, I will be eternally grateful.

I could not have completed this document or the research that it describes without the collaborative assistance from the Bujoli group in Nantes, France. Especially to Fabrice Odobel, who has contributed significant time and energy to

making and teaching others to make the porphyrins and ligands on which this dissertation is focused, *Merci!*

Quick notes of thanks are also due to the Butler Polymer Research Laboratories for sharing their instrumentation and to Eric Lambers and the Major Analytical Instrumentation Center for allowing me to use the XPS. Also, thanks to Joe and Raymond in the chemistry department machine shop for working with me on designing and building the catalysis flow cells.

Without many wonderful friends, my time at University of Florida would have been much less enjoyable. So, I thank Louann Troutman, Tracey Hawkins, Dean and Annie Welsh, Denise Main, and Debby Tindall, and of course, Jen Batten and Leroy Kloeppner (and Alex) – the greatest of friends. I owe Jen and Leroy special thanks, not only for their efforts in editing this dissertation, but also for their support and love along the way.

And lastly, my family. All the gratitude in the world goes to my mom and dad, Pat and Ron, and to my brothers Joe and John and my soon-to-be sister, Jullia. And to my grandmothers, Evelyn Nixon and Margaret Loeber, and in memory of my Grandpas Bill and Lee. I have been truly blessed. Thanks, too, to my new family, George and Agnes, Brian and Greg Lee who are the best second family I could imagine.

To my husband, Larry, my best friend and biggest fan, I owe more thanks than can be expressed.

TABLE OF CONTENTS

LIST OF TABLES

LIST OF FIGURES

Abstract of Dissertation Presented to the Graduate School
of the University of Florida in Partial Fulfillment of the
Requirements for the Degree of Doctor of Philosophy

METALLO-PORPHYRIN CONTAINING ZIRCONIUM PHOSPHONATE
THIN FILMS: STRUCTURE AND CATALYSIS

By

Christine Marie Nixon Lee

August 2000

Chairperson: Daniel R. Talham
Major Department: Chemistry

Thin films containing mono- and tetra-phosphonic acid palladium tetraphenyl porphyrins and tetra-phosphonic acid manganese tetraphenyl porphyrins, PdP1, PdP4, and MnP4, were prepared by both Langmuir-Blodgett (LB) and self-assembly (SA) techniques. Within the hydrophilic regions of these films was incorporated a zirconium phosphonate network which lent significant stability and flexibility of preparation to these films.

In the LB films of the palladium porphyrins, it was found that the mono-phosphonic acid porphyrins aggregated under all film preparation conditions and in solutions at high concentrations. However, the chromophore aggregation could be controlled in the tetra-phosphonic acid porphyrins when the films were transferred at mean molecular areas greater or near the mean molecular area of the chromophore itself. Self-assembling the PdP4 was another means of controlling the chromophore

interaction in the films. Because chromophore aggregation was expected to inhibit catalysis, film preparation conditions were sought in order to avoid this.

LB and SA films of pure manganese porphyrins were successfully prepared by a number of different methods. Aggregation appeared insignificant when transferred at high mean molecular areas and when the films were self-assembled. The pure manganese porphyrin films were successful at catalyzing the epoxidation of cyclooctene using iodosylbenzene as the oxidant.

To activate the porphyrin for catalysis with peroxide oxidants, a heterocyclic ligand was also incorporated into the manganese porphyrin containing films. The heterocyclic ligand used was an imidazole substituted with an octadecylphosphonic acid chain. Both the manganese porphyrin and the imidazole amphiphile were tethered to a zirconium phosphonate network, first for ease of film synthesis and second, to stabilize the film for use in the catalysis reactions.

Though significant catalyst degradation has been reported in homogeneous and alternative heterogeneous catalysis studies, the manganese porphyrin and imidazole containing zirconium phosphonate films were generally more resistant to degradation under catalysis conditions. The stability of the films toward epoxidation conditions has led to easily recyclable catalysts.

CHAPTER 1
INTRODUCTION

1.1 Ultrathin Films

The study of ultrathin films, especially monomolecular thick films, enables the study of two-dimensional systems and allows the simplification of complicated thermodynamic behaviors. Recent interest in monolayers and multilayers focuses on the many potential applications of organized and functional thin films, which include optoelectronics,[1-3] coatings,[4-7] chemical sensors,[1,6,8-10] and heterogeneous catalysts.[11-13] In order to prepare these organized and essentially two-dimensional structures, the Langmuir-Blodgett (LB) and self-assembly (SA) techniques have been developed.

The study of monolayer thick films began long before the early twentieth century investigations of Irving Langmuir and Katharine Blodgett. It is believed that centuries ago drops of oil were used to calm waves in ponds and other small bodies of water.[14,15] Benjamin Franklin studied monolayers of oil on the surface of a pond. Agnes Pockels pioneered the study of a monolayer on the water surface in the laboratory environment, and is credited with building the first trough.[15] However, the first systematic study of monolayers of amphiphilic molecules on aqueous surfaces began with Irving Langmuir's studies at GE Laboratories and, hence his name is associated with a fundamental method of preparing organized, monomolecular thick

films.[16] His associate, Katherine Blodgett first transferred these films from the water surface onto solid supports.[17]

The SA technique was first described in scientific reports in the late 1940's and mid 1950's.[18,19] This technique relies on surface-active molecules and the appropriate surface being placed in contact with one another through a solvent medium. The films prepared by this method tend to be more stable than traditional LB films because of the types of surface interactions that drive their formation.

The traditional LB technique employs different surface interactions depending on the method of transfer. First, as in the case of hydrophilic-hydrophilic transfers of neutral amphiphiles from a pure aqueous subphase, the interactions are primarily hydrogen bonding in nature. Ionic bonding is commonly observed in the case of hydrophilic-hydrophilic transfers from a metal ion-containing subphase. In the case of hydrophobic-hydrophobic transfers, van der Waals interactions are involved. During LB depositions, the film is usually physisorbed to the surface implying some through-space interaction, while in SA films, the molecules are adsorbed to the surface through a chemical bond. The SA method relies on the formation of covalent bonds between the surface-active component of the molecule and the solid substrate often resulting in more stable films.[20]

In LB films, the hydrophilic head group typically dictates the area the molecule fills in the interfacial region. The alkyl groups, therefore, adjust to maximize the van der Waals contacts leading to organized packing within this region.[21] Unfortunately, control over the film packing and organization achieved by the LB technique is absent in the SA method. The molecular organization in SAMs (self-assembled monolayers) is dictated solely by the geometry of the active sites on the surface. However, in LB films, the pressure and area of deposition can be selected to deposit a particular phase of the monolayer and to influence the transferred film organization. An understanding

of the mechanics of both the LB and SA processes is important in appreciating thin film research and its application to many areas of science.[20]

1.1.1 Langmuir-Blodgett Films and Characterization

1.1.1.1 Langmuir monolayer formation: the isotherm. The Langmuir monolayer is achieved by placing droplets of an amphiphile solution, in a volatile solvent such as $CHCl_3$, on the aqueous subphase in such a way as to uniformly spread the compound on the surface. Typically, the presence of an amphiphile works to decrease the surface tension, and the difference is defined as the surface pressure. In Equation 1.1, Π is the two-dimensional surface pressure typically measured in mN m^{-1}, γ_o is the initial surface tension of the subphase and γ_f is the surface tension of the subphase and film.[22,23]

$$\Pi = \gamma_o - \gamma_f \tag{1.1}$$

The record of the monolayer formation on the water surface, the Π vs. area (A) isotherm, depends on the change in the surface pressure with a change in the mean area per molecule (MMA) on the surface.[15,22] The surface pressure is measured using a sensitive microbalance, such as a Wilhelmy balance, while the area is computer controlled using movable barriers, which define the monolayer boundaries.

Upon room temperature spreading, the monolayer is at a very low density and behaves like a two-dimensional gaseous phase (Figure 1.1). In this phase, the molecules are theoretically not in constant contact with one another, although aggregation may occur depending on the affinity of the amphiphilic molecules for one another. There are random collisions, but there is no appreciable increase in surface

pressure because, in effect, there is not a true monolayer, and the presence of the amphiphile has virtually no effect on the surface tension of the subphase.[20] There is some debate on the existence of a two-dimensional gaseous state; some researchers claim that there is always aggregates formed, which interact within the gaseous phase.[23]

As the monolayer is compressed, the molecules will come in contact with one another, and an observable rise in Π occurs. In the initial region of noticeable pressure increase, the molecules are colliding, but the film is in a fluid-like state. The molecules have no long-range orientational order and they are not close-packed or organized. This region is often called the liquid-expanded state (LE) (Figure 1.1). Within the LE phase, the alkyl chains have many degrees of freedom, and gauche conformations are observed within the chains.

The further compression of long chain fatty acid amphiphiles leads to a more crystalline and organized monolayer. In this phase, the hydrophobic tails of the amphiphiles adopt an overall orientational order that is maintained within the film domains. This orientational order seeks to balance the van der Waals interactions between the alkyl chains with the pressure applied by the barriers. Within this region, referred to as the liquid-condensed phase (LC) (Figure 1.1), the slope of the isotherm is very steep, meaning that the pressure goes up rapidly without much change in the MMA. In some cases, the structure of the amphiphiles may prohibit the formation of a close-packed monolayer regardless of the pressure, and therefore, the monolayer enters and remains in the LE phase.[15]

When the monolayer cannot compress any further, additional applied pressure from the barriers causes the monolayer to fold either over or under itself forming collapsed regions. The collapse point is identified as the first point of deviation from the linear slope of the LC region of the isotherm. [15,22]

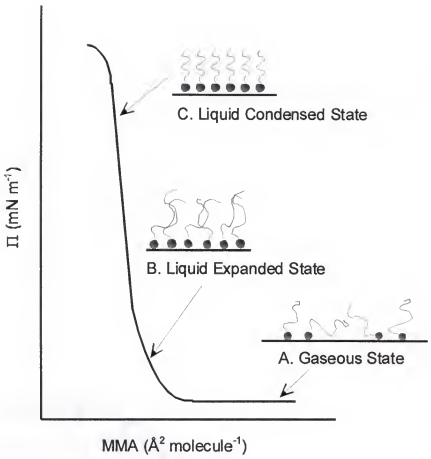

Figure 1.1: Schematic of an isotherm and corresponding monolayer behavior.

1.1.1.2 Langmuir monolayer characterization: creep and hysterisis tests and reflectance spectroscopy. Although the isotherm is very important in identifying the general behavior of a monolayer film, it does not give specific information about such things as the monolayer stability, alkyl chain orientation, or aggregation of the amphiphiles. These more specific ideas of monolayer behavior can be discerned from experiments such as creep and hysterisis tests, reflectance UV-vis, fluorescence microscopy, Brewster angle microscopy, and surface potential measurements,[23] to

name a few.[15,22] The methods applying to the films discussed in this dissertation will be described here.

Creep tests provide information on monolayer quality and can be recorded in two ways. First, the monolayer is compressed to a certain pressure and then that pressure is maintained by the barriers expanding or compressing as necessary while recording the change in area with time. Second, the monolayer is compressed to a defined area, which is maintained by stationary barriers, and the pressure is monitored over time. Stable monolayers will show a static surface pressure or little movement in the barriers after the desired pressure is reached. Unstable monolayers go through constant and sometimes drastic rearrangements, which force contraction or expansion of the barriers. For example, the hydrophobic nature of the amphiphile may be insufficient and the amphiphile may dissolve into the subphase forcing the barriers to compress to maintain Π. Also, the vapor pressure of the amphiphile may lead to their evaporation, causing the surface pressure at constant area to decrease or the barriers to move forward to hold constant pressure in proportion to the instability of the film. Alternatively, the amphiphiles may have a strong affinity for one another, leading to agglomeration and either causing an anomalous change in the surface pressure at constant area or forcing the barriers to work to maintain the surface pressure.[22]

Hysterisis studies monitor the effect of the monolayer stability on the reproducibility of the isotherm upon compression and decompression. If the amphiphiles tend to aggregate, the isotherm will not retrace its compression curve in its decompression cycle. From creep tests and hysterisis experiments, the ability of the monolayer to hold its form and to possibly be transferred can be ascertained.[24]

Reflectance UV-vis spectroscopy is used to understand the optical behavior of monolayers of chromophore-containing amphiphiles on the water surface. One method for studying the Langmuir monolayer by reflectance UV-vis involves placing

a mirror on the base of the trough and reflecting a beam through the monolayer onto this mirror, and back into a detector. These studies can help determine the onset of aggregation in films with such a tendency.[25,26]

1.1.1.3 Langmuir-Blodgett film formation. LB films are formed by vertically transferring Langmuir monolayers from the water surface onto a solid support. There are three common vertical dipping techniques, which form X, Y, and Z-type films (Figure 1.2).[15,23] In X-type LB films, a Langmuir monolayer is transferred onto a hydrophobic substrate in such a way as to maintain head to tail type interactions. In Z-type LB films, the monolayer is transferred onto a hydrophilic substrate also forming head to tail interactions. X- and Z-type films can be prepared on a specially designed trough, which allows one stroke to be made through a monolayer and the next to be made through a clean subphase. However, some amphiphiles have a preference for this type of interaction and upon regular dipping, these structures form spontaneously. Y-type multilayers are most common and can be prepared on either hydrophilic or hydrophobic substrates. Y-type multilayers are typically the most stable due to the strength of the head-head, tail-tail interactions.[15]

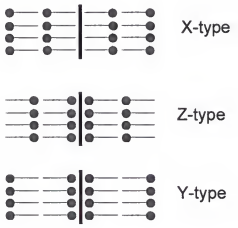

Figure 1.2: Schematic of X-, Y-, and Z-type Langmuir-Blodgett multilayers.

1.1.1.4 Langmuir-Blodgett film characterization. The quality of the transferred film is first indicated by the transfer ratio, which is a measure of the change in the area of the monolayer versus the area of the substrate coated by the monolayer. A transfer ratio of unity indicates that the monolayer is transferred with the same area per molecule that it had on the water surface. This "perfect" transfer ratio assumes that the monolayer on the water surface was stable and was not reorganizing significantly during transfer. A consistent deviation from unity could imply a change in organization upon transfer; however, if the transfer ratio is irregular, the transferred film is probably poor quality.[15]

There are many analytical techniques used to study transferred films. Film characteristics typically of interest are thickness, interlayer spacing, molecular orientation and packing, film coverage, surface topology, chemical composition, and optical and magnetic properties. The techniques used to study these parameters are well described in the literature.[20]

X-ray diffraction is a reliable technique to probe interlayer spacing, and from interlayer spacing, film thickness can be inferred. The X-rays are essentially reflected from planes of higher electron-density. The interaction of X-rays with the crystalline planes can be described by Bragg's law (Equation 1.2):

$$n\lambda = 2d\sin\theta \tag{1.2}$$

where n is an integer, λ is the wavelength of the radiation, d is the interlayer spacing, and θ is the angle of incidence and reflection of the beam.[27]

Ideally, there should be a significant difference between the electron density of the head group and that of the hydrophobic region allowing X-ray diffraction peaks to

be observed in LB films. The d-spacing, which quantifies the periodicity between planes of high electron density, therefore, is the measure of the distance between head groups. This technique is very sensitive to long-range periodicity, and many narrow 00*l* peaks are typically indicative of a well-defined layered architecture (Figure 1.3).[23]

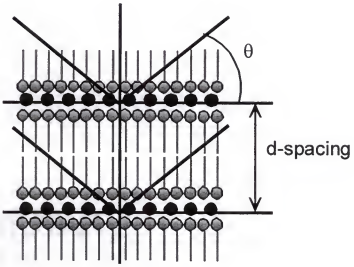

Figure 1.3 X-ray diffraction diagram.

To study the chemical make-up of the surface, attenuated total reflectance FTIR (ATR) and X-ray photoelectron spectroscopy (XPS) are employed. ATR studies involve transferring a film onto a crystal, such as parallelogram-shaped germanium or silicon crystal with ends cut at 45° angles. This is an ideal method for recording the IR spectra of films because it allows the film to be sampled many times due to the internal reflection of the IR beam through the crystal. ATR also provides information about the surface coverage and packing modes. Further, polarized studies using this technique can give information about the film organization and orientation (Figure 1.4).[15] Background information pertaining to films studied by ATR-IR, allows

elucidation of information about films containing new amphiphiles. For example, by comparing the areas of the alkyl stretches of a new amphiphile to that of well-understood fatty-acid films, an idea of the transfer quality can be obtained. This tool is particularly helpful in studying monolayers with transfer ratios varying from unity.

ATR-FTIR can also indicate the packing nature of the alkyl chains. If the chains are in a mostly *trans* configuration and close-packed, the asymmetric CH_2 stretch (ν_aCH_2) will occur at 2918 cm^{-1} and have a full width at its half maximum (FWHM) of ca. 20 cm^{-1}. The symmetric CH_2 stretch (ν_sCH_2) will occur at ca. 2852 cm^{-1}. If there are a significant number of *gauche* interactions in the chains, the ν_aCH_2 and ν_sCH_2 stretches will shift to higher energies (ca. 2924 cm^{-1} for the ν_aCH_2 and ca. 2856 cm^{-1} for the ν_aCH_2 stretches).[28,29]

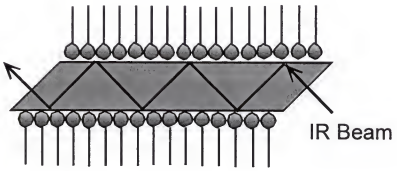

Figure 1.4: Schematic of the ATR-IR Experiment.

XPS is a method used to determine the elemental make-up, and possibly, atomic proportions within a film based on the photoelectron effect. XPS measures the energy of an expelled electron as the surface is bombarded with a monochromatic X-radiation source (Figure 1.5). When a high-energy source is applied, the kinetic energy

of the emitted electrons can be related to the excess energy and to the strength of the electron's binding by Equation 1.3, which is the Einstein photoelectric law:[27]

$$E_{kin} = h\nu - e\phi - E_b \tag{1.3}$$

where E_b is the binding energy, e is the charge of the electron, h is Planck's constant, ν is the frequency of the radiation, and ϕ is the work function corresponding to the minimum energy required for ejection of an electron.

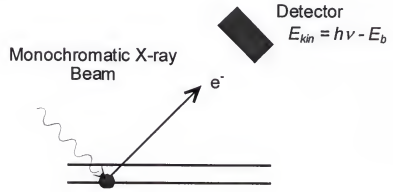

Figure 1.5: Schematic of XPS experiment.

The XPS spectrum plots electron counts versus binding energy. Binding energies are unique to each element present in the film, as well as to that element's chemical environment and oxidation state. Therefore, from a scan over a wide range of binding energies, called a survey scan, XPS results can be used to define the elements present in the sample. A more extensive scan, or a multiplex scan, over a narrow range of binding energies can clarify peak splitting, which can be assigned to a change in the chemical environment or oxidation state. Offord, et. al., in their study of a Ru-porphyrin linked to a thiol on gold SA film containing a percentage of imidazole terminated thiol surfactants, observed two peaks within the N_{1s} region of the XPS

spectrum. These two peaks were associated with the different nitrogen environments in the imidazole and porphyrin, clearly indicating that both species were present in the mixed film.[30]

The intensities of the XPS peaks can be used to determine the relative ratios of the elements present, and can indicate the type of crystalline lattice formed. However, the intensities of the XPS peaks are sensitive to many parameters such as the element's electron escape depth, which can complicate the determination of the elemental ratios. In a given sample, the observed relative peak intensities are compared to a calculated value based on Equation 1.4:

$$I_A = \frac{I_A^{\infty} \sum \exp\left[\frac{-d_m}{\lambda_{e,A}(\sin\theta)}\right]}{I_A^{\infty} \sum \exp\left[\frac{-d_m}{\lambda_{e,A}(\sin\theta)}\right] + I_B^{\infty} \sum \exp\left[\frac{-d_m}{\lambda_{e,,B}(\sin\theta)}\right] + \ldots} \qquad (1.4)$$

where I_A is the relative intensity of element A, I_A^{∞} is the atomic sensitivity factor, d_m is the overlayer thickness, θ is the incident angle of the X-ray beam, and λ_e is the inelastic mean free path. The inelastic mean free path represents the distance over which 60% of the electrons can travel before inter-electron collisions lead to a loss of energy[31] and is defined by:[32]

$$\lambda_e = 10[49/(E_{kin}{}^2) + 0.11(E_{kin})^{0.5}] \text{ (Å)} \qquad (1.5)$$

UV-vis spectroscopy reveals a film's optical behavior. Typically, films are transferred onto glass or quartz substrates and transmittance studies are performed.

Using polarizers and stages that allow careful placement of the substrates at different angles of incidence to the beam, the orientation of the chromophores within the films can be determined. By comparing the absorbance intensity in the s- and p-polarization, a dichroic ratio can be calculated using Equation 1.6:

$$D = \frac{A_s}{A_p} \tag{1.6}$$

Orientational order within the plane of the film and substrate is obtained by looking at results from 0° and 90° (s and p) polarization as the beam is normal to the surface (0° angle of incidence). Studying the polarization at higher angles of incidence (typically 45°) enables the determination of the orientation out of the plane (Figure 1.6).

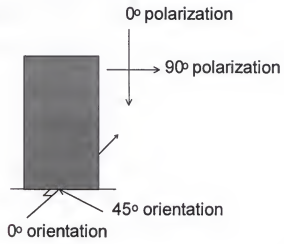

Figure 1.6: Schematic of polarized UV-vis experimental beam directions.

The dichroic ratio can be used to determine the chromophore orientation in a film. In the case of films containing porphyrin chromophores, Orrit et al. determined that the dichroic ratio can be translated into an orientation parameter (P) using the graph shown in Figure 1.7,[25] and hence, an orientation angle (θ) can be established using Equation 1.7:

$$P = \langle \cos^2 \theta \rangle \tag{1.7}$$

θ represents the angel between the surface normal and the chromophore's molecular plane. As is often observed within the plane of a film containing porphyrins, if D is unity, there is no preferred orientation. If D = 1.5, P = 0 and therefore, θ = 90° as measured from the surface normal.

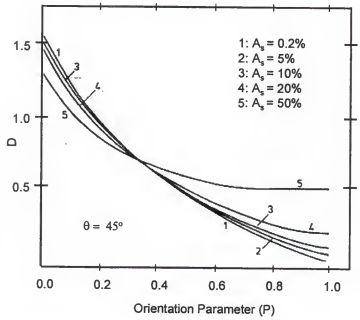

Figure 1.7: Behavior of the oblique dichroic ratio versus an orientation parameter (P).[25]

Porphyrin containing films often have oblique dichroic ratios of approximately 1.5, corresponding to the chromophores lying parallel to the substrate. For example, Zhang et al., obtained such a result in LB films containing a free base tetraphenyl porphyrin either pure or mixed with stearic acid, where the porphyrin was the hydrophilic head group with long alkyl substituents.[33]

1.1.2. Self-Assembled Films

Zisman introduced SAMs to the literature little more than 50 years ago. His studies involved self-assembling long-chained alcohols onto a glass surface using hexadecane as the inert solvent.[18] This study showed that films prepared in this manner had wetting properties similar to those seen in films prepared by the LB technique.

Sagiv et al. studied octadecyltrichlorosilane (OTS) on hydroxylated surfaces, such as glass, to form a siloxane polymer. Multilayers were produced if the amphiphile was terminated at both α and ω positions by surface-active groups.[15,34] When α and ω positions were two different functionalities, subsequent dipping in self-assembly solutions produced non-centrosymmetric films. Unfortunately, studies have shown that small defects in the early layers can magnify upon multilayer formation such that nearly all order breaks down by the tenth layer.[20] The SA of OTS is now commonly used for hydrophobisizing glass slides for LB substrates.

The chemisorption of thiols on gold was initiated by Nuzzo and Allara[35] and continued by Porter,[36] Whitesides,[37] and others. Alkyl thiols, in which the chain lengths range from one carbon to over twenty, have been studied. Closely packed layers were observed when the chain length exceeded eleven carbons.[36] The gold surface used in these studies was formed by vacuum evaporation onto cleaved alkali-

metal halide surfaces.[37] Many of the surfactants studied by self-assembly did not form stable monolayers on aqueous subphases, and therefore, could not be studied by the LB method. However, these surfactants were easily studied by the SA method.

1.2. Hybrid Organic/Inorganic Ultrathin Films Based on Layered Solids

1.2.1. Background

A new class of LB films has been developed, which incorporate an inorganic metal phosphonate network into the polar region.[28,38-41] These films, which can contain a variety of organic groups and metals, were inspired by and show analogous behavior to their solid-state metal phosphonate analogues. In addition, these films are more stable than typical fatty-acid based LB films, and the inorganic lattice provides potential function.[42]

The metal phosphonate solid-state materials are attractive because they can be prepared at low temperatures from aqueous solutions. Further, the structures can provide a model system to which the film properties can be compared. Due to the structure of the metal lattices, which directs the film formation, the orientation and packing of the alkyl region is predictable.

Metal phosphonate materials are especially interesting due to their potential applications in the areas of sorbents[43] and catalysts,[44] and because of their layered structures, these materials can be used as intercalation compounds.[45-49] The interest in the metal phosphonates was sparked by their potential as inorganic ion exchange materials;[50-52] however, the organic region can also be modified and functionalized, providing a straightforward method for preparing a wide variety of materials.

1.2.1.1. Zirconium Phosphonate solids. Clearfield published early work on metal phosphonates and phosphates in the 1960's.[53] The focus at this time was on the zirconium solids which form two preferred phases, α and γ, which have the compositions $Zr(HPO_4)_2 \cdot H_2O$ and $Zr(PO_4)(H_2PO_4) \cdot 2H_2O$, respectively. In these layered materials, a two-dimensional metal lattice is formed and separated from an adjacent metal lattice by the organic layer in the phosphonates or by the hydrogen bonds from the fourth hydroxy site in the phosphates. The interlayer area in these solids forms a possible domain for intercalation of inorganic materials such as amines.[53]

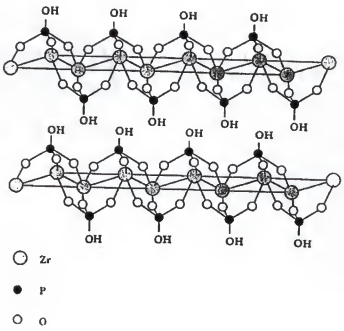

Figure 1.8: Crystal structure of zirconium phosphate.[53]

The crystal structure of the Zr-phenylphosphonate solid was determined in the 1980's and found to form a structure similar to the α-phase. Subsequent studies revealed that any alkyl or aryl group whose area was under 24 $Å^2$ would form an identical metal lattice structure while only the interlayer distance changed. In the n-

alkyl phosphonates, it was found that there is a tilt angle in the chains of between 55° and 60°. This tilt allows for maximization of the van der Waals forces between the chains even within the solid-state materials. Though the structures formed are dictated by the geometry of the inorganic lattice, the hydrophobic region does rearrange to balance these strong forces with the maximization of their overlap.[53] A change in the organic group can lead to very different structures and properties of the solids. Bulkier groups may form new crystal structures or have three-dimensional metal lattice formation. Also, the different organic groups can impart different function to the films.

1.2.1.2. Divalent and trivalent metal phosphonate solids. After extensive research on the zirconium phosphonate solids, interest branched to divalent and trivalent metal phosphonates. The poor solubility of the zirconium phosphonate solids in most standard solvents meant achieving single crystals was difficult; therefore, most of the crystal structure data was achieved from powder X-ray diffraction patterns. However, di- and trivalent metals tend to be soluble in acidic solutions, allowing single crystals to be obtained by slowly changing the solvent pH or the metal ion concentration.

Metal phosphonate materials have been prepared with a variety of different divalent metals such as Mg^{2+}, Mn^{2+}, Zn^{2+}, Ca^{2+}, and Cd^{2+}.[54-56] From the crystal structures, it was determined that the composition of the divalent series metal phosphonates is $M^{II}(O_3PR)\cdot H_2O$ for Mg, Mn, Zn, Ca and Cd. In these materials, layers of the metal atoms are octahedrally coordinated by five phosphonate oxygens and one water molecule, with each phosphonate group coordinating four metal atoms making a cross-linked M-O network. A second structure, the orthorhombic $M^{II}(HO_3PR)_2$, was observed for the Ca phosphonates. A structural exception to the

above divalent series is Cu(II).[48,57] The Cu atoms in these phosphonate materials are five coordinate and form a distorted tetragonal pyramidal geometry.

Mallouk has prepared a series of lanthanide phosphonates. The structure of these materials is given as $Ln(III)H(O_3PR)_2$, where Ln represents La, Sm, or Ce. The lanthanide-series phosphonates are more soluble than the zirconium solids, but less soluble than the divalent materials. Therefore, single crystal data was not easily obtained.[58,59]

ATR-IR provides a facile method for characterization of the metal phosphonate lattice formation. Vibrational modes assigned to the phosphonate are extremely sensitive to the mode of metal binding. Thomas et al. have assigned the $\nu_a(CH_2)$ vibrational frequencies for the divalent metal-phosphonates to be in the range of ca. 1050 - 1100 cm^{-1} where the $\nu_s(CH_2)$ stretches occur ca. 970 - 990 cm^{-1}.[60] Each metal phosphonate material has characteristic stretches in these regions.

1.2.2. Self-Assembled Films Incorporating Metal Phosphonate Binding

After Sagiv's work with self-assembling films of octadecyltrichlorosilane (OTS), it seemed a natural step to translate the formation of the thermodynamically stable and insoluble layered metal phosphonate solids into ultrathin films. Self-assembly was the first technique employed to produce metal phosphonate thin films. Mallouk and coworkers formed the metal phosphonate self-assembled films by first, exposing a silicon or gold surface to an appropriate template forming alkyl-mercaptan that was substituted with a terminal phosphonic acid.[61,62] This phosphonic acid was active toward the metal salt solution in which the substrate was then dipped. After metallating the surface, the substrate was dipped in a solution of an α, ω-bisphosphonic acid, which left another phosphonic acid on the surface to be

subsequently metallated, and the cycle continued until multilayered films were fabricated.

The self-assembly of metal phosphonate films is made possible by a very strong attraction between certain metal ions, particularly the tetravalent metals such as Zr^{4+}, for the phosphonate groups of alkyl phosphonic acids.[61-63] However, the individual metal salts and the phosphonate are themselves soluble. This particular affinity between metal and phosphonate, makes possible the formation of monomolecular layers during each step of the cycle and the ability to assemble controlled multilayers.

1.2.3. Metal Phosphonate Langmuir-Blodgett Films

Two methods of film formation have been employed to incorporate the metal phosphonate lattice into the polar region of LB films, one for the divalent and trivalent metals which are soluble in acidic media, and one for the tetravalent and some trivalent metals which are insoluble even at low pH. A schematic comparing traditional LB films to metal-phosphonate LB films is shown in Figure 1.9.

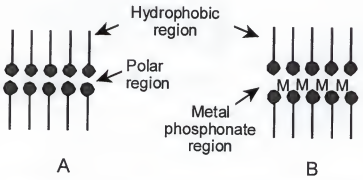

Figure 1.9: Comparison between A) traditional LB films and B) metal-phosphonate LB films.

The zirconium metals have such a high oxophilicity for the phosphonate oxygens, that when a phosphonic acid amphiphile is spread on the surface of a zirconium cation containing aqueous subphase, the monolayer crystallizes before it can be transferred. Therefore, a three-step deposition procedure has been developed. A phosphonic acid containing monolayer is formed on the surface of a pure water subphase and transferred onto a hydrophobic substrate. Onto this phosphonic acid surface, a layer of zirconium is assembled, followed by the transfer of a second LB monolayer containing a phosphonic acid. This three-step deposition technique will be described in detail in Chapter 2.[28,38]

Advantages of this three-step technique include the fact that at the hydrophilic stage, the monolayer is stable and can be independently characterized by ATR-FTIR or XPS, etc. Second, this method allows the formation of alternating films in which the template and capping layers do not have to be formed of the same amphiphile. The option of forming alternating films is important because some amphiphiles do not transfer on the down stroke but will transfer onto an ODPA template layer. A disadvantage of the three-step deposition of the phosphonate films occurs at the self-assembly of the zirconium lattice. The self-assembly of the zirconium onto the ODPA template causes the metal phosphonate lattice to be amorphous, whereas in a one-step deposition, the metal lattice is crystalline.

An alternative technique of film formation is employed for the divalent and trivalent metals.[41] In these cases, the metal salts are dissolved in the aqueous subphase, the phosphonic acid monolayer is formed on the surface, and the hydrophobic substrate is dipped down and then up through the same compressed monolayer forming a complete metal-phosphonate layer or an LB bilayer. The crystallization of the metal-phosphonate lattice occurs on the slow upstroke of the film through the monolayer (Figure 1.10).

In the one-step method, the pH of the subphase is as crucial to successful lattice formation as it is in the formation of the solids in aqueous solutions. If the pH is too high, the affinity of the metals for the deprotonated phosphonates will be too high and crystallization of the lattice will occur in the Langmuir monolayer rather than upon transfer. As with the zirconium films, these films will be too rigid to be successfully transferred.

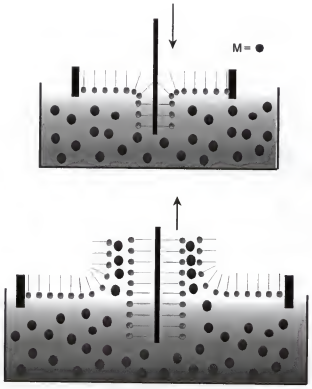

Figure 1.10: Schematic of formation of divalent or trivalent metal phosphonate films.

If the pH is too low, the phosphonate will remain completely protonated, and the films will transfer without metal binding. Fortunately, the pH effects on the crystallization of the monolayer have signatures in the isotherm behavior.[64] When the pH is too high, the rigid monolayer gives an erroneous but characteristic isotherm that has a much

higher onset and shallower incline. We believe this isotherm behavior is due to the rigid films causing deflections in the Wilhelmy balance rather than showing an increase in surface pressure.

1.2.4. Dual-Function Langmuir-Blodgett Films

After the extensive characterization of simple alkyl metal phosphonate LB films, there was interest in incorporating function into the organic region that might be paired with properties in the inorganic lattice to form a "dual function" LB film. As models, phenoxy and biphenoxy alkyl phosphonic acids were prepared, and divalent, trivalent, and tetravalent metal phosphonate films were studied. [65,66] Additionally, films containing azobenzene-derivatized phosphonic acid amphiphiles were synthesized, and metal phosphonate films were formed also with divalent, trivalent, and tetravalent metals.[67] These results prove that larger organic groups can be incorporated into the metal phosphonate LB films while maintaining the integrity of the inorganic lattice structure.

Potential applications of dual functional metal-phosphonate thin films include magnetic switches, in which the magnetic behavior of the inorganic lattice can be altered by a structural change in the organic region. Also, films containing a conductive or non-linear optic organic region as well as a magnetic inorganic lattice could act as a sensor. This dissertation will focus on the preparation of porphyrin containing zirconium phosphonate films where the metal phosphonate lattice acts to stabilize the films toward potential catalytic reaction conditions.

1.3 Background on Porphyrins

1.3.1 Optical Behavior of Porphyrins

Porphyrins are a common research focus in physics, chemistry, and biology. Physical and chemical interest in porphyrins stems, for example, from their highly conjugated structure that allows facile electron-transfer,[68-72] and from their chemical activity at an exposed metal that may be active toward catalysis or chemical sensing.[1,8,73-75] Biologists and biochemists are interested in the common biological building blocks that are based on the porphyrin structure.[76-78]

The core structure of the porphyrin is the completely saturated porphine macrocycle (Figure 1.11).[79] Upon reducing this macrocycle to the unsaturated form, the porphyrin chromophore is achieved. By hydrolyzing one of the pyrrole units, the chlorin compound is prepared. Another important structure based on the porphine core is the phthalocyanine or the tetraazatetrabenzporphyrin. Each of these structures includes either two protons, as in the free base porphyrin, or a coordinated metal within the center of the porphyrin, called the metallo-porphyrin. Examples of biologically active porphyrins include chlorophyll, which is a manganese-coordinated chlorin molecule, and heme, which is an iron-substituted porphyrin.

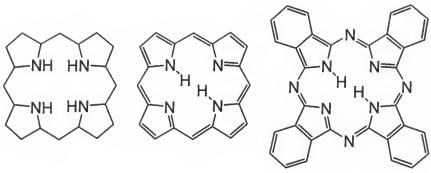

Figure 1.11: Structures of porphyrin-type molecules A) porphine B) free base porphyrin, and C) pthalocyanine.

Porphyrins have characteristic and strong optical transitions by which they can be identified. The bands often observed in visible spectra of porphyrins include the B or Soret Band and Q Bands, as seen in Figure 1.12 for a palladium tetraphenylporphyrin (PdTPP). The Soret Band is associated with the allowed $\pi - \pi^*$ transition and is typically seen between 380 and 420 nm.[80]

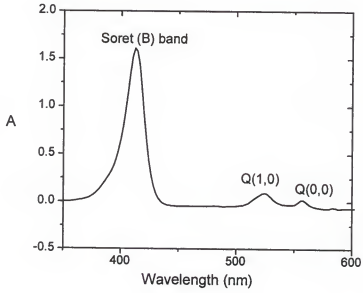

Figure 1.12: UV-vis spectrum of a metallo-porphyrin (PdTPP).

The Q-Bands are observed between 500 and 600 nm. The lower energy Q-Band (Q_α) is associated with the electronic origin, Q(0,0) of the lower energy singlet excited state. The higher energy Q-Band (Q_β) has a contribution from a vibration mode and is denoted Q(1,0). Both Q(0,0) and Q(1,0) are quasi-allowed transitions with relatively low absorbance intentisties. The Q-Bands are highly sensitive to the symmetry of the molecule. In porphyrins of D_{4h} symmetry such as metalloporphyrins, or the diacidic or dibasic forms of the porphyrin, two Q Bands are observed as pictured in Figure 1.12. The free-base porphyrin is of D_{2h} symmetry and the degeneracy of the Q-Bands is disrupted, splitting the Q-Bands into four peaks.[80]

The above described transitions are due to the porphyrin π-electrons and are $\pi-\pi^*$ in nature. If these transitions are unperturbed by the central substituent, the

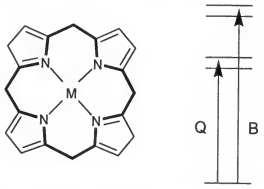

Figure 1.13: Outline of 16-member principal resonance structure of metallo-porphyrin.

porphyrin is classified as "regular". Similarly, the emission spectra of regular porphyrins are determined solely by the chromophore itself. The above explanation of the UV-visible behavior of porphyrins is based on the free-electron model, in which the core of the porphyrin, the 16-member heterocyclic, conjugated ring behaves like a free-electron wire (Figure 1.13). Another popular theory is Gouterman's four-orbital

model (Figure 1.14), which combines the Hückel-MO theory with the free-electron model. In this model, Gouterman describes four orbitals, two LUMOs, $c_1(e_g)$ and c_2 (e_g) each with five nodes, which are degenerate in energy, and two HOMOs, $b_1(a_{2u})$ and $b_2(a_{1u})$, each with four nodes, which are not degenerate. According to the four orbital model, the Soret Band corresponds to the transition from the lower energy a_{1u} orbital to the e_g orbital, giving a higher energy transition. The Q-Bands arise from the transition from the a_{2u} orbital, which is higher in energy giving a lower energy transition.[25,80]

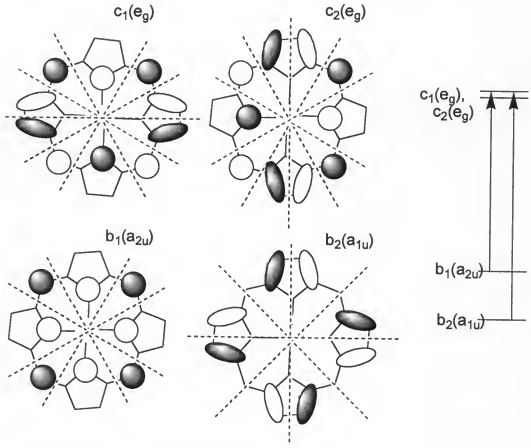

Figure 1.14: Gouterman's four-orbital model.

However, there are also "irregular" porphyrins. Irregular porphyrins, typically metalloporphyrins, are broken down into categories called hypso- and hyper-porphyrins. In the case of irregular porphyrins, the central metal contains partially filled shells, which introduce a possibility of metal electrons mixing with porphyrin π-electrons. This mixing is caused by the possibility of metal to porphyrin back-binding due to similar energies of the metals d-orbitals and the porphyrin's π-orbitals. The central metal ion can lead to significant changes in the optical and emission spectra. The metal and its oxidation state determine which category the porphyrin's optical behavior will fall into. Also, the release of electron density from the metal to the porphyrin enables the metal to stay co-planar with the chromophore as the effective size of the metal is reduced.[79]

Hypsoporphyrins have central metals of groups eight through eleven with configurations d^m where m = 6 - 9 and have filled $e_g(d\pi)$ orbitals. The inclusion of these metal ions is often associated with a bathochromic or blue shift relative to the corresponding free base porphyrin. Common hypsoporphyrins include Ni(II), Pd(II), and Pt(II)-porphyrins. The Ni(II) porphyrins are easily affected by basic axial ligands, whereas Pd(II) and Pt(II) are typically four coordinate and appear insensitive to the potential ligand environment [80,81]

The second class of irregular porphyrins is called the hyperporphyrins, which is further broken down into subclasses called p-type, d-type, and pseudonormal hyperporphyrins. Most metallo-porphyrins classified as hyperporphyrins have central metals with easily accessible lower oxidation states. Of these, Mn(III) and Fe(III) are the most well studied due to their biological implications. The spectra of hyperporphyrins exhibit the Soret and Q-Bands as before with some possible shifting. Additional prominent absorption bands may be seen typically at higher energies relative to the Soret Band. The hyperporphyrin spectra demonstrate the effects due to

metal-ligand charge transfer (MLCT) mixed with the porphyrin $\pi-\pi^*$ transitions even within the Soret Band. The MLCT Bands can be porphyrin to metal, metal to porphyrin, or even axial ligand to metal. Due to the spectral sensitivity to chromophore substituents, to the metal its oxidation state, and to the nature of the axial ligand, and the additional UV-vis Bands, hyperporphyrin spectra are much more difficult to analyze.[80,81]

The d-type hyperporphyrins include metals of groups six through eight. Mn(III)-porphyrin, for example, is d^4 and $S = 2$, or high-spin, and is a characteristic d-type porphyrin. In chloroform, Mn(III) tetraphenylporphyrin shows six peaks. An early researcher of the Mn-porphyrins, Boucher, termed these peaks by Roman numerals going from low to high energy. The first two peaks are in the far-red region between 800 and 650 nm. Bands III and IV absorb in a region similar to the Q-Bands in regular porphyrins, between 500 and 650 nm. Band V is similar to and often called the Soret Band though this band now includes contributions from metal to ligand mixing. Band VI is typically around 350 nm. The ratio of Bands V and VI is very sensitive to axial ligands and ring substituents. These bands are due to porphyrin to metal charge transfer $a_{1u}(\pi)$, $a_{2u}(\pi)$ to $e_g(d\pi)$, which implies a necessity for one or more vacancies in the $e_g(d\pi)$ orbital of the metal and reduction potentials which are not too negative.[80,81]

Finally, pseudonormal hyperporphyrins include VO(IV), Cr(II), Mn(II), Mo(IV), La and Ac where $S \neq 0$. These metals show normal absorption spectra with a weak extra absorption possible in the far-red region. All of these metals have a partially filled or empty $e_g(d\pi)$ orbital, but charge-transfers from the porphyrin to the metal are too high in energy to be observed in the UV-vis region. In addition, further reduction takes these metals to unstable oxidation states which makes this an even higher energy transition and highly unlikely [80,81]

In addition to intramolecular effects such as the metal, substituents, and axial ligands, intermolecular effects such as aggregation can significantly alter the electronic behavior of porphyrins. Aggregation in these chromophores has been described thoroughly by Kasha's exciton theory. This theory looks at aggregation only from the point of view of overlapping transition dipole moments (Figure 1.15) and not as interacting π-systems. In metallo-porphyrins, the transition dipole moments are equivalent due to the symmetry of the chromophore.[76,82,83]

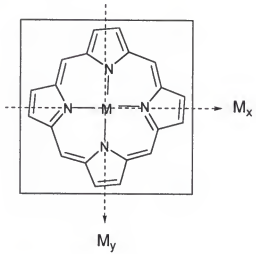

Figure 1.15: Transition dipole moments in metallo-porphyrin.

Aggregation, according to Kasha's model, splits the excitation energy of the monomer (E^o) into high and low energy components. Equation 1.8 describes the energy dependence on aggregation by:

$$E^{\pm} = E^{o} + D \pm V \tag{1.8}$$

where D is the dispersion energy which is highly dependent on the change in environment upon aggregation, and V is the exciton splitting energy. [76,83,84]

When the chromophores are interacting with the transition dipole moments parallel, the exciton energy can be described by Equation 1.9:

$$V = \left\langle \left(\frac{N-1}{N} \right) \frac{M^2}{R^3} \left(1 - \cos^2 \alpha \right) \right\rangle \tag{1.9}$$

where M is the transition dipole moment, R is the center-to-center distance, N is the number of chromophores, and α is the angle between R and M (Figure 1.16). So, if $\alpha < 54.7°$, V will be positive, and the exciton splitting will be greater and a red shift will be observed as the transition shifts to lower energy. A red shift is observed in what are called J-aggregates where both M_x and M_y make angles less than 54.7° with the R vector. If $\alpha > 54.7°$, V will be negative, and the exciton splitting energy will be lower leading to a blue shift in the spectrum. When M_x and M_y are both greater than 54.7° from R, the aggregates are termed H-type. If $\alpha_x < 54.7°$ and $\alpha_y > 54.7°$, the spectral components will split and part of the band will shift red and part will shift blue; this spectral behavior is seen in edge-to-edge type aggregates. There can be combinations and varying degrees of these types of interactions within an aggregated domain possibly leading to complicated spectra, but in general, the optical spectra ease identification of electronic behavior of porphyrin chromophores (Figure 1.16). [76,83,84]

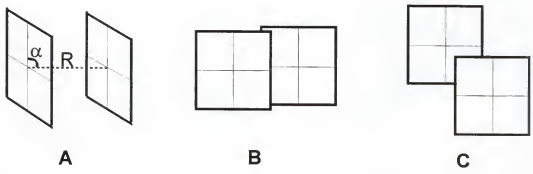

Figure 1.16: Porphyrin chromophore interactions: The square represents the chromophore and its disecting axes. A) H-type or face-to-face aggregates; B) edge-to-edge aggregates; C) J-type or head-to-tail aggregates.

The transition dipoles M_x and M_y are typically parallel to the plane of the chromophore except when the nature of the metal in the chromophore center causes a puckering of the ring. Therefore, polarized UV-vis experiments can easily indicate orientational changes of the chromophore within a film (Figure 1.16).[76,83,84]

Incorporation of porphyrins into LB films is currently of interest in scientific literature. These films are designed in order to prepare selective gas-sensors,[1,74,75] photovoltaic devices,[85] electron-transfer materials,[72,86] molecular wires,[87] and novel heterogeneous catalyst systems.[88] However, a difficulty arises in the stability of the samples using the "typical" LB methods of purely hydrophilic/hydrophobic interactions or by self-assembly involving tethering through a ligand. Including a metal-phosphonate lattice into these films should significantly improve the stability and the applicability of these materials in ultra-thin, organized films.

Typically, LB films containing porphyrin constituents have been studied in which the chromophore itself is the polar head group. These porphyrin films have been successfully prepared with either the molecule sufficiently diluted with a film stabilizing amphiphile,[33,88-90] such as stearic acid, or with long hydrophobic chains

attached to the chromophore to stabilize the monolayer on the water surface.[84,91] There are significant disadvantages to this method of film preparation. First, the chromophore is buried in the film interior on a transfer onto a hydrophilic substrate, and commonly, the hydrophobic interactions necessary to deposit onto a hydrophobic substrate are too weak for successful transfer. Also, the hydrophilic interactions are typically of a hydrogen-binding nature making this a relatively weak interaction destabilizing the film. Finally, the conditions necessary for transferring the traditional porphyrin LB films facilitate aggregate formation, which can be detrimental in certain applications, such as catalysis.

The aggregation, or chromophore π–π interactions, is often a consequence of the film forming procedures. First, compression of the film on the water surface forces the eventual overlap or tilting of the chromophores.[84,88,90] Also, the decreased affinity of the derivatized chromophores for water tends to force the chromophores to aggregate rather than to spread on the water surface.[92] Understanding the molecular orientation, aggregation, and morphology of porphyrin LB films is critical because each is intimately linked to chromophore behavior. For example, aggregation can significantly reduce or eliminate the efficiency of the porphyrin in catalysis[76] or the ability of the porphyrin to bind probe molecules in a sensor.[92] Therefore, it is desirable to find methods for forming porphyrin LB films with no aggregation.

1.3.2. Background on Manganese Porphyrins

Biomimetic systems involving porphyrin catalysts have often been discussed in scientific literature over the past 20 years. Manganese and iron porphyrins are commonly studied oxidation catalysts and are prevalent elements in biological processes.[93-96] Biochemical oxidation reactions employing metallo-porphyrins involve reversible site-specific binding of the substrate such that the substrate is within

reach of the oxygen atom on the metal. After the oxygen has been successfully transferred to the substrate, the product is released and the catalyst is regenerated.[93]

Manganese porphyrins are probably most well known as epoxidation and hydroxylation catalysts whether under heterogeneous or homogeneous conditions. The manganese porphyrin catalysts can utilize a number of different oxidants such as iodosylarenes, alkylhydroperoxides, hydrogen peroxides, and perchlorates among others, in order to accomplish the facile oxidation of deactivated olefins, alkanes, alcohols, ethers, and amines.[97-100] A hyper-valent metal-oxo species is believed to be the active intermediate in the oxidation process in cases such as dioxygen activation of Cytochrome P-450, or in oxygen transfer from iodosylbenzene, peracids, or hypochlorite oxidants.[101] Though there is some debate on the actual mechanism of the epoxidation, there are a few possible routes (Figure 1.17). The suggested first and rate-determining step is the formation of a charge-transfer complex. Whether the reaction then proceeds through epoxidation or rearrangement is dependent on the oxidation potentials of the alkenes and the oxidants, steric and electronic structures of the reactants, and the ability of the substrates to undergo rearrangement.[97]

Porphyrins have also been studied in chiral catalysis. Lai and co-workers studied the asymmetric aziridation of alkenes using a chiral manganese porphyrin catalyst.[102] They found that with bulky chiral substituents on the porphyrin, successful nitrene transfer to alkenes was achieved. Enantiomeric excess ranging from 43 to 68% and product yields greater than 70% were obtained. In these catalysis studies, the reactive intermediate was a Mn(IV) complex.

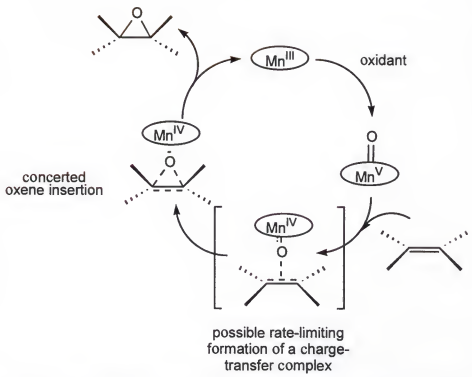

Figure 1.17: Suggested mechanism of olefin epoxidation catalyzed by MnTPP.

1.3.3. Immobilization of Porphyrins

The ability of porphyrins to efficiently catalyze both the epoxidation of olefins and the hydroxylation of alkanes unfortunately leaves the porphyrin and its superstructure vulnerable as potential substrates. However, nature has developed mechanisms to eliminate these unwanted complications. For example, an enzyme and its cofactors may form metal-oxo complexes only when the substrate molecule is confined within an enzymatic cavity. Also, the tertiary protein structure prevents the active porphyrin catalyst from approaching other potentially oxidizable metalloporphyrins, and it makes the structure rigid, protecting the amino acid backbone and the side-chains from intermolecular oxidation by contacting the active site. These biosystems are difficult to mimic in the laboratory; however, successful

biomimetic catalysts have been prepared with bulky, rigid groups substituted on the porphyrin chromophore.[101]

One alternative solution to the problem of internal oxidation or intermolecular oxidative destruction of the porphyrin catalyst is immobilization of the chromophore. Immobilization involves tethering the porphyrin to a surface such as a film,[88] an inorganic solid particle,[103-106] a polymer,[107,108] a membrane,[109] or a resin.[110] Immobilized porphyrins as biomimetics and as heterogeneous catalysts have been well explored in the past several years.[104-106,110] Tethering of porphyrins to a solid support can not only reduce or eliminate oxidative destruction of the active catalyst, but can also aid in the catalyst recovery after the reaction is completed.

Heterocyclic ligands are commonly used as the link between the porphyrin and surface in many immobilized porphyrin systems.[94,98,111] Unfortunately, binding the metallo-porphyrin to the imidazole allows little control over the porphyrin orientation in the films. Additionally, in these circumstances, there is no chemical connection between the porphyrin and the surface other than the ligand, which leaves the porphyrin vulnerable to removal from the surface by ligand displacement, changing the reaction conditions.[30,94,98,111] An alternative method for tethering the porphyrins to surfaces has been established, which uses four alkyl phosphonic acid substituents that can be attached to a zirconium phosphonate network making a very stable catalytic film.

1.3.4 Heterocyclic Ligand Cocatalysts

1.3.4.1. Ligand activation of the porphyrin catalyst. Heterocyclic ligands are well documented in the literature as activating Fe(III) and Mn(III) porphyrins for catalysis with oxidants such as alkyl or hydrogen peroxides.[94,98,99] Porphyrins

immobilized on an ion-exchange resin support showed significant increases in catalytic activity in the presence of either imidazole or 4-methylimidazole. With the heterocyclic ligand present, nearly quantitative conversion of cyclooctene to cyclooctene oxide was achieved, relative to only 5% conversion in the absence of imidazole over the same time period.[112] Likewise, Arasasingham et al. found a 4 to 10 fold increase in the rate of the reaction between a manganese porphyrin and an oxygen source commonly used in olefin epoxidation reactions, t-BuOOH, in the presence of imidazole. Since the oxidation of the porphyrin accelerates, a rate increase should also be observed in the overall epoxidation reaction.[98]

According to Yuan and Bruice, the reaction of the Mn(III)TPP Cl complexes with peroxide oxidants only proceeds in the presence of a heterocyclic nitrogen base ligand such as imidazole or pyridine. The imidazole ligation was pH dependent and was evident only above pH 5. Consequently, the enhanced oxidation rate was also pH dependent. Further, with common oxidants, nitrogen base ligation led to a significant increase in the oxygen transfer rate.[111]

The rate increase could be due to a general-base catalysis and/or ligation of the imidazole (ImH) to the manganese ion.[98] Activation by ligation of ImH is supported by the fact that when 2,4,6-trimethyl-pyridine is used as the base, which is sterically forbidden from porphyrin ligation, no increase in the reaction rate was observed. However, when the ImH concentration was below a saturation level, the rate increase was linear with ImH concentration up to a saturation level. An increase in the oxidation rate with a basic ligand is likely due to the increase in the electron density at the metal center arising from donation of the lone pair of electrons from the ImH.[98] The presence of the ImH as an axial ligand has been shown also to stabilize the metal-oxo compound.[99]

1.3.4.2. Spectral evidence of axial ligand. ImH to porphyrin binding should be apparent in the UV-vis spectra. The formation of a bis-imidazole Mn(III)TPP Cl complex was demonstrated by a broadening shift in the Soret Band from 478 nm for the pure porphyrin to 472 nm.[111] Interestingly, the equilibrium constants for the formation of the mono- and bis-ligated imidazole-porphyrin complexes are similar and their absorption spectra are nearly identical. Therefore, at high concentrations of imidazole in solution, it is possible that the observed spectra arise from the formation of bis-imidazole complexes.[111,113] However, the preferred formation of the mono- vs. bis-imidazole complexes has caused some disagreement, and some authors claim that even at saturated concentrations of imidazole, the principal component is the mono-imidazole only.[114]

In the UV-vis of the Mn-porphyrin, the Soret Band of the Mn-porphyrins is the most sensitive to the axial ligand. The change in the Soret energy is due to the charge induced on the porphyrin chromophore through the metal. Electron-donating axial ligands induce negative charge on the macrocycle, separating the bonding and anti-bonding orbitals of the porphyrin, and increasing the transition energy.[115] Hard anions, whose binding is strengthened by increased ionic character of the central metal, prefer localization of positive charge on the metal, which leaves the chromophore with more negative charge.[115] Similarly, as a basic ligand takes on more hard base character, the λ_{max} will shift to higher energies.

1.4 Dissertation Overview

The overall goal of this dissertation was to prepare zirconium phosphonate thin films by both the SA and LB technique that contained catalytic Mn-porphyrins. The purposes of the zirconium phosphonate network were to stablize the manganese

containing films to reaction conditions and to allow these films to be recycled in a number of catalytic studies. Chapter 2 is an overview of the experimental techniques used to prepare and characterize the films described in this dissertation, and materials and instrumentation used in this pursuit are also presented.

Films containing a Pd-tetraphenyl porphyrin were prepared to develop film preparation procedures and to better analyze the UV-vis properties of porphyrin containing films. Substituted tetraphenyl porphyrins, palladium 5,10,15,20-tetrakis(2,3,5,6-tetrafluorophenyl-4-octadecyloxyphosphonic acid)porphyrin (PdP4) and palladium 5,10,15-tris(2,6-dichlorophenyl)-20- (2,3,5,6-tetrafluorophenyl-4-octadecyloxyphosphonic acid)porphyrin (PdP1), have been studied as Langmuir monolayers and as zirconium phosphonate LB and SA films.

Films were prepared incorporating the pure porphyrins and the porphyrins mixed with octadecylphosphonic acid (ODPA). The Langmuir monolayers were characterized with pressure vs. area isotherms and reflectance UV-vis spectroscopy. Using a three-step deposition technique, symmetric and alternating zirconium phosphonate bilayers and multilayers were prepared by the LB technique. PdP4 containing films were also prepared by the SA technique. In all PdP1 and PdP4 films, the porphyrin constituent resided in the hydrophobic region of the monolayer and the phosphonate substituents bound zirconium ions in the hydrophilic region.

LB and SA films were studied with transmittance UV-vis and the LB films were further investigated using X-ray diffraction. Control over chromophore interaction was achieved by chemical modification of the amphiphiles and by selection of appropriate transfer conditions. For example, reduced aggregation was seen in LB films of the tetraphosphonic acid substituted porphyrin PdP4 transferred at mean molecular areas (MMA) larger than the area per molecule of the substituted porphyrin and in SA films. In these films, the porphyrin macrocycles are non-aggregated and

oriented parallel to the surface. In contrast, the monophosphonic acid substituted PdP1 aggregates under all of the deposition conditions studied.

Stability of the Pd-porphyrin LB and SA films was examined by exposing the films to refluxing chloroform. UV-vis absorbance after immersion in chloroform confirmed conclusions that in films of PdP1, many of the chromophores are not tethered to the inorganic network and are easily removed, whereas in films of PdP4, all molecules bind to the zirconium phosphonate extended network making these films very resilient.

Study of the Pd-porphyrins led to significant understanding of the behavior of tetra- and mono-phosphonic acid porphyrins in LB films. Chapter 3 describes the results of these studies, which were the first to show incorporation of porphyrins at the exterior of metal-lattice containing films.

Manganese tetraphenyl porphyrins are well known epoxidation catalysts,[97,99,116] and the incorporation of these catalysts into zirconium phosphonate films should improve their catalytic efficiency as well as their stability and recoverability. Films containing manganese 5,10,15,20-tetrakis(2,3,5,6-tetrafluorophenyl-4-octadecyloxyphosphonic acid)porphyrin (MnP4) have been prepared using the LB and SA techniques. The formation of these films involved modifying traditional LB procedures with SA techniques, which is possible with the use of zirconium phosphonate networks. From Langmuir monolayer and LB studies of the pure tetraphosphonic acid porphyrin, it appears that the MnP4 amphiphiles tend to form face-to-face aggregates, or H-aggregates, when assembled at the air-water interface, and this aggregation is translated into the transferred films. Attenuated total reflectance (ATR) IR, UV-vis, XPS and stability studies confirm the presence of the porphyrin. Thorough characterization of the MnP4 containing films is described in Chapter 4.

The heterocyclic imidazole ligand has been shown to improve the catalytic efficiency of Mn-porphyrins, and MnP4 films containing the imidazole ligand have been successfully developed. These films were prepared by a variety of methods involving a combination of LB, SA and substitution procedures. In solution, it is seen that binding of a non-amphiphilic imidazole causes a small blue shift of the Mn-porphyrin Soret band; however, a dominant influence on the Soret band in the films and in solutions containing the ImODPA ligand comes from the metals axial environment -- especially halide binding. Mixed films containing both the imidazole phosphonic acid (ImODPA) and the MnP4 molecules have been prepared and characterized by ATR-IR, UV-vis, and XPS. The preparation and characterization of imidazole and MnP4 containing films is presented in Chapter 5.

The epoxidation of cyclooctene using iodosylbenzene was catalyzed by the pure MnP4 containing films with substrate to oxidant ratios of 20:5, 40:5, and 60:5 over a variety of reaction times. The self-assembled MnP4 films proved to have slightly improved catalytic efficiency relative to the analogous LB films likely due to the increased aggregation observed in LB deposited films. The mixed ImODPA/MnP4 films showed catalytic activity in the presence of the peroxide oxidants. These films were examined with different substrate to oxidant ratios. The porphyrin containing films, both with and without ImODPA were resistant to degradation under most examined reaction conditions. The catalysis results involving both PhIO and H_2O_2 oxidants with pure porphyrin and mixed porphyrin/imidazole films are described in Chapter 6.

CHAPTER 2

EXPERIMENTAL

2.1 Langmuir-Blodgett and Self-Assembled Films

2.1.1. General Langmuir-Blodgett and Self-Assembly Procedures

2.1.1.1. Film Formation. The general procedure for forming LB films starts with the Langmuir monolayer, which are prepared on a Langmuir trough. The trough consists of a rectangular piece of Teflon, typically 1 cm deep, supported on a metal base with Teflon barriers, shown as black rectangles in Figure 2.1. A Teflon well is carved in the center of a double barrier trough for transferring monolayers. The spreading solution is prepared by dissolving the amphiphile of interest in a volatile solvent, such as $CHCl_3$. The solution is carefully applied to the subphase surface, ideally spreading the molecules uniformly over the surface.

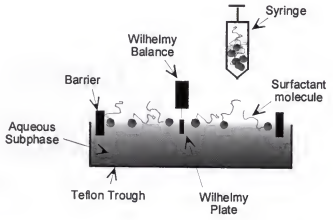

Figure 2.1: Schematic of Langmuir-Blodgett trough and monolayer.

The amphiphiles are shown in Figure 2.1 as gray circles, representing the hydrophilic head group, and black lines, representing the hydrophobic tails. The subphase, which is usually aqueous, must be nanopure. Because there is such a small amount of amphiphile present, the monolayer is extremely sensitive to contaminants – especially lipids and other surfactants and ions found in soaps and tap water.

The barriers compress the amphiphiles at a constant speed. In studying the Π-A isotherm, the film is compressed until it collapses. For LB transfers, the film is compressed until the desired transfer pressure is achieved. At this point, the monolayer is held at constant pressure for approximately two minutes until the monolayer is stabilized, then the solid substrate is dipped vertically down through this monolayer.

The monolayers are first characterized with Π-A isotherms. In modern computer operated systems, the concentration (mg mL^{-1}) and the molecular weight (g mol^{-1}), or the concentration in mol L^{-1}, of the compound being spread is entered into the program along with the spreading surface area in mm^2. From this information, the program can calculate the MMA in $Å^2$ $molecule^{-1}$. As the barriers move together and the surface is compressed, the effective MMA is decreased and the surface pressure increases.

The preparation of the zirconium phosphonate porphyrin films took place by a three-step deposition procedure (Figure 2.2).[28,29,38] A glass sample vial was placed in the subphase in the well of the trough. Octadecylphosphonic acid was spread from 0.3 mg mL^{-1} $CHCl_3$ solutions and compressed at 15 - 20 mm min^{-1} on the water surface. At 20 mN m^{-1}, the substrate was dipped down through the monolayer surface and into the sample vial at 8 mm min^{-1}, transferring the ODPA template layer. The substrate and the vial were then removed from the trough and an amount of zirconyl chloride was added to the vial to make the solution ca. 4×10^{-5} M in Zr^{4+}. After 20 min in the

zirconium solution, the substrate was removed from the vial and rinsed with water. After the template layer was successfully prepared, it was dried and characterized independently by ATR-IR, XPS, and UV-vis if needed.

Capping layers were prepared by a variety of methods, which will be described for each different film type in Chapters 3, 4 and 5. LB or SA methods could be used to form the capping layers. To form the capping layer and complete the zirconium phosphonate bilayer by the LB technique, the now hydrophilic substrate was lowered into the trough, a monolayer was spread on the surface and compressed to the desired pressure, and the substrate was raised through the monolayer at 5 mm min^{-1}. To form the capping layer by self-assembly, the hydrophilic surface was submerged in a solution of the desired molecules at about 10^{-5} M in an appropriate solvent, usually $EtOH/H_2O$ (9/1). The capping layer was then allowed to self-assemble.

2.1.1.2. Materials and Methods. Materials used to prepare the porphyrin containing films included octadecylphosphonic acid (ODPA), zirconyl chloride ($ZnOCl \cdot 8H_2O$), and the porphyrins themselves. The porphyrins were provided by Bruno Bujoli, Fabrice Odobel, Karine LeClair, and Laurent Camus from the Laboratoire de Synthese Organique, at the Faculte des Sciences et des Techniques de Nantes in Nantes, France. ODPA was used as purchased from Alfa Aesar (Ward Hill, MA). Zirconyl chloride, 98% was used as supplied from Aldrich (Milwaukee, WI). Octadecyltrichlorosilane (OTS) 95%, used to silanize and hence hydrophobicize the substrates, was also used as purchased from Aldrich. Amylene stabilized HPLC grade $CHCl_3$ was used as a spreading solvent, and was used as received from Acros (Pittsburgh, PA) and Fisher Scientific (Pittsburgh, PA).

A KSV 2000 system (Stratford, CT) was used in combination with a homemade, double barrier Teflon trough for the Langmuir monolayer studies and LB film preparation.

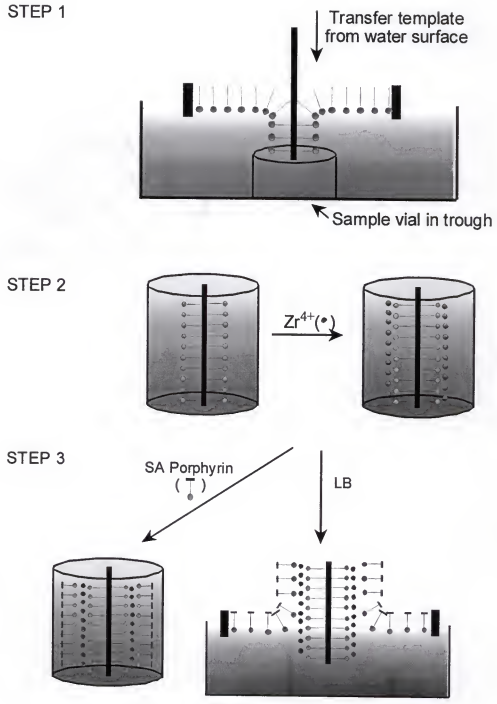

Figure 2.2: Schematic of the three-step deposition process used for zirconium phosphonate films.

The surface area of the 2000 trough was 343 cm^2 (36.5 cm x 9.4 cm). A platinum or filter paper Wilhelmy plate, suspended from a KSV microbalance, measured the surface pressure. Subphases were usually pure water with a resistivity of 17-18 $M\Omega\ cm^{-1}$ produced from a Barnstead NANOpure (Boston, MA) purification system.

The films were transferred from the aqueous surface onto solid supports. Glass microscope slides and glass coverslips were purchased from Fischer (Pittsburgh, PA) and were used as substrates for UV-vis and catalysis studies. Single crystal silicon wafers (1 0 0) were purchased from Semiconductor Processing Company (Boston, MA), and cut using a diamond glass cutter to 25 mm x 15 mm x 0.8 mm for XPS studies. These substrates were cleaned using piranha etch, which is 1:4 H_2SO_4: 30% H_2O_2, a new hydrophilic surface was prepared by the RCA procedure,[117] which involved first, heating in a 5:1:1 solution of water, 30% H_2O_2, and NH_4OH, and second, heating in a 6:1:1 solution of water, 30% H_2O_2 and HCl. Then the substrates were sonicated for 15 minutes each in methanol, 50/50 by volume methanol/ chloroform, and chloroform. The substrates were then sonicated in a 2% octadecyltrichlorosilane (OTS) solution in hexadecane and $CHCl_3$ for two hours. Finally, the substrates were sonicated for 15 minutes each in $CHCl_3$, 50/50 by volume CH_3OH/ $CHCl_3$, and CH_3OH.[118]

2.1.2. Characterization

2.1.2.1. UV-vis. Transmittance UV-visible experiments were performed on a Cary 50 spectrophotometer by Varian with an average resolution of 2 nm. Porphyrin solutions were studied by UV-vis in EtOH, H_2O, $CHCl_3$, and CH_2Cl_2 solvents. The behavior of the porphyrin with different potential ligands was investigated by mixing the porphyrin solution with ethylphosphonic acid, t-butyl ammonium halides (chloride

and bromide) (Aldrich), and imidazole with no alkyl substituents (ImH) (Kodak). A 1 cm x 1 cm x 3 cm quartz cuvette held the sample, and the background using the corresponding pure solvent was subtracted.

A Teflon substrate holder with grooves cut at 45° to one another was used to obtain sampling at 0° (beam normal to the substrate) and 45° incidence to the substrate surface. A plane, visible polarizer was used to select s- and p-polarized light. Reflectance UV-vis experiments were performed on a KSV 2000 mini-trough using an Oriel spectrophotometer and a 77410 filter with a range from 200 - 600 nm.

2.1.2.2. X-ray Photoelectron Spectroscopy. X-ray photoelectron spectroscopy (XPS) was performed on a Perkin-Elmer PHI 5000 Series spectrometer using the Mg Kα line source at 1253.6 eV. The instrumental resolution was 2.0 eV, with anode voltage and power settings of 15 kV and 300 W, respectively. The operating pressure was around 5×10^{-9} atm. Survey scans were performed at a 45° takeoff angle with a pass energy of 89.45 eV. During multiplex scans, 80 - 100 scans were run at each peak over a 20-40 eV range with a pass energy of 37.35 eV.

2.1.2.3 X-ray Diffraction. In order to obtain low angle X-ray diffraction (XRD) patterns, multilayer films were transferred onto a hydrophobic glass slide. The diffraction patterns were obtained using a Phillips APD 3720 X-ray powder diffractometer with the CuKα line, $\lambda = 1.54$ Å, as the source for films ranging from 10 to 15 bilayers.

2.1.2.4. Attenuated Total Reflectance Infrared. Attenuated total reflectance infrared spectroscopy was performed on a Mattson Instruments (Madison, WI) Research Series-1 FTIR spectrometer equipped with a deuterated triglyceride sulfide detector and a Harrick (Ossining, NY) TMP stage which held the Ge crystal substrate. ATR-FTIR spectra consisted of 500 scans at 2 cm^{-1} resolution and were referenced to the silanized crystal or previous bilayers.

2.2 Porphyrin Films

2.2.1. Palladium Porphyrin Films

The palladium porphyrins studied were palladium 5,10,15,20-tetrakis(2,3,5,6-tetrafluorophenyl-4-octadecyloxyphosphonic acid)porphyrin (PdP4) and palladium 5,10,15-tris(2,6-dichlorophenyl)-20- (2,3,5,6-tetrafluorophenyl-4-octadecyloxyphosphonic acid)porphyrin (PdP1). The Bujoli group provided us with these porphyrin amphiphiles.

The Pd-porphyrins made well-behaved monolayers; therefore, these amphiphiles were often transferred by the LB technique. Additionally, the Pd-porphyrins were studied in diluted mixtures with ODPA in an attempt to disrupt the aggregate formation in the films. For mixed, Pd-porphyrin/ODPA films, the two materials were simultaneously dissolved in a $CHCl_3$ solution. The weighted average concentration and molecular weight were calculated and used in the KSV software to monitor the MMA with compression. Ratios of PdP (1 and 4) to ODPA studied included 1:0, 1:1, 1:4, 1:9 and 0:1, respectively.

The creep of the pure palladium-porphyrin Langmuir monolayers was studied at high and low pressures over 30 min, or slightly longer than the time of one deposition. At a constant pressure of 12 - 15 mN m^{-1}, the area changed by 6% and 12% for PdP4 and PdP1, respectively. At low pressure (3 - 5 mN m^{-1}), the change in area was 3% and 7% for PdP4 and PdP1, respectively. The instability in the monolayers led to a necessary correction in the transfer ratios. The corrected transfer ratios for the pure PdP4 were 1.0 - 1.4 at high pressures and 1.0 - 1.1 at low pressures. For the pure PdP1, the corrected transfer ratios were 0.8 - 1.0 and 0.9 - 1.0 for high

pressure and low pressure transfers, respectively. The transfer ratios of the porphyrin films mixed with ODPA consistently showed uncorrected transfer ratios near unity.

Monolayers of PdP1 and PdP4 were also studied on both heated and basic subphases. To heat the trough, an Isotemp Refrigerating Circulating Model 900 (Fisher Scientific) pump with a water/ethylene glycol bath was used. The temperature of the subphase was monitored using a KSV thermosensor. A 0.01 M KOH solution was added to the subphase to adjust the pH to the desired value.

PdP4 films were also studied by self-assembly. The SA solution was prepared by diluting 1 mL of a 0.5 mg mL^{-1} solution of PdP4 in $CHCl_3$ to 30 mL with a 9/1 $EtOH/H_2O$ mixture. The film was allowed to SA for approximately 2 hours before studying by UV-vis.

2.2.2. Manganese Porphyrin Films

Manganese 5,10,15,20-tetrakis(2,3,5,6-tetrafluorophenyl-4-octadecyloxyphosphonic acid)porphyrin (MnP4) and a model porphyrin, manganese 5,10,15,20-tetrakis (pentafluorophenyl)porphyrin (MnP0) were prepared by the Bujoli group. Again, ODPA was used for the template layers, zirconyl chloride was used to prepare the zirconium network, and $CHCl_3$ was used as the spreading solvent. Also, *t*-butylammonium chloride (*t*-$BuNH_2^+$ Cl^-) (Aldrich) was used as a chloride source for SA deposited films. NaCl (Acros) was used as the chloride source for LB transferred films.

To form the MnP4 monolayers, a 0.4 mg mL^{-1} solution was prepared in $CHCl_3$ (often, in order to dissolve the porphyrins, up to 5% ethanol was added and the solution was sonicated for about an hour). An appropriate volume of solution was spread on the aqueous surface in order to reach and hold the desired transfer pressure

throughout the deposition. A variety of surface pressures were used for transfer and will be described in more detail in Chapter 4.

To prepare SA Mn-porphyrin films, 1 mL of a 0.5 mg mL^{-1} MnP4 solution in EtOH was diluted to 30 mL with a 9/1 EtOH/H_2O mixture in a 50 mL vial. Alternatively, a 0.5 mg mL^{-1} MnP4 solution in $CHCl_3$ was diluted with pure $CHCl_3$ or CH_2Cl_2. The zirconated ODPA surface was exposed to the SA solution for 2 hr unless otherwise specified. After 2 hr, there were typically some physisorbed chromophores, which were rinsed off the surface using a hot solvent such as $CHCl_3$ or CH_3CN.

As is discussed in Chapter 4, halogenated solvents were originally chosen as self-assembly solvents to eliminate possible ethoxide or water binding. However, the oxide coating on the exposed zirconated ODPA template is soluble in EtOH/H_2O solvents making the zirconium available for binding the phosphonic acids of the porphyrin capping layer. From UV-vis studies, the films formed from these different solvent systems appeared to behave similarly. Therefore, because the film formation mechanism from EtOH/H_2O was better understood, this solvent mixture was normally used.

To induce chloride binding at the Mn-porphyrin's axial position, a SA solution containing approximately 0.01 – 0.1 M *t*-$BuNH_3^+$ Cl^- along with the porphyrin in EtOH/H_2O was prepared. The zirconated ODPA template was submerged in this solution for 2 hr. Alternatively, chloride ions were incorporated into the aqueous subphase used for LB transfer of the MnP4 monolayers using NaCl at 0.1 M and greater concentrations.

From UV-vis results of the MnP4 and MnP0 with ethylphosphonic acid, it appeared that the phosphonic acid might cause the Mn(III)-porphyrin to go through a spin state crossover from high-spin to low-spin Mn(III). In order to examine this magnetic change, the Evan's NMR method was used.[119,120] A solution of 10% *t*-

butanol in $CDCl_3$ was injected into a small capillary tube using a long syringe needle. The depth of the solution in the capillary tube reached approximately 2". Two standard NMR tubes were then filled to approximately 1" with sample solution. The first was filled with pure MnP0 (0.0106 g, 100 μmol) dissolved in the 10% *t*-butanol/$CDCl_3$ solution. The second was filled with MnP0 (0.0106 g, 100 μmol) and ethylphosphonic acid (0.220 g, 2000 μmol). The reference solution in the capillary was inserted into the porphyrin containing NMR sample, and the magnetic susceptibility of the solute, χ_g ($cm^3\ g^{-1}$) induced by the magnetic porphyrin was approximated by:

$$\chi_g = \frac{-3\Delta f}{4\pi f m} \tag{2.1}$$

where Δf is the diamagnetic frequency shift, f is the spectrometer frequency, and m is the mass of substance per mL of solution. Compared to literature values, the differences in the χ_g of MnP0 with and without ethylphosphonic acid did not correspond to a spin state change in the Mn(III).

2.2.3. Manganese Porphyrin/Imidazole Mixed Films

The general method used to prepare MnP4/imidazole films in this study involved the initial formation of a zirconated octadecylphosphonic acid (ODPA) template, as before. Onto this template, a film of either pure imidazole octadecylphosphonic acid (ImODPA), which was prepared by the Bujoli group, or a mixture of ImODPA and MnP4 could be formed. The zirconium phosphonate network provided a means for locking the porphyrin and the imidazole into the films, resulting in films that were stable toward the conditions used for the catalysis

reactions. Even under relatively harsh conditions such as elevated temperatures or rapid solvent flow, the porphyrins films appeared to be stable. Additionally, the zirconium phosphonate network made preparation of the MnP4-imidazole films possible by a wide variety of mechanisms.

MnP4 and ImODPA could be incorporated into both LB and SA films. In order to accommodate ImODPA into LB films, two types of spreading solutions were used: 1) ImODPA mixed with a stabilizing agent such as hexadecylphosphonic acid (HDPA), or 2) ImODPA mixed with the MnP4 amphiphile. Alone, the ImODPA did not form sufficiently stable monolayers for transfer. The porphyrin, MnP4 was substituted into the films of pure ImODPA or ImODPA/HDPA from an EtOH/H_2O solution. Alternatively, the MnP4 film was transferred by the LB technique and then the ImODPA was substituted into these films.

First, in the case of the mixed 25% ImODPA/75% HDPA films, 200 μL of a solution with a weighted average concentration of 0.17 mg/mL and a weighted average molecular weight of 329.86 mg $mmol^{-1}$ was spread on the water surface and compressed to 12 mN m^{-1}. The film was transferred at 5 mm min^{-1} on the upstroke completing the zirconium network. Films made in this way were abbreviated ODPA/Zr/25% ImODPA. These films were then placed in a solution of the MnP4 at ca.10^{-5} M in 9/1 EtOH/H_2O and the porphyrin phosphonic acids were allowed to substitute into the defect or vacant sites in the film for 2 hr. Transmission UV-vis of these films confirms the ability to include the porphyrins by this method, and the resulting films were called ODPA/Zr/25% ImODPA, SA MnP4.

Films containing both the MnP4 and the ImODPA transferred by the LB technique from a mixed monolayer were also prepared. A 70/30 mixture of MnP4/ImODPA, respectively, was dissolved in $CHCl_3$ with a weighted concentration and MW of 0.289 mg/mL and 992.70, respectively. 175 μL of this solution was

spread and transferred at 3 mm min^{-1} on the upstroke forming the ODPA/Zr/30:70 MnP4:ImODPA films.

For the self-assembly of the imidazole onto a zirconated ODPA template, 2 mL of a 0.5 mg mL^{-1} solution of ImODPA in EtOH was dissolved in a 9/1 EtOH/H_2O mixture in a 50 mL vial. The substrate containing the zirconated ODPA template was placed in the vial and the film was allowed to self-assemble for 2 hr. When the self-assembly procedure was complete, the film was rinsed with nanopure water and dried with forced air. The MnP4 molecules were allowed to substitute into these films as described in section 2.3.2. Similarly, mixed MnP4 and ImODPA solutions were prepared at a variety of ratios in EtOH/H_2O, and the mixed monolayer was allowed to self-assemble for 2 hr.

The ImODPA was deprotonated as mentioned in Chapter 5 by soaking the mixed film in an EtOH solution containing *t*-butyl amine. The *t*-butyl amine was used to deprotonate the imidazole within the films so the ligand would be available for binding the central manganese. The concentration of this solution was not precise but was consistently ca. 0.1 M and rinsing times were ca. 15 min.

2.3 Catalysis

2.3.1. Catalysis using PhIO as an oxidant

Pure porphyrin films behaved as catalysts for the epoxidation of cyclooctene using iodosylbenzene (PhIO) as the oxidant. PhIO was synthesized from the diacetate precursor using NaOH.[121] Iodobenzene diacetate (3.0 g, 9.3 mmol) was placed in an Erlenmeyer flask. 30 mL of 3 N NaOH was added with stirring over 5 min. The mixture was stirred for 15 min and left to sit uncovered 45 min. 100 mL deionized H_2O was added with stirring and the yellow solid was filtered using a Buchner funnel.

The solid was collected and washed with another 100 mL aliquot of H_2O. The solid was filtered again, and washed with $CHCl_3$ 2 times in a beaker and filtered. The solid was dried in a vacuum desiccator. The product's melting point corresponded well to the literature value of 210° C. Iodometric titration, involving converting the PhIO product to PhI and I_2 with HI and titrating with sodium thiosulfate, gave a purity of 99%.[122]

PhIO (27.5 mg, 125 μmol) was diluted in 25 mL CH_2Cl_2. The PhIO compound was only slightly soluble in CH_2Cl_2, so it was diluted and then sonicated for at least 30 min. After sonicating, an amount of the cyclooctene was added and the mixture was stirred for about 1 min. Decane (97 μL, 500 μmol or 24 μL, 125 μmol), the internal standard, was also added with stirring. 1mL samples of this mixture were used for both a blank run and a homogeneous run. In all homogeneous experiments, 1 μL of a 1 mM solution of MnP0 was added to the blank solution to investigate the epoxide yields with the porphyrin in solution.

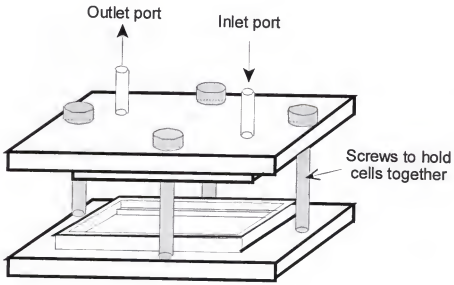

Figure 2.3: Schematic of catalysis cell, side view.

Approximately 5 mL of the above oxidant/substrate solution was transferred into a small Erlenmeyer flask and from there loaded into the flow cells used for studying catalysis with the films. Also, blanks and homogeneous solutions were loaded into cells containing blank films (no catalyst) for studying product yields affected by the flow cell.

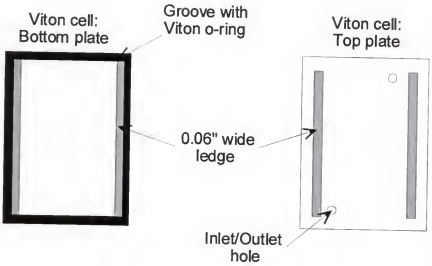

Figure 2.4: Schematic of catalysis cell, top view.

The flow cells were built by the University of Florida machine shop. The cell was made from two blocks of Delrin into which was carved a cell with dimensions: 0.96" x 1.38" x 0.039". Inlet and outlet tubes were place at the cell edges. One end of a 1' length of 1/16" ID Viton tubing (Cole-Parmer, Vernon Hills, IL) was connected to the inlet port and the other end was submerged in the reaction solution. A Cole-Parmer Masterflex peristaltic pump (model 7553-70) (6-600 rpm) with an easy-load head was used to introduce the solution into the cell, then the open end of the Viton tubing was removed from the solution and connected to the outlet port of the cell. The solution was circulated around the film using the peristaltic pump.

The reaction products were studied by GC. The GC instrument was a Shimadzu GC-17A (Columbia, MD) with a hydrogen flame ionization detector. A 1 μL portion of the reaction solution was injected onto the 25 m, 0.025 mm ID RTX-5 column (Crossbond, 5% diphenyl-95% dimethyl polysiloxane). The column was held at 50° C for 3 min and then ramped at 10° C min^{-1} for 15 min.

Sensitivity factors (k) were determined using decane and *o*-dichlorobenzene as the internal standards. A series of runs were performed for both the cyclooctene (CyO) and the cyclooctene oxide (CyOO) standards. Equation 2.2 was used to calculate 'k' from the GC trace areas of the standard (A_s) and the product (A_{CyOO}) and the known sample weights (w_{CyOO} and w_s).

$$k_{CyOO} = \frac{w_{CyOO} A_S}{w_S A_{CyOO}} \tag{2.2}$$

After an average k value was obtained for the CyO and CyOO, the catalysis yields were determined from the reaction mixture using Equation 2.3:

$$w_{CyOO} = \frac{k_{CyOO} w_S A_{CyOO}}{A_S} \tag{2.3}$$

Because the PhIO oxidant was rather insoluble, a series of 1 mL aliquots of a 1.1 g L^{-1} solution of PhIO in CH_2Cl_2 were dried and weighed. The final weights were 1.1 mg ± 9%, assuring us that the amount of oxidant in each reaction was approximately the same.

In order to compare nearly the same concentrations of catalyst in both the homogeneous and heterogeneous cases, the concentration of porphyrins in the films

was calculated to be, at most, 1 nmol. In was, however, difficult to keep this concentration constant. In the homogeneous reactions, 1 nmol of the corresponding non-amphiphilic MnP0 was used.

Imidazole is reported to improve the catalytic efficiency of the Mn-porphyrins in the presence of a peroxide oxidant, but for comparison, we also tried to see if imidazole would improve the catalytic efficiency in the presence of PhIO. For this experiment, 0.1 μmol of ImH was added to the blank and homogeneous solutions using a PhIO solution with 40 μmol CO, 5 μmol PhIO and 20 μmol decane. Also, films prepared by SA ImODPA and SA MnP4 were used in the flow cells with this same PhIO solution. The reactions were, again, stirred for 24 hr.

2.3.2 Catalysis using peroxide oxidants

In studying the catalysis of the epoxidation of cyclooctene (CyO) with H_2O_2, many different substrate to oxidant ratios were studied. The epoxide yields were greatest, however, when very dilute solutions of reactants were used to keep the proportion of reactants to catalyst near a factor of 10 and the substrate was used in excess. The starting materials, CyO and H_2O_2, were dissolved in 250 mL of CH_2Cl_2 with *o*-dichlorobenzene as the internal standard. 1mL aliquots of this solution were used for the reaction blank and homogeneous reactions and contained 8 μmol CyO, 0.2 μmol H_2O_2, and 0.2 μmol of o-dichlorobenzene. To the homogeneous reaction were added 0.4 μmol ImH and 0.001 μmol of MnP0. The original solution was pumped into the flow cells using the peristaltic pump, and these reactions were allowed to stir for 24 hr at room temperature.

CHAPTER 3
PALLADIUM PORPHYRIN CONTAINING ZIRCONIUM PHOSPHONATE LANGMUIR-BLODGETT FILMS

3.1. Background on Palladium Porphyrin Films

Langmuir monolayers and LB films of the derivatized palladium tetraphenyl porphyrin molecules, palladium 5,10,15,20-tetrakis(2,3,5,6-tetrafluorophenyl-4-octadecyloxyphosphonic acid)porphyrin and palladium 5,10,15-tris(2,6-dichlorophenyl)-20- (2,3,5,6-tetrafluorophenyl-4-octadecyloxyphosphonic acid)porphyrin, referred to as PdP4 and PdP1, respectively, are described in this chapter. The central Pd metal is a four-coordinate, diamagnetic d^8 metal, and is co-planar with the porphyrin ligand. Being four-coordinate, there are no complicating axial ligands to consider.

Porphyrins PdP4 and PdP1 are substituted with four and one octadecylphosphonic acid groups, respectively. These molecules differ from many other porphyrin amphiphiles in that there is a hydrophilic group at the end of the alkyl chain substituent. In many literature reports, the porphyrin group is often the hydrophilic part of LB film forming amphiphiles.[91] Molecules PdP4 and PdP1 (Figure 3.1) were designed to investigate whether porphyrins can be incorporated into metal phosphonate LB films. Also, because of their well-understood spectroscopic behavior, the PdP molecules were used to study how the orientation and aggregation of the porphyrin can be controlled in the deposited films.

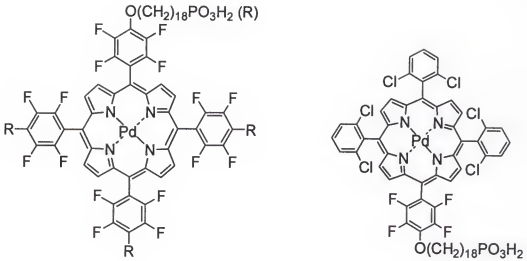

A **B**

Figure 3.1: Structures of A) PdP4 and B) PdP1.

Palladium polyhalogenated porphyrins were chosen based on the following considerations. First, palladium porphyrins are not demetallated in acidic conditions, and their diamagnetic character makes following the synthesis with NMR spectroscopy possible. Second, manganese and iron polyhalogenated porphyrins are well-known catalysts for the oxidation of hydrocarbons;[123] therefore, if palladium is replaced by one of these metals, the films can be used for catalytic applications. Third, pentafluorophenyl substituents on porphyrins allow straightforward functionalization of this ligand by aromatic nucleophilic displacement with an alcohol. In addition, the ether bonds are more stable toward hydrolysis and less hydrophilic than the ester or amide linkages usually used to tether alkyl chains on porphyrins. High hydrophobicity of the linkage is a requirement because competition with the polar phosphonic acid head-group should be avoided during the LB film preparation.

LB films of PdP4 and PdP1 were formed incorporating a zirconium phosphonate network. The strong tendency of zirconium ions to crosslink the phosphonate groups precludes the normal deposition of organophosphonate monolayers with the metal in the subphase.[28] Therefore, a previously developed three-step deposition procedure was used (Figure 2.2) as described in Chapter 2.[28,38] Both symmetric (PdP/Zr/PdP) and alternating (ODPA/Zr/PdP) films have been prepared in this way (Figure 3.2).

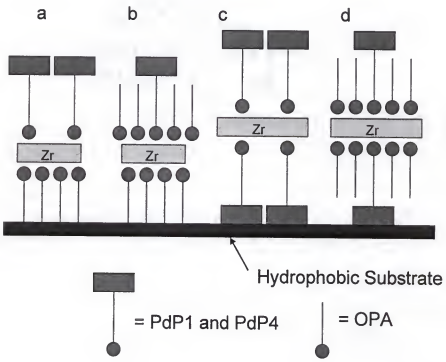

Figure 3.2: Schematic of Pd-porphyrin films formed: a) alternating ODPA/Zr/PdP, b) alternating ODPA/Zr/PdP:ODPA mixed film, c) symmetric PdP/Zr/PdP, d) symmetric PdP:ODPA/Zr/PdP:ODPA.

Control over aggregation of the porphyrin chromophores is achieved through a combination of molecular design and the careful choice of the conditions for transfer

of the films. Aggregation is decreased or eliminated in the films of the tetra-substituted PdP4 when transferred at very high mean molecular area MMA and at high subphase pH. Mixtures of this amphiphile with ODPA transferred at high temperatures (40°C) and high MMA showed a similar decrease in inter-chromophore interaction. The four long-chain phosphonic acid substituents significantly aid the spreading of monomeric porphyrin species and the strength of the zirconium phosphonate interaction assures their isolation in the transferred films. In similar studies of the mono-substituted PdP1, aggregation was observed under all of the transfer conditions explored, indicating that none of the deposition procedures overcome the tendency of the molecules to aggregate.

3.2. Results

3.2.1. UV-vis of Palladium Porphyrin Solutions

The palladium porphyrins show spectral responses in the UV-vis consistent with hypso-type metallo-porphyrins. For each porphyrin, a strong Soret Band (or B Band) is present above 400 nm and two Q Bands are centered around 550 nm.[80,124] Solution studies of the porphyrins PdP4 and PdP1 were performed in ethanol and chloroform, and the absorbance dependence on concentration was investigated. Solutions ranging from 10^{-11} M to 10^{-6} M were studied (Figure 3.3). In $CHCl_3$, the Soret Band was consistently at 410 to 411 nm for the porphyrin PdP4. In $CHCl_3$, therefore, PdP4 shows no sign of solution aggregation. For porphyrin PdP1 at 10^{-11} M, the Soret Band absorbed at 411 nm; however, as the concentration was raised, the Band shifted to 414 nm. Because PdP1 has only one long chain substituent, the likelihood of aggregation is increased; therefore, in $CHCl_3$, the PdP1 chromophores J-aggregate at high concentrations.[76,92] Interestingly, the Soret Bands for both PdP4

and PdP1 absorb at 411 nm at 10^{-11} M, so the long chains have no effect on the Soret Band of the non-aggregated chromophore.

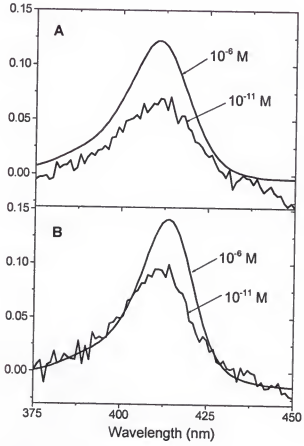

Figure 3.3: Solution UV-vis of Pd-porphyrins in $CHCl_3$: A) PdP4, B) PdP1. The absorbance scale refers to the 10^{-6} M curve. The 10^{-11} M curve has been enlarged for Band comparison.

The studies of the same molecules at identical concentrations in EtOH and water showed very different behavior (Figure 3.4). In EtOH at 10^{-11} M, both PdP4 and PdP1 show Soret Bands at 414 - 415 nm. This peak is significantly to the red of the Soret Bands in $CHCl_3$; however, it is known that more polar solvents tend to stabilize

the excited states in $\pi-\pi^*$ transitions, shifting this Band to lower energies.[25,26] As the concentrations of both PdP4 and PdP1 were raised, the Soret Band systematically shifted blue to 407 and 411 nm for the porphyrins PdP4 and PdP1, respectively, implying H-aggregation of the chromophores in EtOH.[76,92] Going from EtOH to $CHCl_3$ to H_20, at 10^{-6} M, there is an obvious red shift in the λ_{max}. This red shift does not correspond to a solvent polarity shift, but it does correspond to a shift in the solubility of PdP4. PdP4 is very soluble in EtOH and only slightly soluble in water.

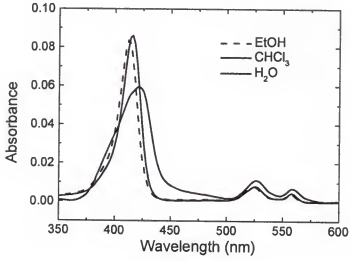

Figure 3.4 Solution UV-vis of PdP4 in EtOH and water compared to $CHCl_3$.

3.2.2 Langmuir Monolayers of Palladium Porphyrins

The room temperature pressure (Π) vs. area (MMA) isotherm of PdP4 on water at pH 5.5 is shown in Figure 3.5. There is a measurable onset of surface pressure near 220 $Å^2$ molecule^{-1}, followed by a gradual increase in pressure as the film is compressed, with an apparent phase transition giving a steeper rise in pressure near

115 Å^2 molecule^{-1}. The MMA of the tetraphenyl porphyrin is 200 Å^2 molecule^{-1} implying that at the onset, the tetrasubstituted porphyrin molecules are not aggregated or stacked.[91] However, this arrangement is not stable to pressure, and as the film is compressed, the molecules are forced to rearrange.

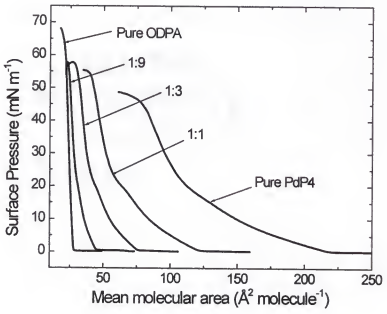

Figure 3.5: Isotherms of PdP4, pure and mixed with ODPA (PdP4:ODPA), on a water subphase.

The change in the aggregation of PdP4 during compression can be observed with reflectance UV-vis spectroscopy of the Langmuir monolayer (Figure 3.6). As the film is compressed from a MMA of 370 Å^2 molecule^{-1} through 220 Å^2 molecule^{-1}, the λ_{max} remains between 416 and 417 nm, similar to the λ_{max} observed for the non-aggregated porphyrin in EtOH. At areas between 220 and 100 Å^2 molecule^{-1}, the Soret Band shifts to 418 - 419 nm, and below 100 Å^2 molecule^{-1} the Soret Band shifts further to near 421 nm. The shift in the Soret Band suggests a change in the

interaction of the chromophores at different pressures. At MMA larger than and comparable to the size of the chromophore itself, the porphyrin rings cannot be aggregating to any significant extent or the onset of surface pressure would occur at lower areas. The red shift of the Soret Band as the area is decreased indicates enhanced chromophore aggregation at lower MMA.

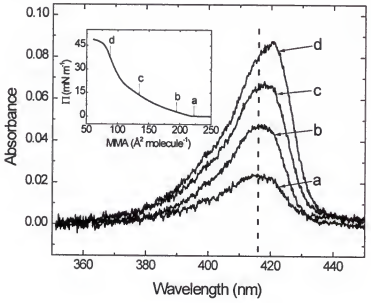

Figure 3.6: Reflectance UV-vis of PdP4 on water subphase.

In contrast to PdP4, the Π-A isotherm of PdP1 (Figure 3.7) indicates that these molecules aggregate even in the absence of applied pressure. No significant increase in surface pressure is seen until areas below 120 $Å^2$ $molecule^{-1}$. The pressure rises to only 5 mN m^{-1} at 60 $Å^2$ $molecule^{-1}$, below which the pressure increases until the film collapses below 36 $Å^2$ $molecule^{-1}$. The isotherm cannot reflect a true molecular monolayer, but rather results from the compression of aggregates at the water surface.

Evidence of aggregation at all MMA is seen in the reflectance UV-vis spectra. Figure 3.8 shows the Soret Band as a function of MMA from greater than 120 $Å^2$ molecule^{-1} to film collapse at 36 $Å^2$ molecule^{-1}. The Soret Band does not shift during compression, and the λ_{max} of 426 nm indicates that the porphyrins are aggregated at each stage of the isotherm.

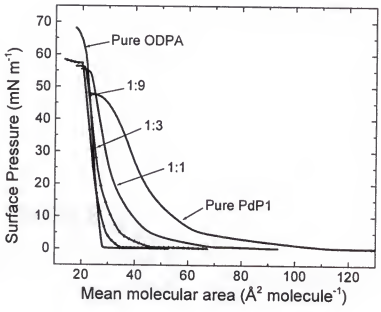

Figure 3.7: Isotherms of PdP1, pure and mixed with ODPA (PdP1:ODPA), on a water subphase.

A common procedure for enhancing the stability and processibility of unstable Langmuir monolayers, and to reduce aggregation, is to mix the amphiphile of interest with a good film-forming amphiphile.[33,88-90] In this pursuit, both of the porphyrins were mixed with ODPA, which is a well-studied amphiphile that forms a liquid-condensed phase on the water surface and easily binds to an exposed Zr-phosphonate surface. As the percentage of ODPA is increased, the isotherms increasingly take on

characteristics of the liquid-condensed phase of ODPA, although features present in the isotherms of the pure porphyrins are also present in the isotherms of the mixed films (Figure 3.5 and 3.7).

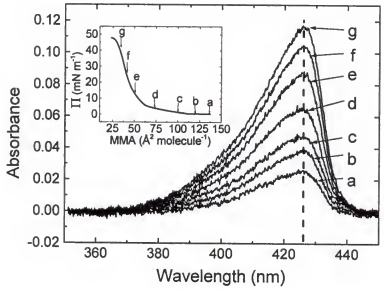

Figure 3.8: Reflectance UV-vis of PdP1 on water subphase.

In addition, the collapse pressure increases with the concentration of ODPA indicating that the films become more stable as ODPA is added. However, diluting the porphyrin film with ODPA does not appear to greatly affect the aggregation. Reflectance UV-vis of a Langmuir monolayer of a 1:9 mixture of PdP4 with ODPA is shown in Figure 3.9. The λ_{max} shifts from 415.5 nm at high MMA to 420 nm as the film is compressed, just as it does in the films of pure PdP4 (Figure 3.9). However, the porphyrins do not appear to be aggregated in the mixed film at high MMA.

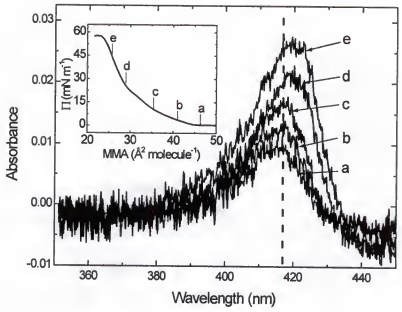

Figure 3.9: Reflectance UV-vis of 10% PdP4: 90% ODPA on a water subphase.

The molecular areas in Figures 3.5 and 3.7 are weighted averages of the porphyrin and ODPA molecules. The MMA of the porphyrin molecules in the mixed films can be calculated using Equation 3.1: [89]

$$S_{MIX} = \frac{(S_{POR} + NS_{OPA})}{(N+1)} \tag{3.1}$$

where S_{mix} is the MMA of the mixture determined from the isotherm, S_{POR} is the MMA of the porphyrin within the mixed films, S_{ODPA} is the MMA of the ODPA amphiphile in pure ODPA films, and N is the molar ratio of ODPA to porphyrin. S_{POR} was calculated in the ODPA mixtures of each porphyrin at pressures of 5 mN m^{-1} and 15 mN m^{-1} and the results are plotted in Figure 3.10.

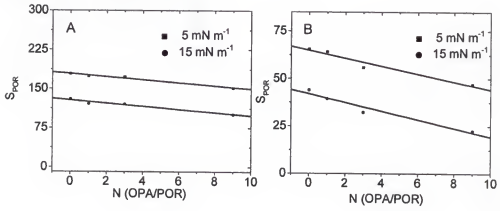

Figure 3.10: Mean molecular area vs. ratio of ODPA/Porphyrin: A) PdP4, B) PdP1.

If the ODPA diluent were breaking apart the preferred organization of the porphyrins in the films, S_{POR} would increase as the aggregates separate. The decrease in S_{POR} in the mixed films suggests that either the porphyrin chromophores are reorienting in the mixed films or aggregation actually increases in the mixed films. However, it does not appear that porphyrin aggregation decreases in the mixed monolayers.

3.2.3 Langmuir-Blodgett Films

LB films of PdP4 and PdP1 were prepared using the deposition procedure described in Figure 2.2. The stepwise deposition allows fabrication of both symmetric films, where the template and capping monolayers are the same, and alternating films, where the two monolayers in the bilayer are different. Both types of films were prepared for each porphyrin (Figure 3.2). It has been shown that a zirconated ODPA template layer frequently provides the best substrate for transferring a capping layer.[65]

The extremely well organized and oxophilic surface allows deposition of almost any phosphonic acid monolayer, including those that are not stable monolayers and would normally not transfer. Monolayers of PdP4 and PdP1 were transferred at a range of temperatures, pressures and subphase pHs (Tables 1 and 2). Films of the porphyrins mixed with ODPA were also transferred under a variety of conditions. Under some conditions, perfect, organized monolayers were obviously not formed, but the films could be transferred onto solid supports and studied.

3.2.3.1 Films of compound PdP4. To form alternating films of PdP4, the Langmuir monolayers were transferred as capping layers onto zirconated ODPA template layers. Films were transferred at different surface pressures and the Soret Band of the transferred films was used to monitor differences in chromophore aggregation in the deposited films. The UV-vis spectrum of a film transferred at 130 $Å^2$ $molecule^{-1}$ (15 mN m^{-1}) is shown in Figure 3.11, where the λ_{max} of the Soret Band appears at 420 nm, significantly red-shifted from any of the solution spectra of PdP4. The red-shift suggests increased aggregation, which is expected because at such a small MMA, the chromophores must be either tilting perpendicular to the surface and organizing side-by-side, or sliding over one another to form bilayers or multilayers. Polarized UV-vis spectroscopy indicates the porphyrins are oriented parallel to the surface, implying the latter arrangement.

Layers of PdP4 were also transferred at 190 (12mN m^{-1}) and 300 $Å^2$ $molecule^{-1}$ (Figure 3.11). The Soret Band shifts to 418 nm for the film transferred at 190 $Å^2$ $molecule^{-1}$ and to 416 nm for the film transferred at 300 $Å^2$ $molecule^{-1}$, indicating less aggregation in films transferred at high MMA. At these larger MMA, the porphyrin chromophores should be lying flat at the air-water interface with little aggregation and they appear to remain non-interacting when transferred.

Table 3.1: UV-vis data from symmetric and alternating films of PdP4. λ_{max} is given for monolayers, and interlayer thickness is given for multilayers of films transferred under a variety of transfer conditions.

Film	Transfer Area ($Å^2$ $mol.^{-1}$)*	Π of Transfer (mN/m)	pH***	Temp (°C)	λ_{max} (nm)	thickness (Å)
OPA/Zr/PdP4	300	—	5.5	23 - 25	416	—
OPA/Zr/ PdP4	190	4	5.5	23 - 25	418	42
OPA/Zr/ PdP4	180	5	5.5	23 - 25	418	—
OPA/Zr/ PdP4	130	15	5.5	23 - 25	420	—
OPA/Zr/ PdP4	100	25	5.5	23 - 25	420	—
OPA/Zr/ PdP4	90	35	5.5	23 - 25	420	—
OPA/Zr/10% PdP4	37	5	5.5	23 - 25	415	—
OPA/Zr/10% PdP4	33	15	5.5	23 - 25	418	47
OPA/Zr/25% PdP4	50	15	5.5	23 - 25	420	—
OPA/Zr/50% PdP4	74	15	5.5	23 - 25	420	—
OPA/Zr/ PdP4	300	—	9.4	23 - 25	416	
OPA/Zr/ PdP4	190	4	9.4	23 - 25	416	—
OPA/Zr/ PdP4	300	—	11.1	23 - 25	414	—
OPA/Zr/ PdP4	85	15	5.5	40	419	—
OPA/Zr/ PdP4	160	4	5.5	40	417	—
OPA/Zr/25% PdP4	50	15	5.5	40	415	—
OPA/Zr/25% PdP4	60	4	5.5	40	415	—
OPA/Zr/10% PdP4	35	15	5.5	40	415	
OPA/Zr/10% PdP4	50	4	5.5	40	415	—
PdP4/Zr/ PdP4	190	4	5.5	23 - 25	416	—
PdP4/Zr/ PdP4	130	15	5.5	23 - 25	418	—
10% PdP4/Zr/ 10% PdP4	37	5	5.5	23 - 25	418	47

* Area of the chromophore and diluent as determined from Figure 3.5 (isotherms)
** Corresponding pressure from Figure 3.5 (isotherm)
*** pH of nano-pure water from filtration system is about 5.5

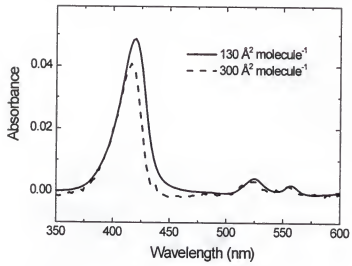

Figure 3.11: Transmission UV-vis of PdP4 films transferred at high and low MMA. Absorbance scale corresponds to the film transferred at 300 $Å^2$ $molecule^{-1}$. The absorbance for the film transferred at 130 $Å^2$ $molecule^{-1}$ has been divided by 10.

As the pH was raised, the amphiphiles became slightly more water-soluble and the monolayer was increasingly susceptible to creep. However, films of PdP4 compressed to 300 $Å^2$ $molecule^{-1}$ were deposited onto zirconated ODPA templates from subphases of pH 9.4 and 11.1. As the pH increased, λ_{max} of the Soret Band of the transferred film decreased to 414 nm for the film deposited at pH 11.1. This was the lowest value of λ_{max}, and therefore, the least aggregated LB transferred film of PdP4. The λ_{max} of this Soret Band corresponds to that of chromophore PdP4 in EtOH at 10^{-12} M which is believed to be non-aggregated.

Consistently, $D = 1 \pm 0.02$ when measured at 0° incidence, indicating no preferred in-plane orientation of the chromophore in the PdP4 and PdP1 films. However, in all films, $D \neq 1$ when measured at 45° incidence. For films transferred at high surface area, it is expected that the porphyrins should lie flat with all four phosphonates tethered to the surface. Indeed, this is observed for films transferred at

190 $Å^2$ molecule^{-1} and 300 $Å^2$ molecule^{-1} where the tilt angle, θ, with respect to the surface normal is observed to be 90°. Interestingly, the porphyrins also appear to lie parallel to the surface in the films transferred at 130 $Å^2$ molecule^{-1} where θ is also measured as approximately 90°. This result implies that in films transferred at areas smaller than the MMA of the flat porphyrin macrocycle, the molecules overlap, stacking in bilayers or multilayers but with very little change in the tilt angle. There is a larger uncertainty, possibly ± 10°, in the measurement as the tilt angles near 90°;[26] however, these results confirm that the chromophores are lying approximately flat in all of the films in this study.

Multilayers of the alternating ODPA/Zr/PdP4 films can be deposited and X-ray diffraction confirms the layered nature of the films. Two or three orders of the (00*l*) Bragg peaks can be observed in each case. Films transferred at 190 $Å^2$ molecule^{-1} have a bilayer thickness of 42 Å, which is smaller than the 48 Å thickness seen in pure ODPA/Zr/ODPA bilayers,[28] suggesting that the 18-carbon tethers of PdP4 are not fully extended in the alternating films. For the film transferred at 130 $Å^2$ molecule^{-1}, the bilayer thickness increases to 47 Å as the tetrasubstituted chromophores begin to overlap.

Symmetric bilayers of PdP4/Zr/PdP4 fabricated according to Figure 2.2, were also studied. Porphyrin PdP4 could be transferred on the down stroke onto a hydrophobic substrate under a variety of conditions. After zirconation, deposition of a capping layer of PdP4 results in a symmetric bilayer. The Soret Band is very similar to that from alternating films deposited at the same area per molecule, and polarized UV-vis indicates the porphyrins are also lying parallel to the surface. However, the layers are poorly organized, as (00*l*) Bragg peaks could not be seen in diffraction from

9-bilayer films. It is probably poor organization in the template layer of porphyrin PdP4 that is responsible for the lack of a well-defined layered structure.[38]

Mixed monolayers of PdP4 with ODPA were transferred onto ODPA templates at different points along the surface pressure vs. area isotherms as shown in Table 1, and the aggregation of the porphyrin in the transferred film parallels that seen in the films of the pure porphyrins. For films transferred at pressures of 15 mN m^{-1}, the Soret Band appeared at 420 nm, shifting to 415 nm when transferred at pressures less than 5 mN m^{-1} which, again, corresponds to the non-aggregated form seen in EtOH. In all cases, polarized UV-vis indicates that the porphyrins orient parallel to the surface.

The mixed monolayers show an interesting effect with increased temperature. A mixed monolayer of 10% PdP4 with ODPA transferred at 15 mN m^{-1} on a subphase heated to 40° C shows a Soret Band λ_{max} of 415 nm, shifted from 420 nm for the same film deposited at room temperature. As the subphase is heated, the aggregates appear to break-up in the mixed film. A similar effect is not seen on the pure films of PdP4. It appears that the ODPA plays a role in breaking up the aggregated domains at higher temperatures.

Films of PdP4 were also prepared by the SA technique. After the zirconated ODPA template had been exposed to a PdP4 solution in $EtOH/H_2O$ for 2 hr, the porphyrins were successfully incorporated into these films. The Soret Band appeared at 414 nm, which then shifted to 411 nm after 60 min rinsing in hot $CHCl_3$. The λ_{max} in the SA film was the closest of any of the PdP films to that seen in the dilute solution. Therefore, it appears that non-aggregated assemblies of PdP4 are easily obtained by self-assembly (Figure 3.12). However, the overall absorbance intensity of these non-aggregated films is lower than observed in the films transferred by the LB technique at high MMA.

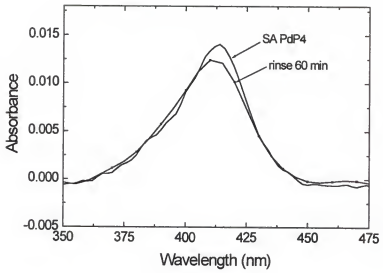

Figure 3.12: UV-vis of SA PdP4 films rinsed in hot $CHCl_3$.

3.2.3.2. Films of compound PdP1. The Π-A isotherms and the reflectance UV-vis experiments described above indicate that the molecules of PdP1 aggregate upon spreading, and this aggregation is preserved in the transferred films. In contrast to PdP4, the monophosphonate PdP1 is only slightly influenced by attempts to break up the aggregates by changing the deposition conditions. The UV-vis spectrum of a capping layer of PdP1 transferred at 52 $Å^2$ $molecule^{-1}$ (12 mN m^{-1}) is shown in Figure 3.13, where the Soret Band appears at 426 nm, consistent with the value observed in the reflectance spectrum taken from the water interface. The shape of the Soret Band does not change for films deposited at higher MMA, higher temperatures, or in mixtures with ODPA. The peak position shifts only slightly (Table 2). The orientation of the chromophores were also unaffected by the deposition conditions. Polarized spectra consistently give tilt angles of 90°, corresponding to the porphyrins lying flat.

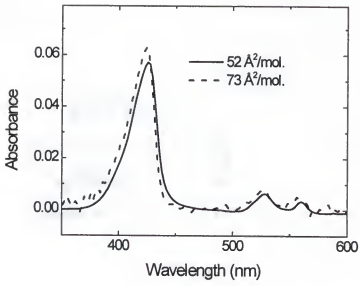

Figure 3.13: Transmission UV-vis of films of PdP1 transferred at high and low MMA.

X-ray diffraction from alternating films of PdP1 transferred at 52 $Å^2$ molecule^{-1} onto a zirconated ODPA template gives a layer thickness of 61 Å (Table 3.2). This thickness is larger than that of the alternating films of ODPA/Zr/PdP4 or ODPA/Zr/ODPA bilayers.[28] Since optical spectroscopy indicates the molecules lie flat, the enhanced thickness of the layer suggests they transfer as stacked bilayers or multilayers. Further evidence for this arrangement comes from the film stability studies, described below, which indicate that part of the transferred film of porphyrin PdP1 is physisorbed to the surface.

Table 3.2: UV-vis data from symmetric and alternating films of PdP1. λ_{max} is given for monolayers, and interlayer thickness is given for multilayers of films transferred under a variety of transfer conditions.

Film	Area of Transfer (Å²/molecule)*	Π of Transfer (mN/m)	Temp (°C)	λ_{max} (nm)	thickness (Å)
OPA/Zr/PdP1	73	4	23 - 25	426	—
OPA/Zr/PdP1	52	12	23 - 25	426	61
OPA/Zr/ PdP1	41	25	23 - 25	428	—
OPA/Zr/ PdP1	38	30	23 - 25	428	—
OPA/Zr/ PdP1	36	35	23 - 25	428	—
OPA/Zr/10% PdP1	27	12	23 - 25	426	48
OPA/Zr/25% PdP1	30	12	23 - 25	426	—
OPA/Zr/50% PdP1	38	12	23 - 25	426	—
OPA/Zr/ PdP1	300	—	23 - 25	416	
OPA/Zr/ PdP1	190	4	23 - 25	416	—
OPA/Zr/ PdP1	300	—	23 - 25	414	—
OPA/Zr/ PdP1	73	4	40	424	—
OPA/Zr/10% PdP1	30	12	40	424	
OPA/Zr/10% PdP1	26	20	40	425	—
OPA/Zr/25% PdP1	30	12	40	424	
PdP1/Zr/ PdP1	52	12	23 - 25	426	—
10% PdP1/Zr/ 10% PdP1	26	20	23 - 25	426	48

* Area of the chromophore and diluent as determined from Figure 3.7 (isotherms)
** Corresponding pressure from Figure 3.7 (isotherm)
*** pH of nano-pure water from filtration system is about 5.5

3.2.3.3. Film stability. Zirconium phosphonate LB films are insoluble in organic solvents due to the cross-linking within the zirconium-phosphonate extended network.[28] In order to monitor how well the porphyrin layers bind to the zirconated template, transferred films of PdP4 and PdP1 were rinsed with chloroform in a Soxhlet extractor. Figure 3.19 shows the Soret Band absorbances as a function of washing time in hot $CHCl_3$. Figure 3.14 shows that none of the film of PdP4 is washed away after 1 hr in chloroform, suggesting that all of the molecules are tethered to the zirconated ODPA template. The same result was obtained for films of PdP4 deposited at both higher and lower pressures or in mixtures with ODPA.

In contrast, the absorbance of the LB films of PdP1 exposed to $CHCl_3$ decreased significantly due to the desorption of chromophores. The absorbance leveled off after 20 min, to a value corresponding to the truly surface confined chromophores (Figure 3.14). This result suggests that the stacked layers of chromophores in the porphyrin PdP1 films were partially physisorbed on the surface.

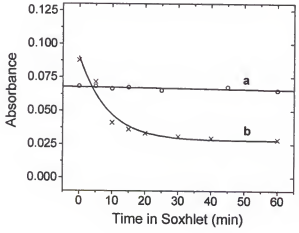

Figure 3.14: Absorbance of Soret vs. time rinsed in hot $CHCl_3$: a) PdP4, b) PdP1.

3.3. Conclusions

The behavior of the monosubstituted and tetrasubstituted porphyrins is very different on the water surface, and the differences are carried over to the transferred films. Porphyrin PdP1 spreads on the water surface to a limited extent. Our proposal for how the molecules behave on the water surface is shown schematically in Figure 3.15. Optical spectroscopy indicates that PdP1 aggregates, but the π-A isotherm and X-ray diffraction from the transferred layers suggest that the aggregates are only a few molecules thick. The aggregates are present at both high and low MMA and can be transferred, as aggregates, onto the zirconated ODPA templates. Some molecules from each aggregate chemisorb to the zirconated surface through zirconium phosphonate linkages, but some are physisorbed as part of the preformed aggregates. When exposed to hot chloroform, the physisorbed part of the film is dissolved away.

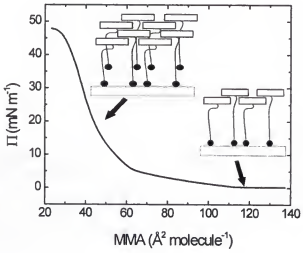

Figure 3.15: Illustration of orientation and packing of PdP1 films transferred at high and low MMA.

Chemical modification with four alkylphosphonic acid sidegroups allows the porphyrin to spread completely. Porphyrin PdP4 spreads to a monolayer thick film at high MMA, and as the film is compressed, an increase in surface pressure is registered near 200 $Å^2$ $molecule^{-1}$, corresponding to the area of the flat porphyrin macrocycle. However, the side-by-side arrangement of the porphyrin chromophores is not stable as the pressure is increased and the film rearranges, with the molecules sliding over one another to form multiple chromophore layers. This behavior is illustrated in Figure 3.16.

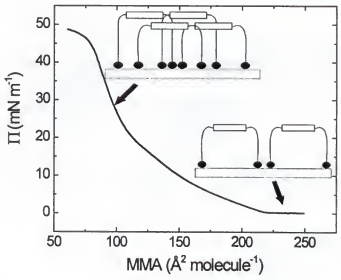

Figure 3.16: Illustration of orientation and packing of PdP4 films transferred at high and low MMA.

The films of PdP4 can be transferred at high MMA onto zirconated ODPA templates to form monolayer or submonolayer films of the porphyrin chemisorbed to the surface with the chromophore ring oriented parallel to the surface. Films of PdP4 can also be transferred at lower MMA, where the reflectance UV-vis indicates the

porphyrins are interacting. Analysis of the transferred films suggests that the porphyrin chromophores are lying flat and overlapping each other to form layers that are a few molecules thick. In contrast to the films of PdP1, all of the molecules in the aggregated films of PdP4 appear to be chemisorbed to the surface. None of the film is lost during rinsing with hot chloroform. The different behavior probably results from the fact that four phosphonic acid groups increase the chance of each molecule bonding onto the zirconium phosphonate network. Any orientation of the porphyrin macrocycle will direct at least one alkylphosphonic acid side chain toward the surface. Also, all of the phosphonic acids have the potential to reach the water surface at high MMA. Forcing a strongly hydrophilic group off of the water surface requires more energy than reorganization of the alkyl chains or shifting the chromophore interactions.

Whether the Langmuir monolayers are transferred intact or reorganized during film transfer is not yet completely clear. At high MMA, molecules of PdP4 lie flat on the water surface and this arrangement appears to be preserved in the transferred films based on the similar λ_{max}. However, when the films are transferred at lower MMA, where the films are clearly aggregated, there could be some rearrangement. There is a significant driving force for forming zirconium phosphonate linkages, and the aggregates could rearrange during transfer to further maximize interactions with the zirconated surface. While the porphyrins are clearly oriented parallel to the surface in the transferred film, providing each porphyrin the chance to form multiple zirconium phosphonate bonds, it is not known if the molecules aggregate the same way on the water surface.

The LB procedure used in these studies takes advantage of the binding energy of the zirconium phosphonate continuous network and is shown to be quite versatile. Both symmetric and alternating layer films can be prepared. Use of the zirconated

ODPA template layer allows almost any phosphonic acid derivatized amphiphile to transfer in a capping layer.[28,38,65,125] Unlike conventional LB depositions, films of PdP4 and PdP1 can be transferred onto the zirconated template layers at any surface pressure, allowing, in the case of PdP4, the arrangement of the molecules in the transferred films to be tuned by choice of the area-per-molecule at deposition. The films do not need to be stable Langmuir monolayers in order to transfer, as the driving force is formation of the zirconium phosphonate bonds. It is the strength of the zirconium phosphonate interaction, in particular the lattice energy associated with the zirconium phosphonate extended network, that is responsible for the exceptional stability of these non-traditional LB films.[28,38]

Zirconium phosphonate LB films, like solid-state zirconium phosphonates, are insoluble in organic solvents and under most aqueous conditions. The inorganic network has also been shown to enhance the thermal stability of LB films.[126] The zirconium phosphonate inorganic extended network adds substantial stability to the films, which are insoluble under most organic and aqueous conditions. The methods developed here with the palladium tetraphenyl porphyrins can also be applied to other porphyrin systems, and in this way the vast array of physical and chemical characteristics of porphyrins, including catalytic activity, should be able to be incorporated in stable LB films.

CHAPTER 4
MANGANESE PORPHYRIN CONTAINING ZIRCONIUM PHOSPHONATE THIN FILMS

4.1 Background

Monolayer and film work using the molecule manganese 5,10,15,20-tetrakis(2,3,5,6-tetrafluorophenyl-4-octadecyloxyphosphonic acid)porphyrin, or MnP4, will be discussed in Chapter 4 (Figure 4.1A). For comparison, work done using a similar molecule without the four alkylphosphonic acid chains, manganese 5,10,15,20-tetrakis(penta-fluorophenyl)porphyrin, or MnP0, will also be discussed (Figure 4.1B). The manganese porphyrins are structurally and chemically more complex than the palladium porphyrins. The Mn(III) central metal is a 5- or 6-coordinate d^4 metal.[80,127,128] Depending on the ligand character, Mn(III) is either S = 2 (high spin) or S = 1 (low spin).[129] Also, depending on the axial ligand or ligands, the Mn(III) may or may not be co-planar with the porphyrin ligand. Mn(III) also has an easily accessible lower oxidation state, which leads to significant metal/porphyrin electronic interactions,[80] the Mn(III)-porphyrins have a tendency to form face-to-face dimers bridged through an axial ligand,[130] and the Mn(III)-porphyrins are vulnerable to demetallation under certain conditions. Therefore, film characterization using these molecules was much more complicated than with the Pd-porphyrins.

To investigate the catalytic properties of manganese-porphyrin films, film preparation procedures involving the tethering of Mn-porphyrins to a metal

phosphonate network were developed. This method involves the initial formation of a zirconated octadecylphosphonic acid (ODPA) template onto which a film of pure MnP4 can be SA or transferred via the LB technique (Figure 2.2). Including MnP4 in a zirconium phosphonate network provided films that were stable toward harsh organic conditions. Also, the strong oxophilicity of the zirconium for the phosphonate oxygens enabled the film preparation procedure to be easily altered and fine tuned and complete film characterization to be carried out.

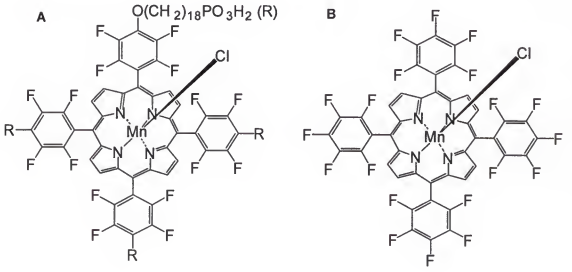

Figure 4.1: Structures of A) MnP4 and B) MnP0.

The MnP4 molecule is similar to the PdP4 molecule described in Chapter 3, in which the manganese tetraphenylporphyrin (MnTPP) chromophore and the strongly hydrophilic phosphonate groups are separated by 18-carbon chains (Figure 4.1A). This geometry allowed for the porphyrin to be sitting at the exterior of the film and available for catalysis while the phosphonates were buried in the hydrophilic region and available for binding to the stabilizing inorganic network. The incorporation of this network significantly improves the resistance of the film to typically destructive

forces such as solvent, heat, or time.[126] In addition, having four amphiphilic chains on the porphyrin permits the formation of Langmuir monolayers of these materials without diluting the amphiphiles with a good film forming amphiphile such as stearic acid.[33,88-90]

The MnP4 films were first investigated on the water surface in a Langmuir monolayer. An isotherm of this material showed significant film compressibility (Figure 4.2). Reflectance UV-vis showed that the porphyrins formed face-to-face dimers above ca. 10 mN m^{-1}, which were maintained upon transfer onto glass substrates.

The procedure for MnP4 film formation was directed by the film characterization results. In most cases, evidence suggests that the phosphonic acid tethers on the porphyrins were able to bind to the metal phosphonate lattice. Film stability was monitored by UV-vis, which displayed no significant chromophore loss after 5 minutes in hot $CHCl_3$ or CH_2Cl_2. Although the zirconium phosphonate lattice contributes no interesting physical phenomena to the final film, the strong oxophilicity of the phosphonate oxygens for the zirconium lattice allow for a wide variety of stable films to be formed.

4.2 UV-vis Behavior of MnTPPs

4.2.1. Solution Studies

Both MnTPPs displayed electronic behavior in solution consistent with d-type hyperporphyrins. Mn(II)-porphyrins have absorption spectra similar to free-base porphyrins due to a lack of metal-porphyrin interaction; however, the absorption spectrum of the Mn(III)-porphyrin is quite different. According to Gouterman,[80] Mn(III)TPP is a classic d-type hyperporphyrin with extra absorption bands at higher

energies relative to λ_{max}. The MnP4 and MnP0 with chloride axial ligands are spectrally consistent with d^4 porphyrins in high-spin configurations.[131] The strong absorption near 450-485 nm is often called Band V, due to the fact that this transition is not pure $\pi-\pi^*$ in nature but includes metal-porphyrin orbital mixing. However, traditionally, it is still often called the Soret Band.[80] One strong band commonly seen to the blue of the Soret Band is called Band VI. A prominent peak, often observed specifically in the MnP4 UV-vis spectrum ca. 410 nm, is referred to as Band Va.

Ligand effects and orientation or aggregation effects are reflected primarily in the shape or shift of the Soret Band and in the extinction coefficient (ε).[132] Therefore, the behavior of this band was carefully monitored. Also, different solvents used for porphyrin investigations caused changes in the absorption spectra. If a coordinating solvent was used, the axial ligand was displaced by a solvent molecule causing a shift in the Soret Band and in the V/VI intensity ratio.[80,132]

4.2.1.1. UV-vis of MnP0 in solution. A concentration study of MnP0 in CH_2Cl_2 showed that the λ_{max} was consistently at 475 - 477 nm between 10^{-5} and 10^{-8} M ($\varepsilon = 1.25 \times 10^7\ M^{-1}\ m^{-1}$). These results suggest that the MnP0 chromophore had little tendency to aggregate in these dilute solutions, and that the axial ligand was probably chloride.[132] In EtOH, the λ_{max} of the MnP0 solution was also constant over the same concentration range; however, the Soret Band was blue shifted to 454 – 456 nm. According to Mu, the coordination of two axial methanol ligands to a MnTPP caused a 10 nm blue shift relative to the chloride bound moieties; therefore, it is believed that this blue shift is due to bis-EtOH binding.[133] Figure 4.2 shows the solution UV-vis of MnP0 in EtOH and $CHCl_3$ at 10^{-6} M. Not only is the Soret Band shifted, but the ratio of Band V to Band VI has also changed, indicating a change in the metallo-porphyrin ligand environment.

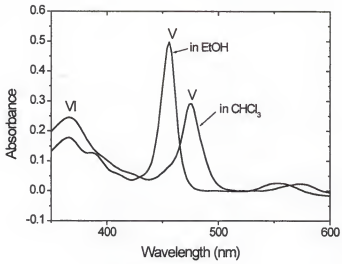

Figure 4.2: UV-vis of MnP0 in $CHCl_3$.

4.2.1.2. UV-vis of MnP4 in solution. Similar solvent shifts were observed in the case of MnP4. In CH_2Cl_2 or $CHCl_3$ at 10^{-6} M or lower concentrations, the λ_{max} appeared at 463 - 464 nm, whereas in EtOH or water, the symmetric Soret Band occurred at 454 nm (Figure 4.3). The peak at 454 nm corresponds to the MnP0 Soret Band in EtOH indicating a similar axial environment, likely a bis-ethanol complex; however, a very clear band, Va, was present at 418 nm in the MnP4 solutions. Additionally, the ratios of Band V to VI were different for each different solvent, implying that coordinating solvents effect the porphyrin axial environment.

The observed MnP4 spectral behavior in $CHCl_3$ was very different from the spectral behavior in EtOH or H_2O. At 10^{-6} M, the λ_{max} occurs at 463 nm with a distinct shoulder present on the red side of the Soret Band. As the concentration of porphyrin in $CHCl_3$ increased from 10^{-6} M to 10^{-5} M, the red shoulder became a distinct second peak at 477 nm (Figure 4.4). The two peaks are hereafter referred to as Vi and Vii for

the first and second Soret Bands. The peak at 477 nm was identified as the formation of a five-coordinate MnTPP Cl structure in the case of MnP0 in $CHCl_3$, and therefore, it clearly represented the analogous structure in MnP4 (Figure 4.2).

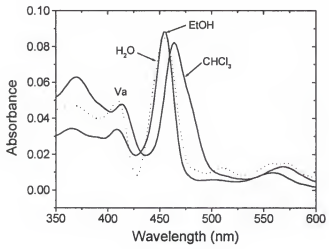

Figure 4.3 Solvent behavior of MnP4 in water, EtOH and $CHCl_3$.

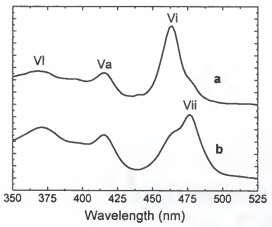

Figure 4.4: UV-vis concentration study of MnP4 in $CHCl_3$: a) 10^{-6} M, b) 10^{-5} M.

The obvious difference between MnP0 and MnP4 is the presence of the four C_{18}-chain phosphonic acid tethers linked to the phenyl rings of the MnP4. Therefore, the peak at 464 nm is, as previously mentioned, probably due to intramolecular phosphonate binding. However, the structures of the two chromophores also differ in that MnP0 has four pentafluoro-phenyl substituents, and MnP4 has an ether linkage to the alkyl chain at the para-position of the phenyl groups. For a more direct comparison, a compound incorporating similar *p*-methoxy-tetrafluoro-phenyl substituents was prepared (MnP-4MeO). This compound's spectral behavior was identical to the MnP0 compound, further indicating that phosphonate binding causes the Soret peak at 464 nm.

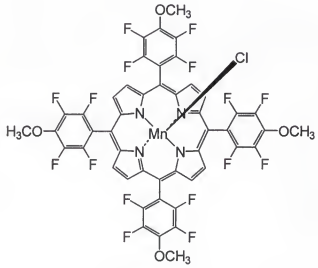

MnP-4MeO

4.2.1.3. MnP0 in solution with ethylphosphonic acid. Though the alkyl chains may have altered the chromophore interaction in solution,[134] the stronger UV-vis effects were likely due to the presence of the intramolecular R-$PO(OH)_2$ ligands. The binding of the phosphonic acids to the central porphyrin metal was confirmed by

studying solutions of MnP0 (1 x 10^{-7} M in $CHCl_3$) with ethylphosphonic acid at high concentrations. In pure MnP0, the λ_{max} was observed at 475 – 477 nm; however, when 1 x 10^{-4} M ethylphosphonic acid was added, a distinct blue shoulder became visible. At ethylphosphonic acid concentrations above 3 x 10^{-4} M (over 1000 times the porphyrin concentration) the dominant peak was the peak at 460 nm (Figure 4.5). Further, upon addition of phosphonic acid to MnP0 solutions in $CHCl_3$, an obvious peak emerged at 418 nm. Band Va was absent in the pure MnP0 solutions, hence, this peak was probably related to phosphonic acid binding.

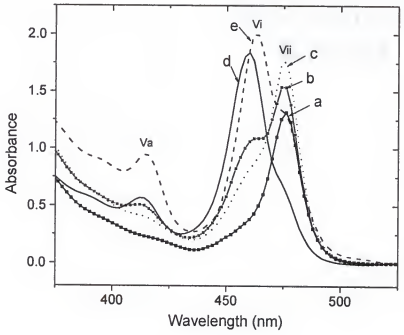

Figure 4.5: MnP0 in $CHCl_3$ (1 x 10^{-7} M) with ethylphosphonic acid: a) pure MnP0, b) 1 x 10^{-4} M ethylphosphonic acid, c) 2 x 10^{-4} M ethylphosphonic acid, d) 3 x 10^{-4} M ethylphosphonic acid, e) pure MnP4.

The peak at 418 nm could represent many different states of the porphyrin. It could be due to the oxidation of the central metal, to a spin state conversion, or even to

demetallation of the manganese porphyrin. This peak was observed in the absence of any strong oxidants indicating that this peak is probably not representing oxidation products.

The electronic spectra of Mn(III)TPP Cl in DMSO was presented by Hansen and Goff.[129] The high spin moiety that was formed by the coordination of the DMSO solvent molecules showed a sharp Soret Band at 465 nm with two prominent higher energy bands at 375 and 397 nm. However, when the molecule was converted to a low-spin Mn(III)-porphyrin complex by the bis-axial ligation of imidazolate anions, the Soret Band shifted to 451 nm and broadened. Also, the band at 397 nm increased in intensity.[129] In a similar way, the phosphonic acid or phosphonate may have been behaving like the imidazolate anion and converting the MnP0 from a high spin to a low spin complex. The spin-state of MnP0 in solution was studied using the Evan's method (described in Chapter 2). The NMR results indicated that the MnP0 with and without phosphonic acid ligands were in the same spin-state, therefore, the observed spectral behavior was due only to the ligand environment of the porphyrin.

The peak at 418 nm aligned with the Soret Band of the corresponding free-base porphyrin in $CHCl_3$ ($\varepsilon = 9.0 \times 10^6$). The strong attraction between manganese and phosphonates is well known; therefore, irreversible binding of the phosphonate to the manganese may result in the demetallation of the porphyrin. The demetallation could be facilitated by the protic nature of the phosphonic acid. This band was often observed, but its relative intensity was not consistent.

When the MnP0/ethylphosphonic acid solution spectra were overlayed with a solution spectrum of pure MnP4, the red shoulder, Band Vii of the MnP4 spectra, aligned with the original MnP0 peak. Also, the blue shoulder, Band Vi, which emerged with the addition of the ethylphosphonic acid to a MnP0 solution, was similar in energy to the original MnP4 peak.

That such high concentrations of ethylphosphonic acid were necessary to induce a change in the MnP0 spectrum indicates that the five-coordinate MnTPP(Cl) structure was generally favored over the six-coordinate MnTPP(Cl)(PA) structure (PA = phosphonic acid). However, with the four phosphonic acids linked to the MnP4 chromophore through the alkyl chains, the effective concentration of phosphonic acid in the vicinity of the metal was very high. Therefore, MnP4 in $CHCl_3$ solutions favor phosphonic acid axial ligation. Considering the Soret Band in the above MnP4 concentration study (Figure 4.4), it is apparent that this preference is stronger in the more dilute solutions of MnP4.

4.2.1.4. MnP4 in solution with chloride ions. If the UV-vis peak at 460 nm demonstrated the porphyrin's propensity to bind phosphonic acids, it was important to determine if the phosphonic acid could be replaced with another ligand such as imidazole (ImH), or chloride. According to Arasasingham, the displacement of a water or hydroxy ion by imidazole is encouraged by the electron-donating nature of the nitrogen base ligand.[114] Unfortunately, no literature precedence was found on the strength of the phosphonate binding. Though chloride binding was implied in concentration studies of MnP4 in $CHCl_3$, it was further tested by adding tetra-butylammonium chloride, $t\text{-}BuNH_3^+ Cl$, to solutions of MnP4 at constant concentrations of 10^{-5} and 10^{-6} M (Figure 4.6). Similar behavior was observed with added bromide ions, with Band Vii shifted to slightly lower energies. As the chloride concentration increased, the red shoulder at 477 nm seen in the original MnP4 spectra in $CHCl_3$ became dominant and the blue shoulder, indicating phosphonic acid binding, disappeared completely.

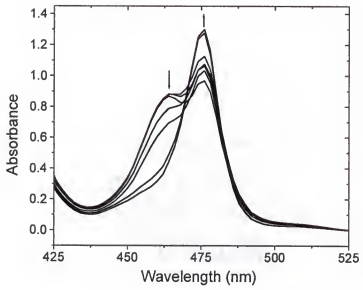

Figure 4.6: Solution UV-vis investigation of MnP4's sensitivity to displacement of R-$PO(OH)^2$ by chloride at 1 x 10^{-5} M ($CHCl_3$). The arrows indicate the changes in the intensity of the peaks as the chloride concentration changes from 0.0 M to 0.1 M while the concentration of MnP4 was constant.

4.2.2. Langmuir Monolayers

The monolayer behavior of MnP4 was studied using surface pressure (Π) vs. Area (MMA) isotherms on water (Figure 4.7). Investigating the tilt angle of the chromophores transferred at various surface pressures by polarized UV-vis gave some indication of the chromophore orientation in the monolayers. The Π-A isotherm showed a distinct Π onset at ca. 250 $Å^2$ $molecule^{-1}$. However, the approximate area of the chromophore itself is ca. 200 $Å^2$ $molecule^{-1}$. This large onset area implied that the alkyl chains were initially buckled so both the chromophores and the phosphonic acid groups were sitting on the water surface. The hydrophilic nature of the porphyrin, especially if the two axial positions are coordinated with water, makes this a viable

scenario. In the first region of the isotherm ('a' of Figure 4.7), the chromophores and the phosphonic acids remained on the water surface and were simply compressed.

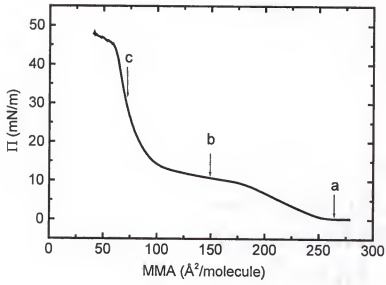

Figure 4.7: Isotherm of MnP4 on water subphase.

During the plateau region of the isotherm ('b' of Figure 4.7), the chromophores were pushed off the water surface and the porphyrin rings started overlapping. There were likely some dimers forming and not all phosphonic acid end groups reached the surface. In region 'c' of Figure 4.7, the MMA was approximately 100 $Å^2$ $molecule^{-1}$, implying the presence of dimers, which were then further compressed until the "monolayer" collapsed. At this point, the film was likely not a true monolayer as the chromophores essentially formed a bilayer.

The separation of the chromophores from the water surface was accompanied by overlapping, which was also indicated by a consequent shift in the λ_{max} detected by reflectance UV-vis (Figure 4.8). In region 'a', the λ_{max} was at 457 nm. While in

region 'b', the Soret Band shifted to and remained at 453 nm. The blue shift corroborates the formation of face-to-face dimers. The mean molecular area of this spectral shift indicated that dimers began forming even before all of the chromophores were pushed off of the water surface.

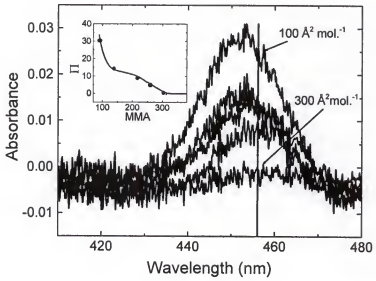

Figure 4.8: Reflectance UV-vis of MnP4 on water subphase.

4.2.3. Langmuir-Blodgett Films of pure MnP4

4.2.3.1. Deposition of MnP4 from a pure water subphase. Using the LB technique, the MnP4 monolayers were transferred at various points along the isotherm. The transmittance UV-vis spectra of these films showed that the blue shift in the λ_{max} followed the shift observed in the reflectance UV-vis experiments on the water surface (Figure 4.9). Films transferred around 5 mN m^{-1} had a λ_{max} at 462 nm, while films transferred at pressures higher than 10 mN m^{-1} were blue shifted to 456 nm. The Soret Band blue shift suggested that the chromophores were interacting as H-type

aggregates. The chromophore interactions observed on the water surface were similar to those observed in the deposited films; however, the λ_{max} at ca. 460 nm also implied that the chromophores were intramolecularly ligating phosphonic acids.

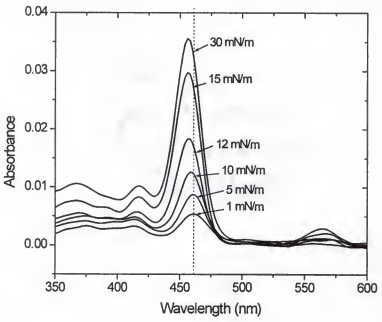

Figure 4.9: UV-vis of MnP4 capping layers transferred onto ODPA/Zr at different surface pressures.

The polarized UV-vis spectra were studied to better understand the orientation of the chromophores within the monolayer. In the case of a high-spin, 6-coordinate Mn(III)TPP, the metal typically lies within the porphyrin macromolecular plane.[127] Therefore, the tilt angle of the chromophore with respect to the surface can be determined from polarized UV-vis as described in Chapter 2.[25,26,135] When the monolayer was transferred in region 'a' of Figure 4.7, the tilt angle was determined to be ca. 90°. Within the plateau region of the Π-A isotherm, the tilt angle immediately after transfer was as low as 60°, but within minutes, the chromophore relaxed back to a

90° orientation relative to the surface normal. When transferred after the plateau region, at areas much smaller than the chromophore itself, the tilt angles were consistently ca. 90°, further confirming the presence of stacked rather than tilted chromophores.

The stability of films transferred by the LB technique before, during, and after the plateau region of the isotherm were tested by exposing the films to hot $CHCl_3$ for up to 60 min each. When transferred at 15 mN m^{-1} (Figure 4.10A), the original Soret Band was at 455 nm. After rinsing, the Band Vi shifted to 463 nm and a second Soret Band appeared at 477 nm. This red shift in the band associated with phosphonate binding is probably due to elimination of H-aggregated, physisorbed chromophores. Band Vi observed before and after rinsing in the films transferred at high MMA, remained at the same energy indicating that there was no significant change in the chromophore interaction at this transfer area. Because chromophore interaction was expected to be low at this MMA before rinsing, it was not surprising that no shift was observed. In each case, the absorbance intensity decreased significantly during the first five minutes of solvent exposure, and then leveled off (Figure 4.10). The formation of two Soret Bands, Vi and Vii, makes it difficult, however, to truly assign the change in absorbance intensities to a removal of chromophores.

The phosphonic acids in the MnP4 would probably have a stronger tendency to be on the water surface than bound to the porphyrin. Considering the strong tendency for the Mn-porphyrins to bind water in the axial positions, the chromophore could be very hydrophilic, promoting their tendency to lay on the water surface. This behavior was observed in MnP4 films transferred at high MMA. In films transferred at lower MMA, chromophore aggregation may have kept many phosphonates from binding to the zirconium network, leaving them available for binding the manganese. Therefore,

the phosphonate ligation was not as reversible when the films were transferred at higher pressures.

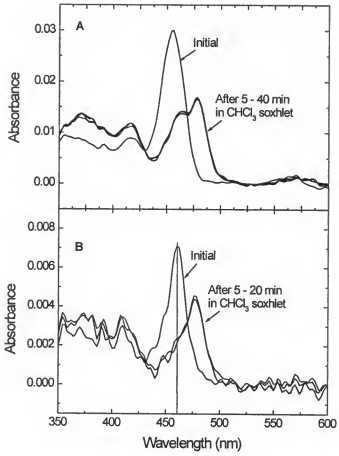

Figure 4.10: LB films of MnP4 transferred at A) 15 mN/m and B) 5 mN/m rinsed in $CHCl_3$.

When LB films of MnP4 transferred at 300 $Å^2$ $molecule^{-1}$ (0.7 mN m^{-1}) were rinsed only in hot CH_3CN, the band at 477 nm (Band Vii) was again observed (Figure 4.11). The Soret Band at 464 nm corresponding to phosphonate binding conversely disappeared. These results suggest that hot solvents were able to eliminate the phosphonic acid binding leading to the stable five-coordinate MnTPP(Cl) structure, and that the appearance of this structure is not a result of chromophore aggregation.

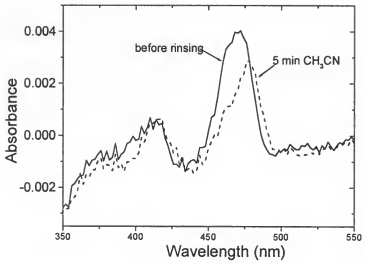

4.11: MnP4 transferred by LB at 0.7 mN m^{-1} and rinsed in CH_3CN: A) transferred from a 0.5 mg mL^{-1} solution.

4.2.3.2. Transfer of MnP4 from a chloride ion-containing subphase. In order to avoid intramolecular phosphonic acid–manganese binding upon LB transfer, chloride ions were incorporated into the subphase at a 0.1 M concentration. The porphyrin was spread and compressed to 4 mN m^{-1} for transfer onto a zirconated ODPA template. In the spectrum shown in Figure 4.12, Soret Bands were observed at 461 nm and 476 nm. Clearly, there exist domains of five-coordinate MnTPP(Cl) and six-coordinate MnTPP(Cl)(PA) structures.

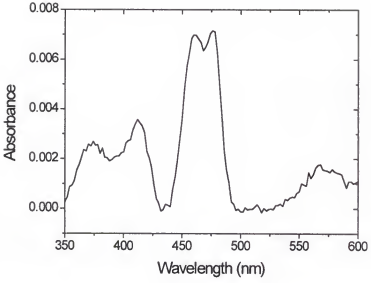

Figure 4.12: MnP4 transferred from 0.1 M [Cl^-] aqueous subphase at 4 mN m^{-1}.

4.2.4. Self-Assembled films of MnP4

4.2.4.1. Self-assembly from pure solvent. MnP4 films self-assembled from EtOH/H_2O (9/1 mixture) or CH_2Cl_2 showed a Soret Band at lower energies than observed in MnP4 LB films. The λ_{max} was now at ca. 463 – 464 nm, which corresponds to the peak in MnP4 solutions and in LB films after rinsing off physisorbed and aggregated chromophores. Therefore, this peak has been attributed to phosphonic acid binding to non-aggregated metallo-porphyrins. When self-assembled films of MnP4 were rinsed in hot $CHCl_3$, the red Soret Band associated with the MnTPP(Cl) increased significantly, and the peak associated with the six-coordinate MnTPP(Cl)(PA) decreased, again proving that hot solvents can remove the phosphonic acid ligands leaving the chloride ligand intact.

However, this five-coordinate structure was not rigid. When the films were left to structurally relax overnight, the peak at 477 nm decreased in intensity and the blue shoulder became more intense. This reversible behavior indicates that the ligand environment, which is very sensitive to solvent and heat, is flexible (Figure 4.13).

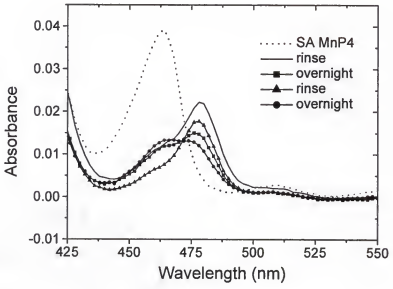

Figure 4.13: MnP4 self-assembled from $EtOH/H_2O$ and rinsed in $CHCl_3$. The legend indicates the spectra after rinsing, after being left overnight and the rinsed again over a three day period.

When these films were rinsed in CH_3CN, behavior similar to $CHCl_3$ rinsing was observed. The band at 477 nm, again, increased and the band at 464 nm decreased in intensity with time in the hot solvent. Again, if the film was left overnight, the band intensities reversed (Figure 4.14). Hot CH_3CN, therefore, also eliminated the phosphonic acid ligand and caused the formation of the five-coordinate MnTPP(Cl). When the film relaxed, the phosphonic acids had a tendency to bind again to the central metal forming the six-coordinate MnTPP(Cl)(PA) structure.

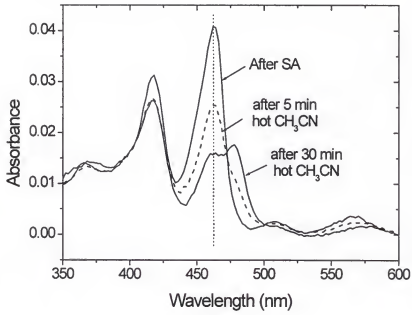

Figure 4.14: SA MnP4 films with rinsing in hot CH_3CN.

All of the described Band Vii intensity increases were observed *after* rinsing in hot solvents. If, as was expected, the axial environment of the porphyrin was associated with the mobility of these anions in solubilized films, the effect should be even more pronounced while these films were in solution. To study this, MnP4 films were self-assembled onto substrates that were cut to fit inside a cuvette filled with hot solvent, and the UV-vis was taken immediately after the solvent was heated. The results were, as predicted, exaggerations of what was observed when the film was removed from the solvent. Figure 4.15 shows that after 5 min in hot solution, the ratio V/VI was ca. 1.0, and dropped drastically up to 60 min in hot solvent as Band VI

increased in intensity and area. But, immediately after the film was removed from the solvent, Band VI dropped leaving the V/VI ratio, again, greater than 1.0.

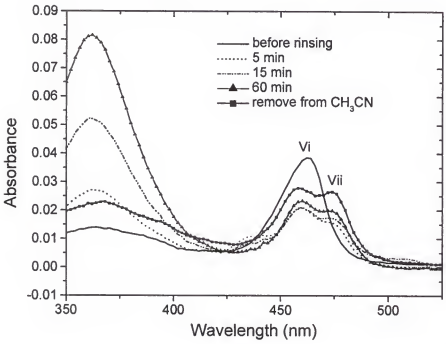

Figure 4.15: UV-vis response of a SA MnP4 film during rinsing with hot CH_3CN.

Polarized UV-vis results were obtained from the self-assembled films of the MnP4. The chromophore tilt angle was 90° at all self-assembly times. The self-assembly of the MnP4 was facilitated by the strong binding between the zirconated phosphonate template and the phosphonic acids on the MnP4 molecules, and the position of the phosphonic acids on the periphery of the chromophore lends it to lie flat in the films.

When the MnP4 was self-assembled onto a zirconated ODPA template, and these films were then rinsed in hot $CHCl_3$ or CH_3CN, the Soret Band conversion from

460 nm to 477 nm was consistently observed. However, when these films were rinsed in hot EtOH, an anomaly occurred. Instead of the increase in the band at 477 nm, as was so commonly observed in $CHCl_3$ and CH_3CN, now a peak to the high-energy side of the original band at 454 nm grew in intensity. This peak aligns with the band seen for the MnP4 and MnP0 in EtOH solutions, indicating that in the films, domains of the chromophores bind EtOH and therefore experience mobility in the axial positions (Figure 4.16).

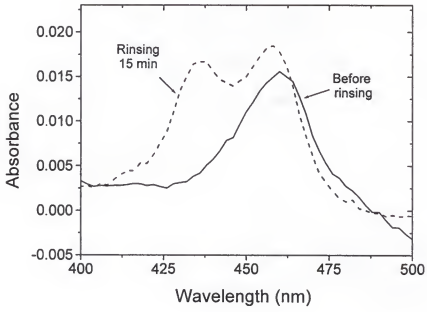

Figure 4.16: UV-vis of MnP4 self-assembled films before and after rinsing in hot EtOH.

4.2.4.2. MnP4 Self-assembly from chloride solutions. To avoid phosphonic acid ligating the porphyrin central metal and to promote the phosphonic acid binding to the zirconium network, the MnP4 was self-assembled out of a 1.4×10^{-5} M solution of porphyrin that was 0.1 M in t-$BuNH_3^+ Cl^-$. Following a successful self-assembly,

the resulting film will appear completely hydrophobic. However, after the SA from a chloride containing solution, the film did not appear totally hydrophobic indicating a potentially incomplete self-assembly. However, the MnP4 was clearly present in the UV-vis. After rinsing in hot $CHCl_3$, the Soret Band at 475 nm was present with a distinct peak at 460 nm. When these films were studied after a night in the desiccator, the Soret showed little change in shape. This behavior is consistent with a preference for the five-coordinate MnTPP(Cl) after rinsing (Figure 4.17). Interestingly, after SA from a chloride containing solution, no peak was observed at 418 nm representing the absense of free-base porphyrin. The excess chloride presumably competes with the ligation of phosphonic acids and prevents their irreversible binding, which consequently prevents the demetallation of the MnTPP.

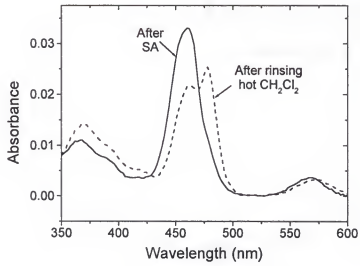

Figure 4.17: MnP4 self-assembled from a 0.1 M chloride solution.

As an additional confirmation of the successful tethering of MnP4 to the zirconated ODPA template, XPS was performed. A clear peak was observed for F_{1s}, N_{1s} and Mn_{2p3} electrons. The Zr_{3d3} and Zr_{3d5} and P_{2p3} were also observed. From the XPS it is apparent that the MnP4 has been incorporated into the film and that the film is stable to UHV.

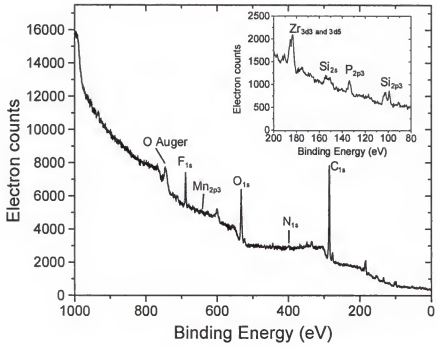

Figure 4.18: XPS of MnP4 SA film. The insert is an enlarged view of the same spectrum between 200 and 80 eV.

4.4 Conclusions

MnP4 molecules can be successfully incorporated into ultrathin films using both the LB and SA techniques. From the UV-vis perspective, these films appear very similar. In each film, there is a characteristic Soret Band. Typically, this band occurs

at 460 - 464 nm, which has been attributed to formation of a six-coordinate MnTPP(Cl)(PA) structure. Also, a band at 376 nm was assigned to Band VI, and Band Va at 418 nm was identified as corresponding to the presence of free-base porphyrins in the films. Further, rinsing in a solvent that can eliminate the intramolecular binding of phosphonic acid causes the Soret Band to shift to ca. 477 nm representing the five-coordinate MnTPP(Cl). This shift is most pronounced in solutions in which chloride ions have been added indicating that excess chloride prevents the binding of the phosphonic acid.

The band representing phosphonic acid binding demonstrated some reversibility. After films of MnP4 were rinsed in $CHCl_3$ or CH_3CN, the structure was that of MnTPP(Cl). When these same films were left to structurally relax, the UV-vis showed the reappearance of the band representing the MnTPP(Cl)(PA), accompanied by a decrease in the intensity of the MnTPP(Cl) peak. When the chromophores were adhered to the zirconated ODPA network by less than four of the phosphonic acid tethers, the non-bound phosphonic acid groups remained in central metal's vicinity. Therefore, displacement of the phosphonic acid ligands with hot solvents does not prevent them from re-ligating as the film conditions change.

The SA MnP4 films have Soret Band absorbance intensities consistently between 0.015 to 0.02 absorbance units. This absorbance intensity corresponds to the LB films transferred at MMA just before the plateau region. When the porphyrin surface coverage is incomplete, as in the LB films transferred below 5 mN m^{-1} and in the films self-assembled for very short times, the absorbance intensity was consistently around or below 0.01 absorbance units. Therefore, depending on the deposition conditions, the amount of chromophore incorporated into the films is reasonably consistent. Consistency in the chromophore loading is helpful in employing these films in catalysis studies.

Unfortunately, though the Soret Band at 477 nm is usually associated with chloride binding, Soret Bands around 460 nm can be associated with a number of axial ligands and chromophore interactions making difficult absolute characterization of the porphyrin's ligand and aggregation environment. However, ultimately, the ligand filling the axial position on the chromophore is less important than its lability. If the metal center of the porphyrin is available for oxidation, the catalyst will be active. Also, as will be discussed in Chapter 5, if the imidazole can displace the axially bound ligand, it can positively influence the catalysis.

CHAPTER 5
INCORPORATION OF AN IMIDAZOLE LIGAND INTO MANGANESE PORPHYRIN CONTAINING ZIRCONIUM PHOSPHONATE THIN FILMS

5.1 Background

As in Chapter 4, the chromophore catalyst studied was a tetraphenyl porphyrin para-substituted with four octadecylphosphonic acid groups (MnP4), which could tether the porphyrin directly to the zirconium surface. For comparison, the model porphyrin MnP0 with no phosphonic acid chains was also examined. The heterocyclic ligand used for these experiments was an alkylphosphonic acid imidazole (ImODPA), which could also be easily attached to the zirconium surface. From the propensity of the imidazole to protonate in the presence of HBr during the ImODPA synthesis, the imidazole unit was the bromide salt upon film preparation (Figure 5.1). Deprotonation of the imidazole was attempted in order to facilitate its binding to the metallo-porphyrin. To study the porphyrin's UV-vis sensitivity to an imidazole ligand in solution, an imidazole with no alkyl chains (ImH) was also used for solution studies.

The anticipated structures of the mixed MnP4/ImODPA and MnP0/ImODPA films are shown in simplified form in Figure 5.2. The chromophore is at the exterior of the film and available to catalyze the reaction of interest. The bulky chromophore leaves vacant sites available for the ImODPA, which is tethered to the zirconium-phosphonate network under and around the chromophore (Figure 5.2). Multiple

ImODPA are anticipated to be located below the chromophore plane; however, only one has the opportunity to bind at a time to the metallo-porphyrin core.

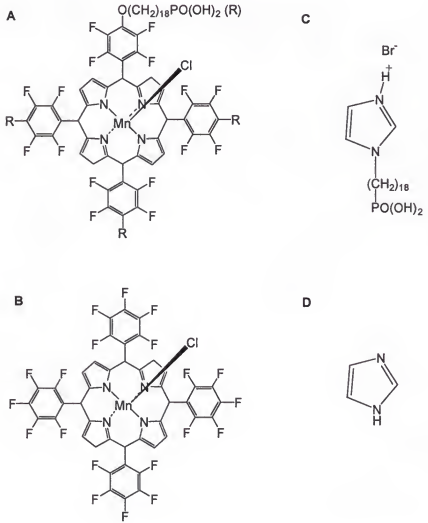

Figure 5.1: Structures of A) MnP4, B) MnP0, C) ImODPA and D) ImH.

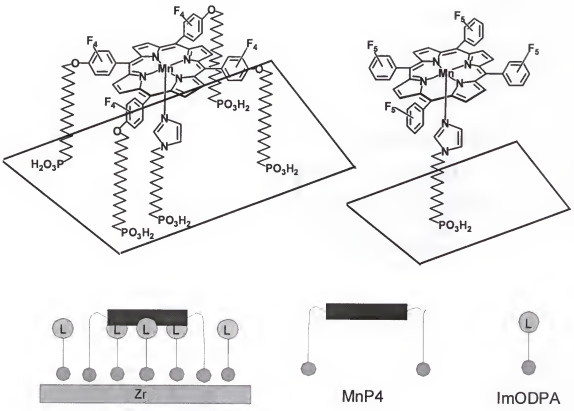

Figure 5.2: Schematic of MnP4 and ImODPA films.

A variety of methods were employed in order to accommodate the porphyrin's large MMA and encourage its binding to the imidazole in the films. These formation procedures, which were motivated by a number of intentions, will be described in this chapter. First, the Mn-porphyrin/imidazole binding is in an equilibrium state. In order to encourage the imidazole binding, or at least its availability for binding, the imidazole had to be present in excess relative to the porphyrin. To insure excess imidazole, this layer was often prepared first by either the SA or LB method. The hydrophilicity of both the phosphonic acid and the imidazole chain terminating groups

of the ImODPA made this molecule impossible to transfer as pure LB films. However, the ImODPA could be mixed with a good film-forming molecule such as ODPA or HDPA (hexadecylphosphonic acid), and these LB films were transferred successfully.

The film preparation methods fall into two general categories. First, the two components, ImODPA and MnP4, were assembled by either LB or SA in two separate steps. Examples include mixed ImODPA/HDPA LB films onto which MnP4 was self-assembled, ImODPA SA films followed by MnP4 SA, and MnP4 LB or SA films with ImODPA SA in the second step. The mechanism of the second SA step is less straightforward than the first. The phosphonic acid tethers on the second amphiphile must either find vacant or defect sites in the zirconium network, or actually replace already existing Zr-phosphonate bonds. Because this step is not a true self-assembly, it will also be referred to as the "substitution" step. The second category of film preparations involves the MnP4 and ImODPA being assembled in one step, either as a mixed SA or LB transfer. All of the described methods were successful in incorporating both components to some degree. The most facile involved SA of ImODPA followed by substitution of MnP4.

Following the formation of the ImODPA film, MnP4 could be substituted from $CHCl_3$, EtOH, or EtOH/water. Immediately after substitution, some MnP4s were physisorbed to the surface and were easily removed by rinsing in a hot solvent. The chromophores that remained contained at least one phosphonic acid tether bound to metal phosphonate base. Film stability was followed by UV-vis, and after the first 5 min of exposure to hot solvents, no more significant chromophore loss was observed.

One goal of this project was to understand the propensity of the imidazole ligand to bind to the porphyrin and to determine certain characterization signatures to confirm that this binding had taken place. That the imidazole/porphyrin binding be

persistent in the films is less important than that the imidazole is present and available to bind.

5.2 Solution Studies

Ligand effects as well as chromophore orientation and aggregation are primarily reflected in the shape or shift of the Soret Band or Band V. Therefore, the behavior of this band was carefully monitored. In addition, the ratio of Bands V to VI could be observed resulting from a change in the ligand environment.[115] Observed changes in the Soret Band in a non-coordinating solvent solution of a potential ligand are partially due to polarizability of the ligand. High polarizability of the axial ligand will lead to less negative charge induced on the porphyrin through the metal, and the Soret will shift to lower energies.[115]

As mentioned in Chapter 4, the MnP4 spectrum demonstrates a strong tendency to intramolecularly bind to the phosphonic acid head-groups on the alkyl chain substituents. Because the imidazole binding is crucial in the catalysis studies, it was important to consider the ability of imidazole to replace phosphonic acid ligands in these systems. According to Arasasingham, the displacement of a water or hydroxy ion by imidazole is favored,[114] however, the ability of imidazole to replace phosphonate ligands had no literature precedence.

5.2.1 MnP0 and MnP4 with ImH

To determine the electronic effects of binding the imidazole in the absence of potential phosphonate ligands, an imidazole containing no long phosphonic acid chain (ImH) was added to a solution of MnP0, where the concentration of the MnTPP was held constant and the ratio of ImH:MnTPP was increased. With MnP0, as an excess

of the imidazole was added, an obvious blue shift of about 20 nm to ca. 458 nm was observed in the λ_{max} (Figure 5.3A).

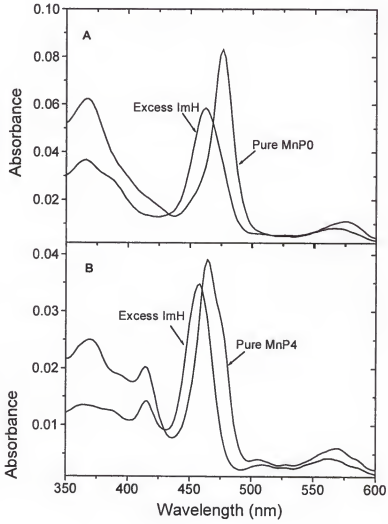

Figure 5.3: Solvent response of A) MnP0 and B) MnP4 to ImH.

Upon addition of ImH to MnP4 solutions in CH_2Cl_2, the original red shoulder on the Soret Band disappeared and was followed by a blue shift of the λ_{max} to 458 nm

(Figure 5.3B). This peak was in reasonable alignment with the peak observed in the MnP0 solutions under the same conditions. Imidazole ligands are not reported to encourage aggregation effects; therefore, these results again imply that the blue shift represents imidazole binding. This blue shift corresponds to a similar shift reported by Bruice et. al in their solution studies of a Mn-porphyrin with an increasing concentration of an imidazole ligand.[111]

At the high concentrations of ImH relative to porphyrin, the imidazole filled either one or both of the axial positions on the metallo-porphyrin. The imidazole, therefore, successfully displaced the phosphonic acid. Also, in the solutions containing excess ImH, Band Va, which was assigned to free-base porphyrin, is reduced. With the competition between imidazole and phosphonic acid for the axial position, the phosphonic acid is obviously less likely to demetallate the Mn-porphyrin. At lower imidazole concentrations, the blue shift was less obvious. However, the effective concentration of phosphonic acids on the MnP4 in the vicinity of the metal was very high, so the solution concentration of ImH had to be large to compensate.

5.2.2. MnP4 and MnP0 with ImODPA

When ImODPA was added to MnP0 in $CHCl_3$, the blue shift indicating imidazole or phosphonic acid binding was not observed. Instead, the Soret Band shifted from 477 nm to 483 nm. This red shift in the Soret Band is due to bromide displacing chloride as the axial ligand. Bromide originates from the ImODPA, which is originally a protonated amine-bromide salt. Mn-porphyrins with bromide ligands absorb at higher wavelengths than with chloride ligands because bromide is less electronegative and more polarizable than chloride shifting the Soret Band to lower energies.[115] A close look at the region ca. 418 nm shows that Band Va is also appearing. This band has been attributed to the presence of free-base porphyrins,

which again, exist due to an irreversible binding of the phosphonic acid to the manganese central metal under certain conditions causing the demetallation of the Mn-porphyrin.

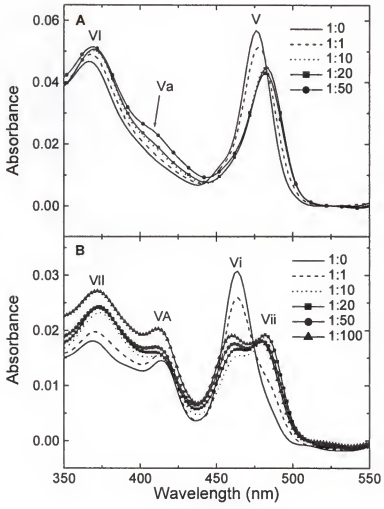

Figure 5.4: Solvent response of A) MnP0 and B) MnP4 to ImODPA. Legends indicate the molar ratio of MnP to ImODPA.

ImODPA was also added to a $CHCl_3$ solution of MnP4. The spectral behavior of this solution was more unusual. With 1 eq. of ImODPA, the red shoulder appeared

at 483 nm and the blue shoulder at 463 nm was reduced in absorbance intensity. This spectral behavior corresponds to some of the phosphonic acid ligands being displaced by bromide. However, the bromide ligation did not appear to be quantitative, as was the case with the MnP0. After the addition of 10 eq. of the ImODPA, the intensity of the peak at 483 nm leveled off, and the 463 nm peak was at a minimum. With 20 or more equivalents of ImODPA, the blue Soret peak, or Band Vi, shifted to 460 nm and increased in intensity (Figure 5.4). This blue shift may indicate imidazole binding.

Since the ImODPA amphiphile is terminated by a phosphonic acid, it would seem, again, that addition of this amphiphile would only serve to increase phosphonic acid binding. The competing ligands, however, make definitive identification of the peak at 460 nm difficult. Above a certain ImODPA concentration, it appeared that the imidazoles were displacing the remaining phosphonic acids and possibly some bromides and shifting Band Vi to higher energies. Therefore, a MnP(Br)(Im) species was probably present in solution at high ImODPA concentrations. In the films of the Mn-porphyrin, this competition may be avoided if the phosphonic acids are bound to the zirconated ODPA template.

5.3 Film Studies

5.3.1. Langmuir-Blodgett Films containing substituted MnP4

5.3.1.1. MnP4 substituted into an HDPA LB film. To understand the ability of the porphyrin to bind to the zirconium network in a preformed bilayer, a film was prepared by substituting a MnP4 layer into a LB film of hexadecylphosphonic acid (HDPA). By substituting the porphyrin film into an aliphatic capping layer, the hope was that the phosphonic acids could secure the porphyrin to the surface while the HDPA would be able to prevent porphyrin aggregation. The HDPA film formed in

this manner was well-organized and represented the most compact, and therefore most challenging, bilayer for MnP4 substitution.

With the potential phosphonic acid binding sites in the Zr-network occupied with HDPA, the phosphonic acid tethers on the porphyrin were available for intramolecular ligation. From solution results, however, chloride or bromide could displace these phosphonic acid axial ligands (Figure 5.4). When the substituted film was studied by UV-vis immediately after the MnP4 SA process was complete, the λ_{max} appeared at 454 nm. At such a high energy, the Soret Band implied that the chromophores were aggregating. Two lower energy shoulders could also be identified in the broadened Soret Band. The first appeared at ca. 463 nm, which may represent non-aggregated porphyrin domains, and the second appeared at ca. 478 nm at lower intensity indicating the presence of MnTPP(Cl) moieties.

The film stability was examined by exposure to hot $CHCl_3$ and a loss in absorbance intensity and a significant peak broadening was observed. After the first 5 min in hot $CHCl_3$, no further decrease in the overall absorbance intensity of the film was perceived, and this spectrum represented only the chemisorbed porphyrins. With the physisorbed chromophores removed, the original red shoulder at 478 nm, which was also observed previously in the solution and films of pure MnP4, was more distinct, and there appeared to be two peaks, Bands Vi and Vii. From the two apparent Soret Bands, it seems that the remaining porphyrins were either MnTPP(Cl)(PA) (peak at 463 nm) or MnTPP(Cl) (peak at 478 nm) (Figure 5.5).

Due to the splitting and broadening of the Soret Band, it is impossible to attribute a change in absorbance intensity just to removal of physisorbed chromophores. Some physisorbed chromophores were indeed removed, which was found by calculating the differences in peak areas before and after rinsing. Figure 5.5 also reveals a decrease in the absorbance intensity ratio of Band V to Band VI. A

change in the ratio of Band V to Band VI is often reportedly associated with a change in the ligand environment.[79,81] Unfortunately, many possible ligand changes are present in these systems. Most likely, as the film was rinsed, the chloride ligands could have displaced the phosphonic acid ligands. However, from the solvent studies of the pure MnP0 with ethylphosphonic acid described in Chapter 4, a decrease in V/VI was associated with increased phosphonic acid binding. Therefore, trends in these ratios were difficult to follow because so many scenarios were possible.

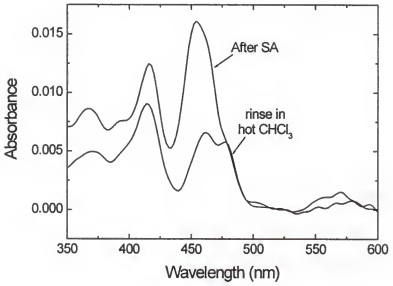

Figure 5.5: UV-vis of ODPA/Zr/HDPA, SA MnP4 film rinsed in hot $CHCl_3$.

5.3.1.2. MnP4 substituted into an ImODPA/HDPA LB film. Though HDPA was easily transferred onto the Zr-ODPA template using the LB method, imidazole was much more difficult to deposit in this manner. The hydrophilic nature of both the phosphonic acid and the imidazole made this molecule unsuitable for Langmuir

monolayer formation. Therefore, the imidazole was diluted with HDPA or ODPA to avoid this problem. After the LB transfer of the ImODPA:HDPA mixtures, the MnP4 was substituted into this layer. When films containing solutions ranging from 10% to 75% ImODPA in HDPA were prepared and the MnP4 was substituted into these films, a pattern was observed (Figure 5.6). In the films of 10% ImODPA, SA MnP4, the ratio of V/Va was clearly less than 1.0. This ratio increased with an increased concentration of ImODPA. Band Va, associated with the free-base porphyrin, drops in intensity with the addition of an imidazole ligand to compete with the phosphonic acid, as was seen in solution studies with MnP4 and ImH (Figure 5.3B). The presence of free-base porphyrin is possibly due to the irreversible binding of phosphonic acid to manganese that then pulls the manganese out of the center of the chromophore. Therefore, if the imidazole prevents the phosphonic acid from binding, it may preserve the integrity of the metallo-porphyrin.

Likewise, though less dramatic, the ratio of V/VI also appeared to increase with added ImODPA. Unfortunately, the ratio of V/VI in these films was not always reproducible or controllable, and this ratio fluctuation was observed in films when imidazole was absent. These inconsistencies could be due to the inability to completely direct the axial binding of the metallo-porphyrins.

The Soret Band in Figure 5.6 demonstrates splitting after rinsing in hot $CHCl_3$. The blue side of the peak occurs at 462 nm, which is slightly red shifted from the peak previously attributed to imidazole binding. However, as the percentage of imidazole increases, Band Vi appears to shift slightly to the blue. Also, the occurrence of the second, red band at 477 nm indicates the presence of halide axial ligands assigned to MnTPP(Cl). Due to the steric constraints from the film environment, it is unlikely that these porphyrins would form bis-imidazole complexes [$MnTPP(Im)_2$]. Therefore, this

peak splitting has been assigned to the formation of asymmetric axially bound porphyrins coexisting with domains of MnTPP(Cl).

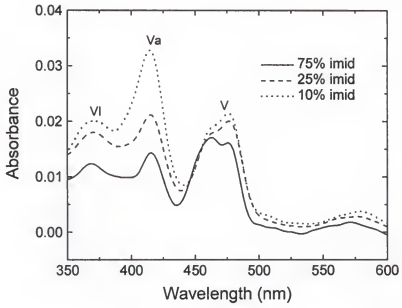

Figure 5.6: MnP4 substituted onto ImODPA:HDPA LB films after $CHCl_3$ rinsing.

Rinsing in hot $CHCl_3$ successfully eliminated any physisorbed chromophores. However, hot $CHCl_3$ had a tendency to also cause a change in the ligand environment. Therefore, room temperature $CHCl_3$ was examined in order to eliminate the physisorbed chromophores. After rinsing a 25% ImODPA/HDPA LB film, MnP4 SA film in room temperature $CHCl_3$, the UV-vis showed behavior different compared to hot $CHCl_3$. The absorbance intensity of the Soret Band decreased along with a shift from 456 nm to 458 nm (Figure 5.7).

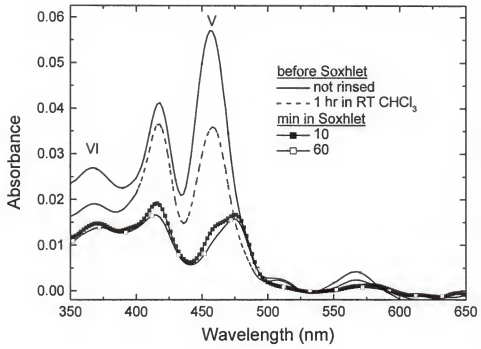

Figure 5.7: MnP4 substituted onto a 25% ImODPA/HDPA film, rinsed in room temperature and hot $CHCl_3$.

When the film was then exposed to hot $CHCl_3$, the absorbance intensity decreased further and the red component of the Soret Band appeared at 477 nm. Therefore, physisorbed chromophores can be eliminated from the surface by using room temperature or hot solvents, but a change in the axial environment was only associated with rinsing in hot solvents. The band representing halide binding at ca. 477 nm was not permanent and relaxed back to the original peak at ca. 460 nm after 24 hr (Figure 5.8).

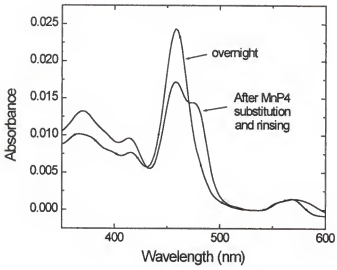

Figure 5.8: UV-vis of an ImODPA/ MnP4 film after drying.

5.3.1.3. MnP0 linked to ImODPA containing LB films. MnP0, a porphyrin with no alkylphosphonic acid chains, was assembled into ImODPA SA films to study the imidazole binding in a simplified system. The only available methods of absorbing MnP0 to these films were through the imidazole or through aggregation of chromophores, i.e. physisorption, to already chemisorbed porphyrins. Upon rinsing, any physisorbed MnP0's should be washed away. Figure 5.9 shows the UV-vis of a layer of MnP0 attached to a 25% ImODPA/HDPA LB film. The absorbance intensity of the MnP0 film was much less than films containing the MnP4, but the porphyrin was clearly present indicating the imidazole binding was active. After 60 min in a hot $CHCl_3$ solution, the absorbance intensity of the film did decrease indicating chromophore loss. However, the imidazole binding was somewhat stable to hot $CHCl_3$, as the chromophores were not completely removed after 60 min in the solvent.

The ratio of ImODPA to HDPA has been varied, and MnP0 films were still successfully formed. Further, using an ImODPA/ODPA mixture instead of ImODPA/HDPA also worked to prepare the MnP0 films. The 25% ImODPA films were studied primarily because of the balance of high imidazole loading and stable film behavior. HDPA was the primary diluent used because its chain length was appropriate to form a film with the imidazole group fully exposed and available for binding.

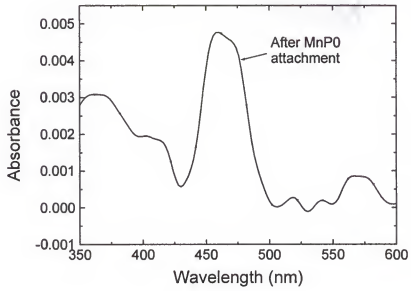

Figure 5.9: MnP0 attached to a 25% ImODPA/HDPA LB film and rinsed in hot $CHCl_3$.

5.3.2. Mn-porphyrins substituted into self-assembled films of ImODPA

5.3.2.1. UV-vis response of MnP4 film to *t*-butyl amine and $CHCl_3$ rinsing.

MnP4 was successfully substituted into a SA layer of ImODPA. After substitution, the films were rinsed with a solution of *t*-butyl amine (*t*-$BuNH_2$) to deprotonate the imidazole and facilitate its binding to the porphyrin. The base *t*-$BuNH_2$ was chosen

for its bulky nature, which should prevent its binding to the porphyrin. Rinsing the films in *t*-$BuNH_2$ caused a blue shift in the Soret Band from 461 nm to 458 nm, which was therefore, assigned to imidazole binding to the central metal. It was unclear if imidazole binding was encouraged by deprotonation or if the elimination of some physisorbed and therefore, non-imidazole bound porphyrins made it easier to observe the imidazole binding. Because of the film structure, the complex is most likely a 6-coordinate MnTPP(Cl)(Im) system.

After rinsing with hot $CHCl_3$, the Soret absorbance intensity decreased significantly. Band Vii shifted to 477 nm, which was again associated with the formation of the five-coordinate MnTPP(Cl). Twenty-four hours after rinsing, the halide-binding peak at 477 nm was no longer detected. Instead, the band at 465 nm increases in intensity as the films were left to reorganize overnight as was observed in the pure MnP4 films. From the energy of the band at 465 nm, which is at lower energies than the Soret Band observed with imidazole binding, this peak was likely due to the binding of phosphonic acid ligands and not imidazoles (Figure 5.10). The Soret Band absorbance in this film was comparable to that of previous examples of pure MnP4 substituted imidazole films, implying roughly the same number of chromophores were present.

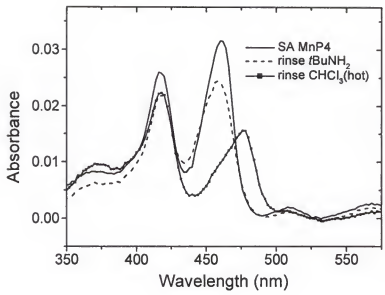

Figure 5.10: MnP4 substituted onto a pure ImODPA SA film.

5.3.2.2. Reversibility of the chloride binding in MnP4 substituted films. The same reversibility of the halide binding was observed in the films of MnP4 substituted into SA ImODPA films. As shown in Figure 5.11, after 24 hr, the peak at 477 nm reduced in intensity while the peak at 460 nm increased in intensity. The halide binding could be achieved again by rewetting this film, and the cycle continued for up to a week. However, with each cycle, the halide binding became slightly more persistent. The reversibility of the binding, as observed by the shifts in the Soret Bands, indicated that the molecular behavior in these ultrathin films was not static. In fact, in thin films, the porphyrins were keenly sensitive to the environment, especially environments containing potential axial ligands.

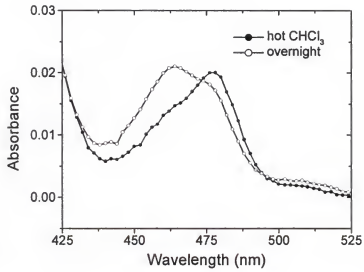

Figure 5.11: Reversibility of the chloride/phosphonic acid binding.

5.3.2.3. Rinsing the substituted MnP4 films in chloride ion solutions. Chloride ions were deliberately added to the system by rinsing the films in a solution of tert-butylammonium chloride (t-$BuNH_3^+$ Cl^-). These results confirmed that the peak at 477 nm in the films represented the MnTPP(Cl). When the MnP4 substituted film was rinsed in a room temperature EtOH solution of chloride ions, there was a clear Soret peak splitting with the red peak occurring at 477 nm indicating that in excess, chloride can bind at room temperature. When this film was then placed in a room temperature chloride solution in 9/1 EtOH/H_2O (the SA solvent mixture), Band Vii disappeared and Band Vi intensified (Figure 5.12).

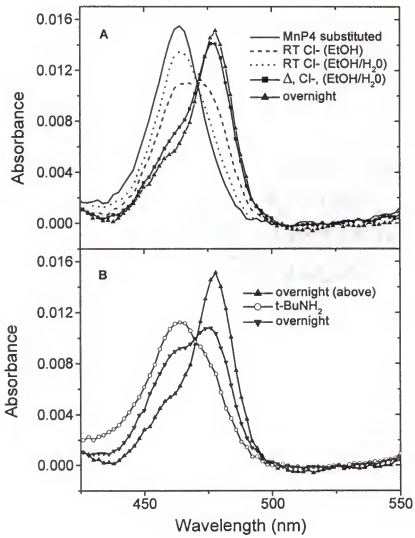

Figure 5.12: MnP4 substituted film rinsed in chloride and t-butylamine solutions.

To further promote chloride binding, the chloride-containing $EtOH/H_2O$ solutions were heated. Heating the solution worked remarkably well at incorporating chloride binding, and the low energy peak developed significantly. After being left overnight, the red peak was much more persistent. This result may indicate that in the

presence of a large excess of chloride ions, chloride binding is much less mobile and more difficult to displace (Figure 5.12).

Rinsing in *t*-$BuNH_2$ in room temperature EtOH caused the complete and immediate displacement of the chloride ligands. It is known that imidazoles tend to bind more efficiently to the porphyrins than chlorides, and so it is possible that the band at 462 nm represents imidazole binding.[111]

5.3.2.4. Preparing the substituted film from a chloride containing solution. To avoid phosphonic acid binding upon film formation, a layer of MnP4 was assembled from a 0.1 M solution of chloride onto an ImODPA layer (Figure 5.13). Initially, the chloride binding was not obvious, and the Soret was slightly blue shifted relative to phosphonic acid binding.

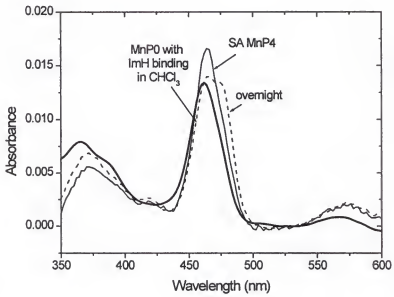

Figure 5.13: MnP4 substituted from a 0.1 M Cl^- solution onto an ImODPA layer, and compared to a MnP0 solution with ImH binding.

After sitting overnight, the red chloride peak again emerged. This behavior is contradictory to results obtained previously where the chloride peak seemed to disappear with time. By adding a sufficient amount of chloride to fill the porphyrin axial positions, the phosphonic acids may be forced to bind to the zirconium network. The chloride axial binding is in equilibrium while the zirconium-phosphonate binding is not. Once the phosphonates are unavailable for ligation, the imidazole binding, which is evidenced by a blue shifted Band Vi, is more likely to be observed. Further proof of imidazole binding is in Band Va, which was earlier associated with phosphonic acid binding causing the demetallation of the Mn-porphyrin. This band was clearly absent in these films.

5.3.3. Self-assembling the MnP4 and ImODPA from a mixed solution

As an alternative method, a self-assembly solution of a 70/30 mixture of the ImODPA and MnP4 was prepared. The UV-vis of this mixed SA solution showed Band Vi at 460 and Band Vii at 477 (Figure 5.14). Band Vi in solution may represent phosphonic acid binding; however, as the film was formed these phosphonic acids were attracted to the zirconium network leaving the manganese available for binding the imidazole. The blue shift may also demonstrate some contribution from porphyrin aggregation. Rinsing with a hot solvent was consistently done to remove any physisorbed chromophores from these films, though in some cases, as shown in Figure 5.14, there often was very little loss in absorbance intensity overall indicating that there were few physisorbed chromophores present initially.

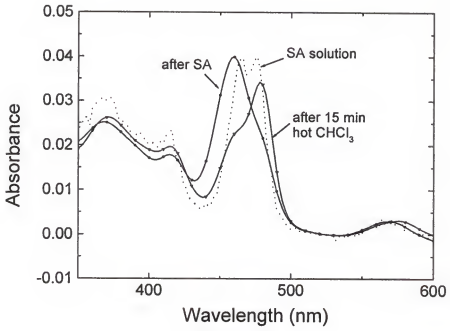

Figure 5.14: ImODPA/MnP4 self-assembled from 70/30 mixture and rinsed in hot $CHCl_3$.

5.3.4. Other methods for preparing ImODPA and MnP4 containing films.

5.3.4.1. LB deposition of MnP4 followed by substitution of ImODPA. Films of MnP4 were transferred from a water subphase at 5, 10, and 15 mN m^{-1} (before, during and after the plateau region of the isotherm shown in Figure 4.7). ImODPA was substituted into these films from an $EtOH/H_2O$ solution. It was thought that, if the MnP4 could form a complete monolayer with phosphonic acids bound to the zirconium network prior to imidazole being present, it may be more likely that there would be imidazole binding instead of phosphonic acid binding the central metal. The UV-vis behavior of these films after the substitution of ImODPA and after rinsing with CH_2Cl_2 at room temperature is shown in Figure 5.15. Unfortunately, there are

many complications with the films prepared in this way. First, the imidazole will most likely want to bind to the exposed surface of the porphyrin first; however, the phosphonic acid will be trying to bury into the film to find the zirconium network. Further, it is very difficult to confirm the presence of the imidazole in these films by any means. Therefore, this method was not rigorously pursued.

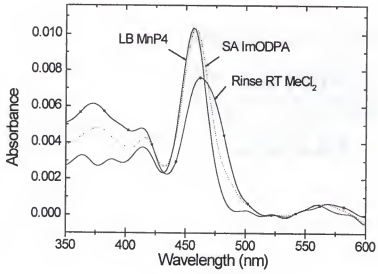

Figure 5.15: ImODPA substituted into a MnP4 LB film transferred at 10 mN m^{-1}.

5.3.4.2. LB transfer of mixed MnP4/ImODPA film at high pH. For comparison, a LB film was prepared from a spreading solution containing MnP4 and ImODPA in a 1 to 3 ratio. Ideally, a monolayer richer in ImODPA would have been used, but again, this is a poor amphiphile for LB films, and so this was impossible. These films were transferred at a variety of pressures and pHs. In a film transferred before the onset of the isotherm at a pH of 11.3 (Figure 5.16), the Soret Band after was at 459 nm. When the film was transferred at a MMA associated with little

chromophore aggregation, the Soret Band at 459 nm possibly corresponds to imidazole binding. The basic subphase was intended to deprotonate the imidazole and encourage its binding to the porphyrin while reducing the porphyrin aggregation, as seen in the case of the Pd-porphyrins in Chapter 3. Additionally, the basic subphase would deprotonate the phosphonic acids causing them to be even more hydrophilic and more likely to be on the water surface. Unfortunately, it is very difficult to confirm the presence or binding of the imidazole in these films. XPS scans of the N_{1s} region were not helpful in determining if there were two nitrogen environments present; therefore, these films were not a major focus for the preparation of catalytic films.

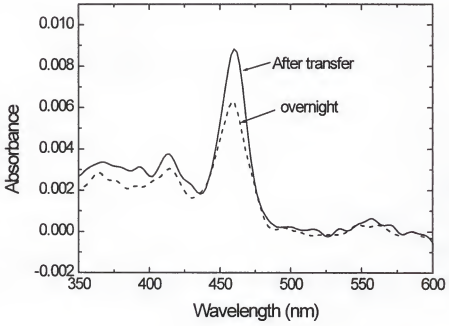

Figure 5.16: LB film of MnP4/ImODPA transferred from a 25/75 mixture on an aqueous subphase, pH 11.3.

5.3.5. Characterization of films containing MnP4 and ImODPA by XPS and ATR-IR

5.3.5.1. XPS results of pure MnP4 and pure ImODPA films. Though the UV-vis is the most well documented method of characterization for porphyrin films, the ImODPA had no clear transition in the UV-vis. Therefore, to characterize the ImODPA self-assembled film prior to the MnP4 substitution, ATR-IR and XPS were employed. To study the formation of the ImODPA films by XPS, a layer of ImODPA was self-assembled onto a zirconated ODPA template on a silicon wafer.

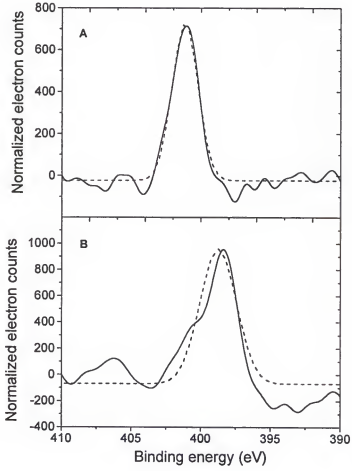

Figure 5.17: XPS multiplex scan over the N_{1s} region of A) ImODPA, and B) MnP4 self-assembled films. The dashed line represents the Gaussian peak fit.

The layer of pure imidazole was scanned by the multiplexing technique over the nitrogen peak (N_{1s}), between 410 and 390 eV. The nitrogen peak, which could only be due to the presence of imidazole, was clearly a single Gaussian peak centered at 401.0 eV with a FWHM of 2 eV (Figure 5.17A).

When a capping layer of pure MnP4 was self-assembled onto the zirconated ODPA template, a nitrogen peak was also seen (Figure 5.17B). However, in these films, the nitrogen peak was broadened to 3 eV and shifted to 399.0 eV. The nitrogen atoms of the imidazole and the porphyrin are in two different environments, and a small change in their binding energies would be expected. Therefore, in the mixed film, two peaks should be present in the N_{1s} region, one representing the imidazole and one representing the porphyrin.

5.3.5.2. XPS results from mixed self-assembled films. A film SA from a 70/30 mixture of ImODPA and MnP4 in CH_2Cl_2 was studied by XPS to determine if two nitrogen environments could be detected. There was a strong peak at about 402.0 eV and a distinct shoulder or second peak of weaker intensity at 399.0 eV indicating the presence of both nitrogen environments, and hence of both the imidazole and porphyrin within the films (Figure 5.18). Alternatively, a mixture of the porphyrin and imidazole in a similar ratio was self-assembled from 9/1 $EtOH/H_2O$. The nitrogen region of these self-assembled films showed two peaks, the first centered at 402.0 eV and the second, a broader peak of approximately equivalent intensity centered at ca. 400.0 eV (Figure 5.19). These peaks align reasonably well with those of the XPS studies of the pure imidazole (401.0 eV) and porphyrin (399.0 eV).

Again, these results indicate the presence of both the imidazole and the porphyrin in these self-assembled films. Similar results were observed by Offord et al. in films of ruthenium or osmium metallo-porphyrins that were adhered to a SA thiol-

on-gold surface.[30] XPS, therefore, clearly demonstrated the presence of both the porphyrin and the imidazole in the films.

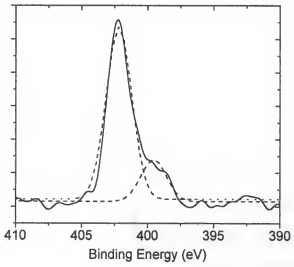

Figure 5.18: XPS multiplex scan of N1s region of ImODPA/MnP4 film self-assembled out of 70/30 CH_2Cl_2 solution. The dashed lines represent the Gaussian peak fits.

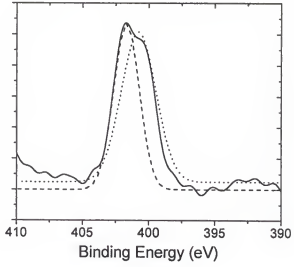

Figure 5.19: XPS multiplex scan of ImODPA/MnP4 film self-assembled from a 70/30 mixture in EtOH/H_2O. The dashed and dotted lines represent gaussian peak fits.

5.3.5.3. ATR-IR characterization of the films containing substituted MnP4 on a self-assembled ImODPA layer. An ODPA monolayer transferred by the LB technique onto a Zr-ODPA template leads to alkyl peaks at 2918 cm^{-1} and 2850 cm^{-1} corresponding to the $\nu_a(CH_2)$ and $\nu_s(CH_2)$ stretches, respectively. For alkyl chains in a majority *trans*-configuration with crystalline order, the $\nu_a(CH_2)$ peak usually falls between 2918 cm^{-1} and 2920 cm^{-1}. A shift to higher energies indicates the introduction of disorganization within the hydrophobic region of the film. In addition, the full width at half maximum (FWHM) of the $\nu_a(CH_2)$ peak can be a measure of the packing and conformational order within the alkyl region. An organized, close-packed film has a FWHM of approximately 17 cm^{-1}, which can stretch to 35 cm^{-1} upon disorganization of the film.

In films formed by both the LB and SA of ODPA from a 9/1 EtOH/H_2O solution onto a zirconated ODPA template, the $\nu_a(CH_2)$ stretch comes at 2918 cm^{-1} and the $\nu_s(CH_2)$ is at 2850 cm^{-1}. Therefore, these films are mostly *trans* and close-packed. In addition, the absorbance intensity of the $\nu_a(CH_2)$ peak in the capping layer is between 0.012 and 0.015 au. An alkyl absorbance intensity of this magnitude is therefore associated with the formation of a complete, organized monolayer of an octadecyl amphiphile.

In order to further confirm the presence of imidazole in the films formed by the SA of ImODPA onto a zirconated ODPA template, the $\nu_a(CH_2)$ and $\nu_s(CH_2)$ peaks were monitored and compared to the ATR-IR results obtained from the ODPA monolayer. The ATR-IR spectra of the ImODPA films were referenced to the zirconated ODPA template; therefore, what was plotted were the results from just the ImODPA capping layer. When the Zr-ODPA template had soaked in a 9/1 EtOH/H_2O

solution of ImODPA for five minutes, the absorbance intensity of the $\nu_a(CH_2)$ peak was 0.004 au, and the $\nu_a(CH_2)$ and $\nu_s(CH_2)$ peaks appeared at 2926 cm^{-1} and 2854 cm^{-1}, respectively. After 20 min, the absorbance increased to 0.0065 au and the peaks shifted to 2920 cm^{-1} and 2850 cm^{-1}. There was no further shift observed in these peaks; however, the absorbance slowly increased over 2 hr, at which time the absorbance intensity remained constant at 0.012 au. These results proved the presence of a monolayer of ImODPA (Figure 5.20 and 5.21). However, the FWHM of 28 cm^{-1} was significantly greater than those seen in ODPA monolayers, indicating a level of disorganization in these self-assembled films. A peak was also observed at 1307 cm^{-1}, which corresponds to the presence of C=N stretches from the imidazole. Hence, ATR-IR studies confirm the presence of a monolayer of ImODPA formed from the SA of this amphiphile from $EtOH/H_2O$.

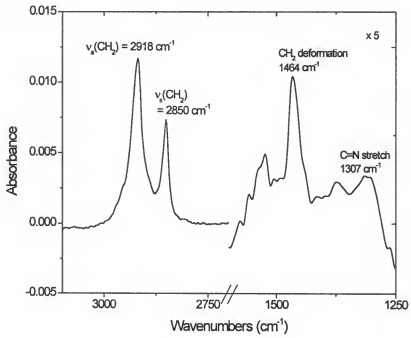

Figure 5.20: ATR-IR of ImODPA SA film.

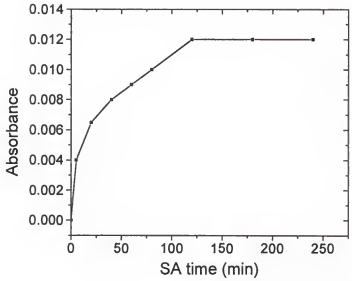

Figure 5.21: Increase in absorbance intensity of 2918 cm^{-1} peak in ImODPA with SA time.

After a layer of pure ImODPA was formed, a layer of MnP4 was self-assembled to monitor the incorporation of the porphyrin into these films. After 1 hr, the absorbance intensity of the $\nu_a(CH_2)$ peak leveled off at 0.016 au (as referenced to the ImODPA monolayer), but the peak consistently appeared at 2924 cm^{-1}. With such a large chromophore on the exterior of the hydrophobic region, the alkyl groups would be expected to be more dispersed and hence, show significantly lower absorbance intensity. Also, the addition of these bulky amphiphiles would be expected to increase the disorganization of the monolayer and shift the alkyl peaks to higher energies. However, the absorbance intensity implies a relatively high density of alkyl chains from the MnP4 units with only slightly more disorganization than seen in SA ODPA films. The physisorption of the MnP4s could result in the alkyl chains burying into the hydrophobic region of the chemisorbed film, leading to a high density of alkyl chains along with some semblance of organization within this region. The possible

physisorption of a number of chromophores is expected due to the propensity of the porphyrins to aggregate. However, this implies a significant reorganization of the underlying imidazole monolayer in order to have room to incorporate these alkyl chains.

After 30 min in hot $CHCl_3$, the absorbance intensity leveled off at 0.011 au and $\nu_a(CH_2)$ peak occurred at 2928 cm^{-1}, as referenced to the imidazole monolayer (Figure 5.22A). This result indicates that the true porphyrin containing monolayer contains alkyl chains that are disorganized and include a number of *gauche* interactions. After removing the physisorbed chromophores, the true MnP4 monolayer characteristics were better defined.

Also, the SA of this film for only 5 min, leading to an absorption intensity of 0.004 au, formed a SA film containing approximately 30% of a complete imidazole monolayer. This incomplete film was then exposed to a MnP4 solution. After 30 min, the absorbance intensity leveled off at 0.018 au and the $\nu_a(CH_2)$ was at 2926 cm^{-1}. After only 10 min in hot $CHCl_3$, the absorbance dropped drastically to 0.005 au and $\nu_a(CH_2)$ shifted to 2937 cm^{-1} (as referenced to the imidazole monolayer). However, the IR shows that the SA of a 30% ImODPA layer resulted in a relatively poor monolayer, which left many defect sites. Originally, it was thought that these defect sites would allow for the more straightforward inclusion of the porphyrin. Unfortunately, the imidazole layer in such a state may be easily removed from the zirconated ODPA template, and the final film may include less imidazole and porphyrin (Figure 5.16B), and therefore, have a lower overall alkyl absorbance in the IR.

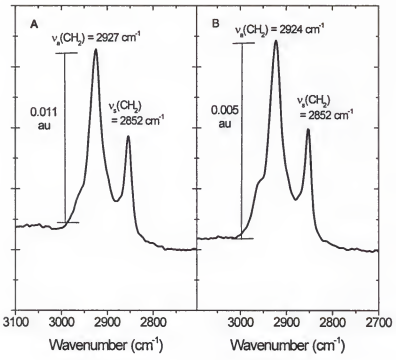

Figure 5.22: ATR-IR of alkyl region of: A) MnP4 substituted on a 100% ImODPA base capping layer, B) MnP4 substituted on a 25% ImODPA base capping layer.

5.4 Conclusions

Thin films containing both the MnP4 and the imidazole on the surface of a zirconium phosphonate film have been successfully prepared by a variety of methods. The imidazole is present in the films for the purpose of acting as a heterocyclic ligand to promote the catalytic behavior of the MnP4 chromophore. Because of the flexibility of assembling the zirconium phosphonate thin films, the procedure for preparing these films has been varied to optimize the incorporation of ImODPA and MnP4. Though aggregation is difficult to identify due to the strong optical influences

of the different axial ligands, the evidence indicates that the aggregation is probably not significant in these films.

Originally the spectral changes observed with rinsing were considered due to some chromophore reorganization or possible solvent effects. However, the peak at 477 – 478 nm aligns with the porphyrins' solvent UV-vis spectra only in the presence of added chloride or bromide; therefore, halide binding has been concluded to cause this red peak in the films as well. As mentioned, the chloride or bromide ligand causing the Soret Band change is probably associated with the MnP4 as the original axial ligand or bound to the imidazole through the HBr salt. When solubilized in hot solvents, the halides then have the opportunity and the preference for binding at the porphyrin metal center. The halide binding can be seen after rinsing in hot $CHCl_3$ or hot CH_3CN, as shown in Figures 4.11 and 4.14.

From ATR-IR, XPS, and UV-vis, the existence of ImODPA and MnP4 within the films is confirmed. From the ATR-IR, the formation of the imidazole-containing capping layer was determined. In addition, UV-vis and XPS confirms the presence and behavior of the pure MnP4 capping layer. XPS results show a nitrogen environment within the porphyrin, which differed in binding energy from the nitrogen peak for a pure imidazole film. In the mixed films, the ATR-IR demonstrated the addition of porphyrin alkyl and aryl environments upon substitution into the imidazole-capping layer.

The ability of the MnP4 films to reversibly bind different axial ligands is inferred from the activity in the Soret region of the UV-vis spectra upon heat and solvation. It appears that the Soret Band splits into two peaks, which typically represent the binding of a chloride ligand and the binding of either a phosphonic acid or an imidazole ligand in the fifth and sixth coordination sites. Further, it is possible that porphyrin domains form with slightly different ligand environments.

From solvent studies, it is clear that the imidazole can displace either phosphonic acid or chloride ligands if present in a high enough concentration. This binding is in equilibrium, making this again, difficult to consistently observe in the UV-vis. However, it is believed that in the case of the catalysis reaction, the binding will be favored due to the excess of imidazole present and that this binding will cause the activation of the porphyrin for catalysis using peroxide oxidants even if it is not consistently observed by UV-vis.

CHAPTER 6
MANGANESE PORPHYRIN AND IMIDAZOLE CONTAINING ZIRCONIUM PHOSPHONATE THIN FILMS AS CATALYSTS

6.1 Background

Reactions using immobilized catalysts have recently gained much interest. First, the immobilized porphyrins are somewhat protected from destructive oxidation because they are ideally isolated from one another on the surface. Elimination of destructive oxidation can improve the catalyst's turnover rates and overall reaction yields. Secondly, when the catalyst is immobilized, its recovery is trivial. Therefore, if the catalyst is still active, the film can be recycled and used in another catalytic reaction. With these motivations, reactions using the MnP4 films, either pure or with ImODPA, were studied. Along with the overall reaction yield, the optical intensities of the porphyrin films before and after the reaction were monitored to determine if the porphyrins were bleached or removed from the surface during the course of the reaction.

Battioni et al. examined the epoxidation of olefins using hydrogen peroxide as the oxidant.[116] In this report, Battioni investigated conditions using 5,10,15,20-tetrakis(2,6-dichlorophenyl)porphyrin (MnTDCPP(Cl)) and 5,10,15,20-tetrakis(pentafluorophenyl)porphyrin (MnTFPP(Cl)) with both A) excess substrate and B) excess oxidant. The molar ratio in condition Awith MnTDCPP(Cl) was 800:10:20:1, cyclohexene to imidazole to H_2O_2 to catalyst, and under these conditions, reported cyclohexene oxide yields of 97% were observed. The molar ratio

investigated under condition B, 40:20:200:1 cyclohexene to imidazole to H_2O_2 to catalyst, with the same porphyrin gave epoxide yields of ca. 91%. When the catalyst was MnTFPP(Cl), called MnP0 in our studies, the yields were 58% under conditions A and 74% under conditions B. The porphyrins containing halide substitutents on the phenyl rings appeared to be fairly resistant to bleaching over the course of the homogeneous reactions.

Baciocchi et al. studied the homogeneous epoxidation of cyclooctene to cyclooctene oxide using both manganese and iron porphyrins as catalysts, comparing the effects of electron donating vs. electron-withdrawing substituents on the tetraphenyl rings.[99] The porphyrins studied included 5,10,15,20-tetrakis(2,6-dimethoxyphenyl)porphyrin (MnTDMeOPP(Cl)), the above MnTDCP(Cl), and 5,10,15,20-tetraphenylporphyrin (MnTPP(Cl)). Results indicate that MnTPP(Cl), in a 1:40:200 ratio to substrate and hydrogen peroxide gave epoxide yields of 15% as referenced to the initial substrate concentration. The MnTDCPP(Cl) derivative in the same molar ratio to substrate and oxidant gave a 36% yield (as compared to 91% in the Battioni report), and the MnTDMeOPP(Cl) catalyst gave a 78% yield.

When the oxidant was instead iodosylbenzene, or PhIO, the substrate was used in excess with a molar ratio of 1:400:20, porphyrin to substrate to PhIO, respectively. The epoxide yields ranged from 73 to 80% with reference now to the oxidant. In both the PhIO and H_2O_2 epoxidation reactions, the bleaching effects observed with the MnTDCPP(Cl) and MnTDMeOPP(Cl) catalysts were mild, under 5%. Only the unsubstituted MnTPP(Cl) showed up to 10% bleaching reported over the course of the 2 hr reaction in the presence of PhIO.

Thin films of catalytic porphyrins have also been studied. Abatti et al. investigated LB films containing an iron(III) 5, 10, 15, 20-tetrakis(tetradecyl-2-N-pyridyl) porphyrin. With the inclusion of alkyl chains on the four-pyridine rings, clear

hydrophobic and hydrophilic regions were defined in the molecule and this amphiphile formed monolayers on the water surface. These monolayers could be transferred onto hydrophobic substrates placing the chromophore on the exposed surface. The immobilization of these porphyrins saw a doubling of the epoxide yield as compared to the same catalyst to reactant ratios in solution with PhIO as the oxidant. Unfortunately, the transferred monolayer by itself was not stable and was removed almost instantly from the surface in room temperature CH_3CN. Abatti et al. used a poly-vinylalcohol film to stabilize the porphyrin film for up to 4 hr.[88]

As an alternative to the homogeneous reactions and coated LB films using porphyrins as catalysts, our work focused on immobilizing active porphyrins in independently stable film structures. As mentioned in Chapters 4 and 5, the process involved incorporating manganese(III) 5, 10, 15, 20-tetrakis(tetrafluorophenyl-4-octadecyloxyphosphonic acid)porphyrin (MnP4), with and without imidazole octadecylphosphonic acid (ImODPA), into zirconium phosphonate LB and SA films. The film structures were stable in hot CH_2Cl_2 over 60 min and were expected to be stable in the catalysis reactions.

The flow cells described and illustrated in Chapter 2 were employed to run reactions using the porphyrin containing films with or without imidazole. The different reaction mixtures were prepared and the blank and homogeneous solutions were separated into different vials, where they were stirred for a given length of time. The blank solution was pumped through a cell containing the film of interest for the same amount of time. In most cases, the reactions were run for 2, 6, or 24 hr.

Because the extent of the reaction would be measured by GC, the first step in this study involved determining the GC sensitivity factors for the cyclooctene and cyclooctene oxide. A decane standard was used in PhIO reactions, and an *o*-

dichlorobenzene standard was used in the H_2O_2 reactions. The sensitivity factors were calculated using Equation 2.2:

$$k_{CyOO} = \frac{w_{CyOO} A_S}{w_S A_{CyOO}} \tag{2.2}$$

and were found to be 1.297 for cyclooctene oxide (CyOO) and 1.008 for cyclooctene (CyCO) with decane. After average k values were obtained for the CyO and CyOO, the catalysis yields were determined from a GC of the reaction mixture using Equation 2.3. The amount of product was calculated in grams, and referenced to the theoretical mass to obtain a percent yield. An empirical sensitivity factor for each compound is necessary due to the fact that the GC detector does not respond identically to each solute.

$$w_{CyOO} = \frac{k_{CyOO} w_S A_{CyOO}}{A_S} \tag{2.3}$$

6.2 Results

6.2.1 Catalysis with PhIO as the oxidant

6.2.1.1. Time dependence of oxidation yields. A stock solution of CyO and PhIO with decane was prepared in CH_2Cl_2 solution at a 1000:125:500 molar ratio in CH_2Cl_2. A 1 mL aliquot contained 40 μmol CyO, 5 μmol PhIO and 20 μmol of decane, which was then used for the blank reactions with no porphyrin present. Considering the amount of porphyrin in the films to be approximately 1×10^{-9} moles, the molar ratio of the corresponding homogeneous reaction was .001:40:5:20 in, again, 1 mL of CH_2Cl_2. Also, ca. 1 mL of the stock solution was introduced into the flow

cells containing the MnP4 film. The films used in these experiments were prepared by self-assembling a monolayer of MnP4 onto a zirconated ODPA template and rinsing this template with hot CH_2Cl_2. The UV-vis band, Va, which has previously been assigned to the free-base porphyrin, is clearly present in the films used for the 24 hr and 2 hr experiments.

When these reactions were allowed to proceed over 24 hours, GC results indicated that the average yield in the blank was ca. 1.5 %, in the homogeneous reaction was 8.4%, and in the films, between 20% and 35%. These percent yields, as calculated relative to the internal standard peak, were fairly consistent.

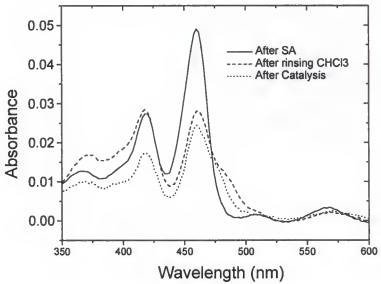

Figure 6.1: SA MnP4 film before and after 24 hr. catalysis run with 40:5:20 cyclooctene: PhIO:decane in CH_2Cl_2.

Interesting to note is the fact that, even after 24 hr in the catalysis reaction, there does not appear to be a significant bleaching effect. The porphyrin appears to still be present and intact in the film. What is noticeable is the fact that the Soret Band

has reverted back to its peak energy at 460 nm. From the known mechanism of this epoxidation reaction, the porphyrin loses its axial ligand and becomes oxidized; therefore, there is evidence for this ligand exchange, which is witnessed in the UV-vis of the films after the catalysis (Figure 6.1).

When this same reaction was run for only 2 hr, the overall yields, as expected, decreased (Table 6.1). These films were prepared in the same manner, as were the films studied in the previous catalysis experiment. The ratio of Bands V:VI changes slightly, as the axial ligand environment is not identical in both cases. Again, the UV-vis behavior before and after the catalysis reaction was studied and is shown in Figure 6.2.

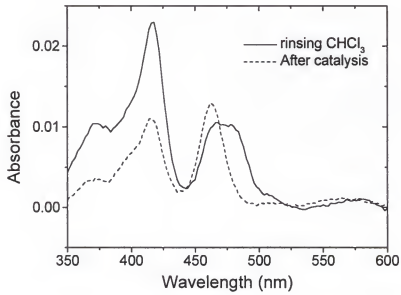

Figure 6.2: SA MnP4 film before and after 2 hr. catalysis run with 40:5:20 cyclooctene: PhIO:decane in CH_2Cl_2.

Considering the original UV-vis spectra of the films indicated in the 2 hr and 24 hr experiments, there appeared to be a significant contribution from free-base porphyrin in these films. From the studies described in Chapter 4 and 5, it was known that self-assembling the MnP4 from a solution containing chloride ions helped discourage the phosphonate from demetallating the porphyrin. To test if a decrease in the film loading of free-base porphyrin affected the catalytic results, a film SA from a chloride containing solution was employed for the 6 hr experiment. Again, some bleaching of the porphyrin was observed, but it did appear that there was a significant amount of the original chromophore present after catalysis. Also, there was no significant contribution from free-base porphyrin to the UV-vis spectra even after the catalysis run, so the catalysis does not cause the Mn-porphyrin to demetallate (Figure 6.3). However, the epoxide yield was not dramatically improved by eliminating the free-base porphyrin from the films.

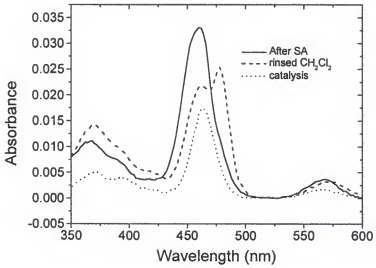

Figure 6.3: UV-vis of MnP4 film SA from chloride containing solution used in catalysis with PhIO after 6 hr.

The behavior of the MnP4 films in the epoxidation reaction with PhIO over 6 hr showed up to a 20% reduction in the absorbance intensity of the peak at 464 nm. The film could be recycled with ca. a 50% loss in catalytic activity, but catalysis could still be observed.

For comparison, the bleaching of the porphyrin in the homogeneous solution was studied (Figure 6.4). It appears that after 6 hr., there was as much as a 50% bleaching of the active chromophores in solution. After 12 hr, the bleaching observed was about the same as at 6 hr. The porphyrins immobilized in the zirconium phosphonate films appear to be slightly more stable under most catalysis conditions.

Table 6.1: Time dependence of epoxidation of cyclooctene using 40 μmol cyclooctene and 5 μmol PhIO in 1mL of solution. To the homogeneous reaction was added 1nmol of MnP0.

Experiment	Cyclooctene oxide Yield	Turnovers*	Porphyrin Bleaching**
24 hr			
Blank	4.98%		
Homogeneous	8.43%	422	
Films	35.1%, 20.8%	1755, 1040	<20%
6 hr			
Blank	1.0%-1.5%		
Homogeneous	6.0%-7.0%	300	< 50%
Films	30.3%, 29.0%	1515, 1450	<20%
2 hr			
Blank	0.5%-1.0%		
Homogeneous	3.0%-3.4%	150-170	
Films	13.3%, 12.7%	665, 635	None

* Turnovers calculated on number of oxidation cycles
** Bleaching determined from decrease in intensity of Soret Band in UV-vis

From Table 6.1, it is clear that the conversion of CyO to CyOO is time dependent. The best yields were usually achieved after 24 hr; however, the difference between 6 hr and 24 hr was small in some cases. Although the absorbance intensity prior to the reaction was roughly the same as in the case of the SA films, after 24 hr, the overall absorbance intensity has decreased. This result indicates that a percentage of the chromophores have been bleached or removed from the surface. Considering studies done previously on the stability of the porphyrin containing zirconium phosphonate SA and LB films after rinsing in hot solvents, the chromophores are probably not removed but have likely been oxidized rendering them useless as catalysts. However, the bleaching process was not complete and there were still a number of catalytic porphyrins available on the surface.

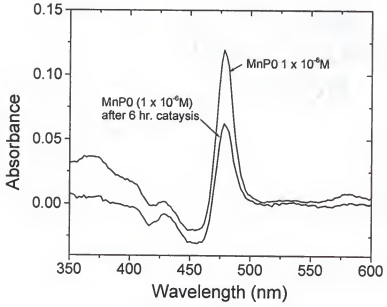

Figure 6.4: Bleaching of MnP0 in homogeneous catalysis reaction with PhIO.

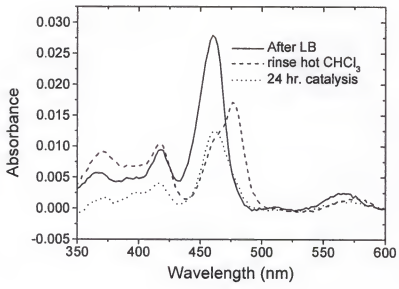

Figure 6.5: MnP4 LB film before and after 24 hr catalysis reaction.

6.2.1.2. Oxidation yield dependence on film preparation method. The above described catalysis results were observed using MnP4 SA films. Alternatively, pure LB films of MnP4 were also used in the reaction cells. A MnP4 film was transferred by the LB technique at 20 mN m^{-1} where the density of chromophores was high and aggregation was observed. The film was rinsed to remove any possibly physisorbed chromophores present due to the compressed nature of the film. These films were then used in the reaction flow cells over 24 hr with a 40:5:20 ratio of CyO to PhIO to decane. The corresponding blank and homogeneous reactions gave yields of, again, around 4% and 10% respectively; however, the yields with the films were around 15%, which is slightly lower than that seen in the case of the self-assembled porphyrin

films (Figure 6.5). The lower yield could be due to the aggregated nature of the chromophores reducing the active porphryin surface area.

Table 6.2: Conversion of cyclooctene to cyclooctene oxide with 40 μmol cyclooctene and 5 μmol PhIO in 1mL of solution using MnP4 LB film in 24 hr.

LB MnP4	Cyclooctene oxide Yield	Turnovers	Bleaching
Blank	4.0%		
Homogeneous	11.0%	550	<50%
Film	15.0%	750	<20%*

* The amount of bleaching was difficult to determine due to the broadened Soret Band observed prior to the catalysis reaction.

6.2.1.3. Oxidation yield dependence on reactant ratios. Changing the ratio of substrate to oxidant was also investigated. Whereas the prior studies focused on a ratio of 40:5, 60:5 and 20:5 substrate to oxidant ratios were also examined over 24 hr. Changing the substrate to oxidant ratio resulted in yields similar to that seen for the 40:5 experiment. In the 60:5 case, the overall yield was, again, around 20%; however, the porphyrin film experienced slightly less bleaching than observed previously with less substrate. The 20:5 case behaved similarly to the 60:5 and 40:5 experiments, and the yields were approximately the same (Table 6.3).

Table 6.3: Conversion of cyclooctene to cyclooctene oxide with varying cyclooctene to PhIO ratios in 1mL of solution using MnP4 SA films over 24 hr.

Experiment	Cyclooctene Oxide Yield	Turnovers	Bleaching
60:5:20			
Blank	3%		
Homogeneous	7%	350	
Films	20%	1000	<15%
20:5:20			
Blank	2%		
Homogeneous	5%	250	
Films	18%	900	<15%

6.2.1.4 Oxidation dependence on presence of heterocyclic ligand. Addition of an imidazole heterocyclic ligand is commonly reported to enhance the catalytic behavior of Mn-porphyrins in the presence of a peroxide oxidant. However, little was mentioned in the literature about the porphyrin response to this ligand when using PhIO as the oxidant. The imidazole was not only expected to encourage the heterolytic cleavage of the O-O bond of the peroxides but also to stabilize the oxidized manganese state; therefore, some extent of catalysis improvement might be expected. To examine this sensitivity, a SA ImODPA/SA MnP4 film was prepared and rinsed to remove physisorbed chromophores. Using a 40:5 substrate to PhIO ratio, the catalysis reaction was run over 24 hr (Table 6.4).

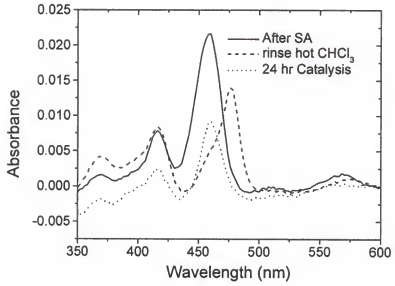

Figure 6.6: SA ImODPA/SA MnP4 studied with PhIO for epoxidation of cyclooctene.

The CyOO yields using these mixed films were actually reduced relative to the pure porphyrin films with PhIO. The lower yield could be due to a decreased porphyrin concentration in the mixed films. The UV-vis spectrum of the films used for this study demonstrated that the overall absorbance of the Soret Band prior to catalysis was lower than that observed in the pure porphyrin film (Figure 6.6). This result corresponded to the behavior often observed in Chapters 5 where porphyrin substitution into a preformed capping layer resulted in a slightly lower loading than in the pure self-assembled films.

Table 6.4: Conversion of cyclooctene to cyclooctene oxide with 40 μmol cyclooctene and 5 μmol PhIO in 1mL of solution and in films containing imidazole.

SA ImODPA/SA MnP4 Film	Cyclooctene oxide Yield	Turnovers	Bleaching
Blank	1.5%-2.5%		
Homogeneous	17.0%-20.0%	850-1000	
Film	15.0%	750	<20%

6.2.1.5. Oxidation yield dependence on cell vs. vial used for reaction. The above results appeared encouraging, with the epoxide yield consistently greater in the immobilized catalyst reactions run in the flow cells over the homogeneous and blank reactions run in the vials. When blank solution mixtures were run through the catalysis cell with blank films, surprising results were obtained. After 6 hr, the blanks in the vials ranged in product yield from 1.0% to 2.0%; however, in the flow-cells, the epoxide yield was 6.0%-6.5%. The discrepancy between the yield in the blank cell and in the vial was not related to a change in the overall concentration. However, the difference was probably due to either the loss of internal standard into the flow-cell material or the fact that the solution experiences more efficient stirring in the flow-cell than in the vial.

Further, homogeneous reactions were also run in the flow-cell to examine if the observed increased product yield with the catalytic films was due to the immobilized catalyst or the act of performing the reaction in the cell. These results are shown in Table 6.5. From a series of experiments, including GCs of a solution run after the

PhIO reaction contents were removed from the cell, it appeared that decane is retained in the cell. The decane is even observed in the GC traces after the cell has been thoroughly cleaned, implying that this molecule has a tendency to adsorb onto the tubing and/or cell material and dissolves out slowly. The amount of decane seen after the cells were cleaned is small relative to the original peak, but this may be the source of some discrepancy observed between blanks and homogeneous reactions run in and out of the cell.

Overall, it appears that there is an improvement observed in the catalytic activity of the porphyrin from the homogeneous solution to that seen in the immobilized films. These systems clearly need to be studied using an alternative internal standard to potentially eliminate the discrepancy observed with leeching of the decane into and then out of the flow cell.

Table 6.5: Comparison of blanks and homogeneous epoxidation yields in vials vs. in the reaction cells.

SA MnP4	Cyclooctene oxide Yield	Turnovers
Blank in vial	1.3%-2.0%	
Blank in cell	6.0%-6.5%	
Homogeneous in vial	6.0%	300
Homogeneous in cell	9.0%-14.0%	450-700
Film in cell	20.0%-21.0%	1000

6.2.2. Catalysis using H_2O_2 as the oxidant

6.2.2.1. Oxidation with 10^4 times less catalyst vs. other reactants (80 μmol H_2O_2 or 40 μmol cyclooctene vs.1 nmol MnP). The above-described PhIO epoxidations were performed with 1nmol of catalyst relative to 40 μmol of substrate and 5 μmol of oxidant. The catalyst in these studies is ca. 10^3 times lower in concentration than that suggested in the literature studies. The results, however, suggest that the catalyst is still active at this concentration under these conditions. Additionally, in the PhIO reactions, excess substrate was used to protect the catalyst from bleaching. As mentioned in section 6.1, with peroxide oxidants, both excess substrate and excess oxidant have been investigated.

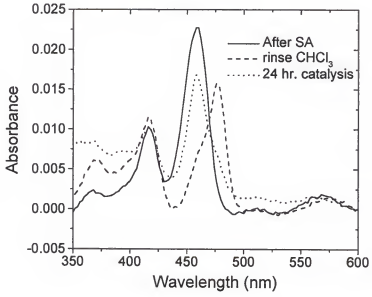

Figure 6.7: SA ImODPA/SA MnP4 studied in the epoxidation of cyclooctene using H_2O_2.

When experiments similar to the Bacciochi study with excess substrate were reproduced using 400 μmol cyclooctene and 80 μmol H_2O_2 in 1mL of solution, with 25 μmol imidazole and 1 nmol of MnP added to the homogeneous reaction, very little epoxide was detected in the blank or homogeneous reactions.[99] Fortunately, a clear increase in the yield was observed with the immobilized porphyrins (Table 6.6). As in the PhIO reactions, the immobilized catalyst appeared to be relatively stable toward the reaction conditions (Figure 6.7).

Table 6.6: Conversion of cyclooctene to cyclooctene oxide with 400 μmol cyclooctene and 80 μmol H_2O_2 in 1mL of solution using imidazole and porphyrin.

SA ImODPA/SA MnP4	Cyclooctene oxide Yield
Blank	0.2%-0.3%
Homogeneous*	0.5%-1.0%
Films	12.6%, 12.8%

* Homogeneous solution contains 40 μmol ImH and 1nmol of MnP0

The epoxidation of cyclooctene was also run in the presence of excess oxidant with approximately the same molar ratio of catalyst (10^{-3} vs other reactants). The ratio examined using excess oxidant was 80 μmol cyclooctene to 400 μmol H_2O_2. The results were surprising in one aspect. After the 24 hr catalysis reaction was concluded, the UV-vis of the film showed nearly complete demetallation of the porphyrin (Figure 6.8).

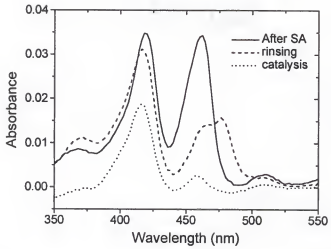

Figure 6.8: SA ImODPA/SA MnP4 after rinsing and after 24 hr in catalysis reaction with excess H_2O_2.

Also, the epoxide yield with the film was now around 0.5% -- nearly identical to that seen in the homogeneous and blank reactions run in vials. Interestingly, when this reaction was run in a vial with 1 μmol of MnP0, mimicking the literature procedure, the yield was 74%, closely resembling the yield reported with a MnTFPP Cl catalyst.[116]

6.2.2.2. Oxidation with 10^2 times less catalyst vs. other reactants (.8 μmol H_2O_2 or .4 μmol cyclooctene vs.1 nmol MnP). Because the epoxide yield in the above reactions may be lower than usual due to the very small amount of catalyst present relative to reactants, an attempt was made to bring these concentrations closer to the literature ratios of 10:1 reactant to catalyst. Additionally, this oxidant concentration (400 μmol vs. 1 nmol catalyst) clearly causes the degradation of the porphyrin films.

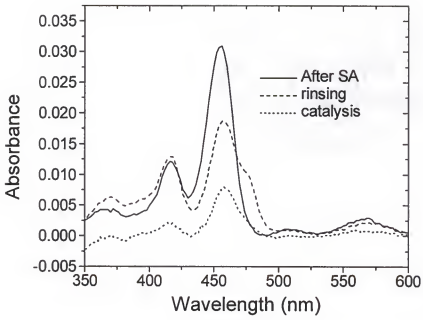

Figure 6.9: SA ImODPA/SA MnP4 film with catalysis using 8 μmol cyclooctene to 0.2 μmol H_2O_2.

The solutions were, therefore, diluted 100-fold and similar reactions were investigated. The new reaction molar ratio was 8 μmol cyclooctene to 0.2 μmol H_2O_2 to 1 nmol of catalyst. The concentration of catalyst in the homogeneous case was set by the concentration in the films, which could not be increased. Unfortunately, even with excess substrate to protect the porphyrin structure, more serious catalyst bleaching was observed in these films than in those with PhIO (Figure 6.9). In addition, the epoxide yield with the immobilized catalyst under these conditions was similar to or less than that observed in the homogeneous case. The reasons behind these results are not clear.

6.3 Conclusions

From the above results, it appears that the immobilization of the porphyrins does slightly improve the catalytic efficiency of the Mn-porphyrin with PhIO as the oxidant. An improvement is also observed in the catalyst stability in the zirconium phosphonate films relative to the homogeneous and previous LB film examples. The stability and easy recovery of these immobilized porphyrins is an advantage over previous literature cases.

The improvement of the epoxide yields using H_2O_2 using the immobilized porphyrin and imidazole did show promise when the molar ratio was ca. 400 μmol cyclooctene to 80 μmol H_2O_2 to 1 nmol of catalyst. Additionally, these films appeared to be significantly more stable over 24 hr than the homogeneous catalysts. Unfortunately, with excess oxidant, the Mn-porphyrin in the film completely demetallates.

Overall, zirconium phosphonate templates allowed the successful incorporation of both catalytic porphyrins and imidazoles into thin film environments. The inorganic template also introduced significant film stability and overall improved the catalytic efficiency of the immobilized catalysts.

REFERENCES

(1) Papkovsky, D. B. *Sensors and Acts. B: Chem.* **1995**, *1-3*, 213-218.

(2) Jung, G. Y., Pearson, C., Kilitziraki, M., Horsburgh, L.E., Monkman, A.P., Samuel, I.D.W., Petty, M.C. *J. Mater. Chem.* **2000**, *10*, 163-167.

(3) Ogata, N. *Makromol. Chem.-Macromol. Symp.* **1992**, *53*, 191-200.

(4) Papkovsky, D. B., Ovchinikov, A.N., Ponomarev, G.V., Korpela, T. *Anal. Lett.* **1997**, *30*, 699-719.

(5) Fabianowski, W., Jaccodine, R., Kodnani, R., Pearson, R., Smektala, P. *Adv. Mat. Opt. Elec.* **1995**, *5*, 199-213.

(6) Papkovsky, D. B., Desyaterik, I.V., Ponomarev, G.V., Kurochkin, I.N., Korpela, T. *Anal.Chim.Acta* **1995**, *310*, 233-239.

(7) Aramaki, K. *Corrosion Sci.* **1999**, *41*, 1715-1730.

(8) Arnold, D. P., Manno, D., Micocci, G., Serra, A., Tepore, A., Valli, L. *Thin Solid Films* **1998**, *327-329*, 341-344.

(9) Penza, M., Milella, E., Anisimkin, V.I. *IEEE T. Ultrason. Ferr.* **1998**, *45*, 1125-1132.

(10) Kauffman, F., Hoffman, B., Erbach, R., Heiliger, L., Siegmund, H.U., Volker, M. *Sensors and Acts B-chemical* **1994**, *18*, 60-64.

(11) Marlow, A. L., Davis, J.T. *Tet. Lett.* **1999**, *40*, 3539-3542.

(12) Petrucci, M. G. L.; Kakkar, A. K. *Chem. Mater.* **1999**, *11*, 269-276.

(13) Suh, J. H., Hong, S.H. *J. Am. Chem. Soc.* **1998**, *120*, 12545-12552.

(14) Agarwal, V. K. *Physics Today* **1988**, 40.

(15) Roberts, G. G. *Langmuir-Blodgett Films*; Plenum Press: New York, 1990.

(16) Langmuir, I. *J. Am. Chem. Soc.* **1917**, *39*, 1848-1906.

(17) Blodgett, K. A.; Langmuir, I. *Phys. Rev.* **1937**, *51*, 964.

(18) Levine, O., Zisman, W.A. *J. Phys. Chem.* **1957**, *61*, 1068.

(19) Bartell, L. S., Ruch, R.J. *J. Phys. Chem* **1956**, *60*.

(20) Ulman, A. *An Introduction to Ultrathin Organic Films: From Langmuir-Blodgett to Self-Assembly*; Academic Press: Boston, 1991.

(21) Zasadzinski, J. A.; Viswanathan, R.; Madsen, L.; Garnaes, J.; Schwartz, D. K. *Science* **1994**, *263*, 1726-1733.

(22) Gaines, G. J. *Insoluble Monolayers at Liquid-Gas Interfaces*; Wiley-Interscience: New York, 1966.

(23) Tredgold, T. H. *J. Mater. Chem.* **1995**, *5*, 1095-1106.

(24) Aston, M. S. *Chem. Soc. Rev.* **1993**, 67-71.

(25) Orrit, M.; Mobius, D.; Lehmann, U.; Meyer, H. *J. Chem. Phys.* **1986**, *85*, 4966-4979.

(26) Mobius, D.; Orrit, M.; H., G.; Meyer, H. *Thin Solid Films* **1985**, *132*, 41-53.

(27) Drago, R. S. *Physical Methods for Chemists*; Saunders College Publishing: Orlando, 1992.

(28) Byrd, H.; Pike, J. K.; Talham, D. R. *Chem. Mater.* **1993**, *5*, 709-715.

(29) Byrd, H.; Whipps, S.; Pike, J. K.; Talham, D. R. *Thin Solid Films* **1994**, *244*, 768-771.

(30) Offord, D. A.; Sachs, S. B.; Ennis, M. S.; A.Eberspacher, T.; Griffin, J. H.; Chidsey, C. E. D.; Collman, J. P. *J. Am. Chem. Soc.* **1998**, *120*, 4478-4487.

(31) *Practical Surface Analysis*; 2nd ed.; Briggs, D.; Seah, M. P., Eds.; John Wiley and Sons: Chichester, 1990; Vol. 2.

(32) Seah, M. P.; Dench, W. A. *Surface Interface Analysis* **1979**, *1*, 1-11.

(33) Zhang, Z.; Nakashima, K.; Lal Verma, A.; Yoneyama, M.; Iriyama, K.; Ozaki, Y. *Langmuir* **1998**, *14*, 1177-1182.

(34) Sagiv, J. *J. Am. Chem. Soc.* **1980**, *102*, 92.

(35) Nuzzo, R. G., Allara, D.L. *J. Am. Chem. Soc.* **1983**, *105*, 4481.

(36) Porter, M. D.; Bright, T. B.; Allara, D. L.; Chidsey, C. E. D. *J. Am. Chem. Soc.* **1987**, *109*, 3559-3568.

(37) Strong, L., Whitesides, G.M. *Langmuir* **1988**, *4*, 316.

(38) Byrd, H.; Whipps, S.; Pike, J. K.; Ma, J.; Nagler, S. E.; Talham, D. R. *J. Am. Chem. Soc.* **1994**, *116*, 295-301.

(39) Byrd, H.; Pike, J. K.; Talham, D. R. *Syn. Met.* **1995**, *71*, 1977-1980.

(40) Seip, C. T.; Byrd, H.; Pike, J. K.; Whipps, S.; Talham, D. R. In *Physical Supramolecular Chemistry*; Echegoyen, L., Kaifer, A. E., Eds., 1996; Vol. 485.

(41) Seip, C. T.; Byrd, H.; Talham, D. R. *Inorg. Chem.* **1996**, *35*, 3479-3483.

(42) Seip, C. T.; Granroth, G. E.; Meisel, M. W.; Talham, D. R. *J. Am. Chem. Soc.* **1997**, *119*, 7084-7094.

(43) Clearfield, A. *Chem. Mater.* **1998**, *10*, 2801-2810.

(44) Cemto, G., Trifiro, F., Ebner, J.R., Franchetti, V.M. *Chem. Rev.* **1988**, *88*, 55.

(45) Frink, K. J.; Wang, R.-C.; Colón, J. L.; Clearfield, A. *Inorganic Chemistry* **1991**, *30*, 1438-1441.

(46) Cao, G.; Mallouk, T. E. *Inorganic Chemistry* **1991**, *30*, 1434-1438.

(47) Cao, G.; Lynch, V. M.; Yacullo, L. N. *Chem. Mater.* **1993**, *5*, 1000-1006.

(48) Drumel, S., Janvier, P., Bujoli-Doeuff, M., Bujoli, B. *J. Mater. Chem.* **1996**, *6*, 1843-1847.

(49) Kaschak, D. M., Johnson, S.A., Hooks, D.E., Kim, H.-N., Ward, M.D., Mallouk, T.E. *J. Am. Chem. Soc.* **1998**, *120*, 10887-10894.

(50) Kraus, K. A., Phillips, H.O. *J. Am. Chem. Soc.* **1956**, *78*, 644.

(51) Alberti, G. *Acc. Chem. Res.* **1978**, *11*, 163.

(52) Clearfield, A. *Chem. Rev.* **1988**, *88*, 125-148.

(53) Clearfield, A. In *Progress in Inorganic Chemistry*; John Wiley & Sons: NY, 1998; Vol. 47.

(54) Cao, G.; Lee, H.; Lynch, V. M.; Mallouk, T. E. *Solid State Ionics* **1988**, *26*, 63-69.

(55) Cao, G.; Lee, H.; Lynch, V. M.; Mallouk, T. E. *Inorg. Chem.* **1988**, *27*, 2781-2785.

(56) Cunningham, D.; Hennelly, P. J. D. *Inorg. Chim. Acta* **1979**, *37*, 95-102.

(57) Zhang, Y.; Scott, K. J.; Clearfield, A. *Chemistry of Materials* **1993**, *5*, 495-499.

(58) Cao, G.; Lynch, V. M.; Swinnea, J. S.; Mallouk, T. E. *Inorganic Chemistry* **1990**, *29*, 2112-2117.

(59) Wang, R.-C.; Zhang, Y.; Hu, H.; Frausto, R. R.; Clearfield, A. *Chem. Mater.* **1992**, *4*, 864-870.

(60) Thomas, L. C.; Chittenden, R. A. *Spectrochimica Acta* **1970**, *26A*, 781-800.

(61) Lee, H.; Kepley, L. J.; Hong, H.-G.; Mallouk, T. E. *J. Am. Chem. Soc.* **1988**, *110*, 618-620.

(62) Lee, H.; Kepley, L. J.; Hong, H.-G.; Akhter, S.; Mallouk, T. E. *J. Phys. Chem.* **1988**, *92*, 2597-2601.

(63) Cao, G.; Hong, H.-G.; Mallouk, T. E. *Acc. Chem. Res.* **1992**, *25*, 420-427.

(64) Fanucci, G. E.; Seip, C. T.; Petruska, M. A.; Ravaine, S.; Nixon, C. M.; Talham, D. R. *Thin Solid Films* **1998**, *327-329*, 331-335.

(65) Petruska, M. A.; Fanucci, G. E.; Talham, D. R. *Chem. Mater.* **1998**, *10*, 177-189.

(66) Fanucci, G. E.; Petruska, M. A.; Meisel, M. W.; Talham, D. R. *J. Solid State Chem.* **1999**, *145*, 443-451.

(67) Petruska, M. A.; Talham, D. R. *Chem. Mater.* **1998**, *10*, 3673-3682.

(68) Croney, J. C., Helms, M.K., Jameson, D.M., Larsen, R.W. *J. Phys. Chem. B* **2000**, *104*, 973-977.

(69) Hsiao, J.-S., Krueger, B.P., Wagner, R.W., Johnson, T.E., Delaney, J.K., Mauzerall, D.C., Fleming, G.R., Lindsey, J.S., Bocian, D.F., Donohoe, R.J. *J. Am. Chem. Soc.* **1996**, *118*, 11181-11193.

(70) Ishida, A.; Sakata, Y.; Majima, T. *Chem. Lett.* **1998**, 267-268.

(71) Jolliffe, K.; Bell, T.; Ghiggino, K.; Langford, S.; Paddon-Row, M. *Angew. Chem. Int. E.* **1998**, *37*, 916-919.

(72) Florsheimer, M., Mohwald, H. *Thin Solid Films* **1988**, *159*, 115-123.

(73) Amini, M. K., Shahrokhian, S., Tangestaninejad, S. *Analyst* **1999**, *124*, 1319-1322.

(74) Arnold, D.; Manno, D.; Micocci, A.; Tepore, A.; Valli, L. *Langmuir* **1997**, *13*, 5951-5956.

(75) Smith, V. C., Batty, S.V., Richardson, T., Foster, K.A., Johnstone, R.A.W., Sobral, A.J.F.N., Rocha Gonzales, A.M.d'A. *Thin Solid Films* **1996**, *284-285*, 911-914.

(76) Schenning, A.; Hubert, D.; Feiters, M.; Nolte, R. *Langmuir* **1996**, *12*, 1572-1577.

(77) Lahiri, J., Fate, G.D., Ungashe, S.B., Groves, J.T. *J. Am. Chem. Soc.* **1996**, *118*, 2347-2358.

(78) Schenning, A. P. H. J., Lutje Spelberg, J.H., Driessen, M.C.PF., Hauser, M.J.B., Feiters, M.C., Nolte, R.J.M. *J. Am. Chem. Soc.* **1995**, *117*, 12655-12656.

(79) *The Porphyrins*; Dolphin D. Academic Press: New York, 1978; Vol. IA.

(80) *The Porphyrins*; Gouterman, M., Dolphin D. Ed.; Academic Press: New York, San Francisco, London, 1978; Vol. III.

(81) Gouterman, M. *J. Mol. Spec.* **1961**, *6*, 138-163.

(82) Kroon, J. M., Koehorst, R.B.M., van Dijk, M., Sanders, G.M., Sudholter, E.J.R. *J. Mater. Chem.* **1997**, *7*, 615-624.

(83) *The Porphyrins*; Academic Press: New York, 1978; Vol V.

(84) Kroon, J.; Sudholter, E.; Schenning, A.; Nolte, R. *Langmuir* **1995**, *11*, 214-220.

(85) Zhang, J.; Wang, D.; Chen, Y.; Li, T.; Mao, H.; Tian, H.; Zhou, Q.; Xu, H. *Thin Solid Films* **1997**, *300*, 208-212.

(86) Gregory, B. W., Vaknin, D., Gray, J.D., Ocko, B.M., Stroeve, P., Cotton, T.M., Struve, W.S. *J. Phys. Chem. B* **1997**, *101*, 2006-2019.

(87) Tour, J. M., Jones, LeRoy III, Pearson, D.L., Lamba, J.J.S., Burgin, T.P., Whitesides, G.M., Allara, D.L., Parikh, A.N., Atre, S.V. *J. Am. Chem. Soc.* **1995**, *117*, 9529-9534.

(88) Abatti, D.; Zaniquelli, M. E.; Iamamoto, Y.; Idemori, Y. *Thin Solid Films* **1997**, *310*, 296-302.

(89) Anikin, M.; Tkachenko, N.; Lemmetyinen, H. *Langmuir* **1997**, *13*, 3002-3008.

(90) Honeybourne, C.; Barrell, K. *J. Mater. Chem.* **1996**, *6*, 323-329.

(91) Ruaudel-Teixier, A.; Barraud, A.; Belbeoch, B.; Roulliay, M. *Thin Solid Films* **1983**, *99*, 33-40.

(92) Song, X.; Miura, M.; Xu, X.; Taylor, K.; Majumder, S.; Hobbs, J.; Cesarano, J.; Shelnutt, J. *Langmuir* **1996**, *12*, 2019-2027.

(93) Breslow, R., Zhang, X., Huang, Y. *J. Am. Chem. Soc.* **1997**, *119*, 4535-4536.

(94) Robert, A., Loock, B., Momenteau, M., Meunier, B. *Inorg. Chem.* **1991**, *30*, 706-711.

(95) Beck, M. J., Gopinath, E., Bruice, T.C. *J. Am. Chem. Soc.* **1993**, *115*, 21-29.

(96) Mohajer, D., Monfared, H.H. *J. Chem. Res. S* **1998**, 772-773.

(97) Arasasingham, R. D., He, G.-X., Bruice, T.C. *J. Am. Chem. Soc.* **1993**, *115*, 7985-7991.

(98) Arasasingham, R. D. J., S., Bruice, T.C. *J. Am. Chem. Soc.* **1992**, *114*, 2536-2544.

(99) Baciocchi, E., Boschi, T., Galli, C., Lapi, A., Tagliatesta, P. *Tetrahedron* **1997**, *53*, 4497-4502.

(100) Guo, C.-C., Li, H.-P., Xu, J.-B. *J. Cat.* **1999**, *185*, 345-351.

(101) Collman, J. P., Zhang, X., Lee, V.J., Uffelman, E.S., Brauman, J.I. *Science* **1993**, *261*, 1404-1411.

(102) Lai, T.-S., Kwong, H.-L., Che, C.-M., Peng, S.-M. *Chem. Commun.* **1997**, 2373-2374.

(103) Gilmarten, C.; Lindsay Smith, J. *J. Chem. Soc. Perkin Trans.* **1995**, *2*, 243-251.

(104) Miki, K.; Sato, Y. *Bull. Chem. Soc. Jpn.* **1993**, *66*, 2385-2390.

(105) Deniaud, D.; Schollorn, B.; Mansuy, D.; Rouxel, J.; Battioni, P.; Bujoli, B. *Chem. Mater.* **1995**, *7*, 995-1000.

(106) Martinez-Lorente, M. A., Battioni, P., Kleemiss, W., Bartoli, J.F., Mansuy, D. *J. Mol. Cat. A* **1996**, *113*, 343-353.

(107) Cooke, P. R., Lindsay Smith, J.R. *Tet. Lett.* **1992**, *33*, 2737-2740.

(108) Neys, P. E. F., Severeyns, A., Vankelecom, I.F.J., Ceulemans, E., Dehaen, W., Jacobs, P.A. *J. Mol. Cat. A Chemical* **1999**, *144*, 373-377.

(109) Groves, J. T., Ungashe, S.B. *J. Am. Chem. Soc.* **1990**, *112*, 7796-7797.

(110) Campestrini, S., Meunier, B. *Inorg. Chem.* **1992**, *31*, 1999-2006.

(111) Yuan, L.-C., Bruice, T.C. *J. Am. Chem. Soc.* **1986**, *108*, 1643-1650.

(112) Tangestaninejad, S., Moghadam, M. *Syn. Comm.* **1998**, *28*, 427-432.

(113) Coyle, C. L., Rafson, P.A., Abbott, E.H. *Inorg. Chem.* **1973**, *12*, 2007-2010.

(114) Arasasingham, R. D., Bruice, T.C. *J. Am. Chem. Soc.* **1991**, *113*, 6095-6103.

(115) Boucher *Coord. Chem. Rev.* **1972**, *7*, 289-329.

(116) Battioni, P., Renaud, J.P., Bartoli, J.F., Reina-Artiles, M., Fort, M., Mansuy, D. *J. Am. Chem.Soc* **1988**, *110*, 8462-8470.

(117) Kern, W. *J. Electrochem. Soc.* **1990**, *137*, 1887-1892.

(118) Advincula, R. *Dissertation*, University of Florida, 1994.

(119) Evans, D. F. *J. Chem. Soc.* **1950**, 2003.

(120) Schubert, E. M. *J. Chem. Ed.* **1992**, *69*, 62.

(121) Saltzman, H., Sharefkin, J.G. *Organic Synthesis , 43*, 60-61.

(122) Lucas, H. J., Kennedy, E.R. *Organic Synthesis , Coll. Vol. 3*, 483, 1955.

(123) Montanari, F. *Metalloporphyrins Catalysed Oxidations*; Kluwer Academic Publishers, 1994.

(124) Caughey, W.; Deal, R.; Weiss, C.; Goutermann, M. *J. Mol. Spec.* **1965**, *16*, 451-463.

(125) Talham, D. R.; Seip, C. T.; Whipps, S.; Fanucci, G. E.; Petruska, M. A.; Byrd, H. *Comments Inorg. Chem.* **1997**, *19*, 133-151.

(126) Petruska, M. A., Talham, D.R. *Langmuir* **2000**, *submitted.*

(127) Day, V. W., Stults, B.R., Tasset, E.L., Day, R.O., Marianelli, R.S. *J. Am. Chem. Soc.* **1974**, *96*, 2650-2652.

(128) Tulinsky, A., Chen, B.M.L. *J. Am. Chem. Soc.* **1977**, *99*, 3647-3651.

(129) Hansen, A. P., Goff, H.M. *Inorg. Chem.* **1984**, *23*, 4519-4525.

(130) Schardt, B. C., Hollander, F.J., Hill, C.L. *J. Am. Chem. Soc.* **1982**, *104*, 3964-3972.

(131) Boucher, L. J. *J. Am. Chem. Soc.* **1970**, *92*, 2725-2730.

(132) Powell, M. F., Pai, E.F., Bruice, T.C. *J. Am. Chem. Soc.* **1984**, *106*, 3277-3285.

(133) Mu, X. H., Schultz, F.A. *Inorg. Chem.* **1992**, *31*, 3351-3357.

(134) Maiti, N. C., Mazumdar, S., Periasamy, N. *J. Phys. Chem. B* **1998**, *102*, 1528-1538.

(135) Nixon, C. M.; Claire, K. L.; Odobel, F.; Bujoli, B.; Talham, D. R. *Chem. Mater.* **1999**, *11*, 965-976.

BIOGRAPHICAL SKETCH

Christine M. Nixon Lee was born in Dayton, Ohio, on February 17, 1973. She moved with her family to Mansfield, Ohio, in fifth grade, and she graduated from Lexington High School in June of 1991. Christine entered Baldwin-Wallace College in Berea, Ohio, in September 1991 as a music major, and in the fall of 1992, she began her chemistry major. Christine graduated from Baldwin-Wallace College *summa cum laude* in June of 1995 with a B.S. in chemistry and a minor in music.

In the summer of 1995, she started studying at the University of Florida, and joined Dr. Dan Talham's group in the spring of 1997–just in time to do her oral qualifying exam. She married Lawrence Lee in July of 1999, and will be joining him in New York City after she graduates in the spring of 2000 with her Ph.D. in chemistry.

I certify that I have read this study and that in my opinion it conforms to acceptable standards of scholarly presentation and is fully adequate, in scope and quality, as a dissertation for the degree of Doctor of Philosophy.

Daniel R. Talham, Chairman
Associate Professor of Chemistry

I certify that I have read this study and that in my opinion it conforms to acceptable standards of scholarly presentation and is fully adequate, in scope and quality, as a dissertation for the degree of Doctor of Philosophy.

William Weltner
Professor of Chemistry

I certify that I have read this study and that in my opinion it conforms to acceptable standards of scholarly presentation and is fully adequate, in scope and quality, as a dissertation for the degree of Doctor of Philosophy.

Martin Vala
Professor of Chemistry

I certify that I have read this study and that in my opinion it conforms to acceptable standards of scholarly presentation and is fully adequate, in scope and quality, as a dissertation for the degree of Doctor of Philosophy.

Kenneth Wagener
Professor of Chemistry

I certify that I have read this study and that in my opinion it conforms to acceptable standards of scholarly presentation and is fully adequate, in scope and quality, as a dissertation for the degree of Doctor of Philosophy.

David P. Chynoweth
Professor of Agricultural and Biological Engineering

This dissertation was submitted to the Graduate Faculty of the Department of Chemistry in the College of Liberal Arts and Sciences and to the Graduate School and was accepted as partial fulfillment of the requirements for the degree of Doctor of Philosophy.

August 2000

Dean, Graduate School